Alfred-Wegener-Institut für Polar- und Meeresforschung
Sektion Periglazialforschung

Thermokarst and thermal erosion: Degradation of Siberian ice-rich permafrost

Dissertation
zur Erlangung des akademischen Grades
"doctor rerum naturalium"
(Dr. rer. nat.)
in der Wissenschaftsdisziplin "Terrestrische Geowissenschaften"

als kumulative Arbeit eingereicht an der
Mathematisch-Naturwissenschaftlichen Fakultät
der Universität Potsdam

von
Anne Morgenstern

Potsdam, Juli 2012

Published online at the
Institutional Repository of the University of Potsdam:
URL http://opus.kobv.de/ubp/volltexte/2012/6207/
URN urn:nbn:de:kobv:517-opus-62079
http://nbn-resolving.de/urn:nbn:de:kobv:517-opus-62079

Abstract

Current climate warming is affecting arctic regions at a faster rate than the rest of the world. This has profound effects on permafrost that underlies most of the arctic land area. Permafrost thawing can lead to the liberation of considerable amounts of greenhouse gases as well as to significant changes in the geomorphology, hydrology, and ecology of the corresponding landscapes, which may in turn act as a positive feedback to the climate system. Vast areas of the east Siberian lowlands, which are underlain by permafrost of the Yedoma-type Ice Complex, are particularly sensitive to climate warming because of the high ice content of these permafrost deposits.

Thermokarst and thermal erosion are two major types of permafrost degradation in periglacial landscapes. The associated landforms are prominent indicators of climate-induced environmental variations on the regional scale. Thermokarst lakes and basins (alasses) as well as thermo-erosional valleys are widely distributed in the coastal lowlands adjacent to the Laptev Sea. This thesis investigates the spatial distribution and morphometric properties of these degradational features to reconstruct their evolutionary conditions during the Holocene and to deduce information on the potential impact of future permafrost degradation under the projected climate warming. The methodological approach is a combination of remote sensing, geoinformation, and field investigations, which integrates analyses on local to regional spatial scales.

Thermokarst and thermal erosion have affected the study region to a great extent. In the Ice Complex area of the Lena River Delta, thermokarst basins cover a much larger area than do present thermokarst lakes on Yedoma uplands (20.0 and 2.2 %, respectively), which indicates that the conditions for large-area thermokarst development were more suitable in the past. This is supported by the reconstruction of the development of an individual alas in the Lena River Delta, which reveals a prolonged phase of high thermokarst activity since the Pleistocene/Holocene transition that created a large and deep basin. After the drainage of the primary thermokarst lake during the mid-Holocene, permafrost aggradation and degradation have occurred in parallel and in shorter alternating stages within the alas, resulting in a complex thermokarst landscape. Though more dynamic than during the first phase, late Holocene thermokarst activity in the alas was not capable of degrading large portions of Pleistocene Ice Complex deposits and substantially altering the Yedoma relief. Further thermokarst development in existing alasses is restricted to thin layers of Holocene ice-rich alas sediments, because the Ice Complex deposits underneath the large primary thermokarst lakes have thawed completely and the underlying deposits are ice-poor fluvial

sands. Thermokarst processes on undisturbed Yedoma uplands have the highest impact on the alteration of Ice Complex deposits, but will be limited to smaller areal extents in the future because of the reduced availability of large undisturbed upland surfaces with poor drainage. On Kurungnakh Island in the central Lena River Delta, the area of Yedoma uplands available for future thermokarst development amounts to only 33.7 %. The increasing proximity of newly developing thermokarst lakes on Yedoma uplands to existing degradational features and other topographic lows decreases the possibility for thermokarst lakes to reach large sizes before drainage occurs.

Drainage of thermokarst lakes due to thermal erosion is common in the study region, but thermo-erosional valleys also provide water to thermokarst lakes and alasses. Besides these direct hydrological interactions between thermokarst and thermal erosion on the local scale, an interdependence between both processes exists on the regional scale. A regional analysis of extensive networks of thermo-erosional valleys in three lowland regions of the Laptev Sea with a total study area of 5,800 km² found that these features are more common in areas with higher slopes and relief gradients, whereas thermokarst development is more pronounced in flat lowlands with lower relief gradients. The combined results of this thesis highlight the need for comprehensive analyses of both, thermokarst and thermal erosion, in order to assess past and future impacts and feedbacks of the degradation of ice-rich permafrost on hydrology and climate of a certain region.

Kurzfassung

Die gegenwärtige Klimaerwärmung wirkt sich auf arktische Regionen stärker aus als auf andere Gebiete der Erde. Das hat weitreichende Konsequenzen für Permafrost, der weite Teile der terrestrischen Arktis unterlagert. Das Tauen von Permafrost kann zur Freisetzung erheblicher Mengen an Treibhausgasen sowie zu gravierenden Änderungen in der Geomorphologie, Hydrologie und Ökologie betroffener Landschaften führen, was wiederum als positive Rückkopplung auf das Klimasystem wirken kann. Ausgedehnte Gebiete der ostsibirischen Tiefländer, die mit Permafrost des Yedoma Eiskomplex unterlagert sind, gelten aufgrund des hohen Eisgehalts dieser Permafrostablagerungen als besonders empfindlich gegenüber Klimaerwärmungen.

Thermokarst und Thermoerosion sind zwei Hauptformen der Permafrostdegradation in periglazialen Landschaften. Die zugehörigen Landschaftsformen sind auf der regionalen Skala bedeutende Indikatoren klimainduzierter Umweltvariationen. Thermokarstseen und -senken (Alasse) sowie Thermoerosionstäler sind in den Küstentiefländern der Laptewsee weit verbreitet. Die vorliegende Dissertation untersucht die räumliche Verbreitung und die morphometrischen Eigenschaften dieser Degradationsformen mit dem Ziel, ihre Entwicklungsbedingungen während des Holozäns zu rekonstruieren und Hinweise auf potenzielle Auswirkungen zukünftiger Permafrostdegradation im Zuge der erwarteten Klimaerwärmung abzuleiten. Der methodische Ansatz ist eine Kombination aus Fernerkundungs-, Geoinformations- und Geländeuntersuchungen, die Analysen auf lokalen bis regionalen räumlichen Skalen integriert.

Thermokarst und Thermoerosion haben die Untersuchungsregion tiefgreifend geprägt. Im Eiskomplexgebiet des Lena-Deltas nehmen Thermokarstsenken eine weitaus größere Fläche ein als Thermokarstseen auf Yedoma-Hochflächen (20,0 bzw. 2,2 %), was darauf hin deutet, dass die Bedingungen für die Entwicklung von großflächigem Thermokarst in der Vergangenheit wesentlich günstiger waren als heute. Die Rekonstruktion der Entwicklung eines einzelnen Alas im Lena-Delta belegt eine andauernde Phase hoher Thermokarstaktivität seit dem Übergang vom Pleistozän zum Holozän, die zur Entstehung einer großen und tiefen Senke führte. Nach der Drainage des primären Thermokarstsees im mittleren Holozän erfolgten Permafrostaggradation und -degradation parallel und in kürzeren abwechselnden Etappen innerhalb des Alas und führten zu einer komplexen Thermokarstlandschaft. Trotzdem die spätholozäne Thermokarstentwicklung im Alas dynamischer ablief als die erste Entwicklungsphase, resultierte sie nicht in der Degradation großer Teile pleistozäner Eiskomplexablagerungen und einer wesentlichen Veränderung des

Yedoma-Reliefs. Weitere Thermokarstentwicklung in bestehenden Alassen ist begrenzt auf geringmächtige Lagen holozäner eisreicher Alas-Sedimente, da die Eiskomplexablagerungen unter den großen primären Thermokarstseen vollständig getaut waren und die unterlagernden Sedimente aus eisarmen, fluvialen Sanden bestehen. Thermokarstprozesse auf ungestörten Yedoma-Hochflächen wirken am stärksten verändernd auf Eiskomplexablagerungen, werden aber in Zukunft auf geringere Ausmaße begrenzt sein, da die Verfügbarkeit großer ungestörter, schwach drainierter Yedoma-Hochflächen abnimmt. Auf der Insel Kurungnakh im zentralen Lena-Delta beträgt der für zukünftige Thermokarstentwicklung verfügbare Anteil an Yedoma-Hochflächen nur 33,7 %. Die zunehmende Nähe von sich entwickelnden Thermokarstseen auf Yedoma-Hochflächen zu bestehenden Degradationsstrukturen und anderen negativen Reliefformen verringert die Möglichkeit der Thermokarstseen, große Ausmaße zu erreichen bevor sie drainieren.

Die Drainage von Thermokarstseen durch Thermoerosion ist in der Untersuchungsregion weit verbreitet, aber Thermoerosionstäler versorgen Thermokarstseen und –senken auch mit Wasser. Neben diesen direkten hydrologischen Wechselwirkungen zwischen Thermokarst und Thermoerosion auf der lokalen Ebene existiert auch eine Interdependenz zwischen beiden Prozessen auf der regionalen Ebene. Eine regionale Analyse weitreichender Netze von Thermoerosionstälern in drei Tieflandgebieten der Laptewsee mit einer Fläche von insgesamt 5800 km² zeigte, dass diese Formen häufiger in Gebieten mit höheren Geländeneigungen und Reliefgradienten auftreten, während Thermokarstentwicklung stärker in flachen Tiefländern mit geringeren Reliefgradienten ausgeprägt ist. Die kombinierten Ergebnisse dieser Dissertation zeigen die Notwendigkeit von umfassenden Analysen beider Prozesse und Landschaftsformen, Thermokarst und Thermoerosion, im Hinblick auf die Abschätzung vergangener und zukünftiger Auswirkungen der Degradation eisreichen Permafrosts auf Hydrologie und Klima der betrachteten Region und deren Rückkopplungen.

Table of contents

1 Introduction

1.1 Scientific background and rationale

1.1.1 Permafrost and climate change

Permafrost, i.e. ground that remains frozen for at least two consecutive years (van Everdingen, 2005), underlies about one quarter of the Earth's land surface and is particularly widespread in the Arctic (Figure 1-1). Recent global climate warming is occurring in the Arctic at a much faster rate than in other parts of the world and therefore significantly affects polar permafrost regions (AMAP, 2011). Consequently, of major concern in current periglacial research is the question of how permafrost reacts to climate warming and which effects and consequences this reaction may have on the local, regional, and global scales.

Figure 1-1. Permafrost distribution in the northern hemisphere and location of the study region (black rectangle).

The Snow, Water, Ice and Permafrost in the Arctic (SWIPA) Scientific Assessment Report (AMAP, 2011), which synthesizes the scientific knowledge on arctic changes, describes various effects of changes in the distribution and extent of permafrost on:

- hydrological processes,
- geomorphological processes,
- ecological processes,
- feedbacks to climate through trace gas emissions and albedo changes.

Observations and analyses of these processes often show contrasting changes and effects in different regions, under different conditions, or at different developmental stages. The processes are interrelated and the interactions between factors and feedbacks are highly complex (Jorgenson et al., 2010). This also applies for a certain type of permafrost degradation, thermokarst. Thermokarst is defined as the thawing of ice-rich permafrost or the melting of massive ice resulting in surface subsidence and characteristic landforms such as thermokarst lakes and thermokarst basins (alasses) (van Everdingen, 2005). The formation of thermokarst lakes is accompanied by changes in surface hydrology, disturbance of vegetation, thawing of the underlying permafrost up to depths of several tens to hundreds of meters because of the higher heat capacity of the lake water, mobilization of deep pools of fossil organic carbon and their release to the atmosphere (Zimov et al., 1997; Osterkamp et al., 2000; West and Plug, 2008; Grosse et al., 2011). After the drainage of thermokarst lakes, their basins remain in the landscapes as topographic lows, permafrost starts to aggrade, vegetation reestablishes, organic matter accumulates and can act as a carbon sink (Hinkel et al., 2003; Grosse et al., 2012). While lake formation and lake drainage can occur simultaneously in the same area, remote sensing studies of thermokarst lake area changes have shown increasing as well as decreasing lake area trends for different regions (Payette et al., 2004; Smith et al., 2005; Riordan et al., 2006; Kravtsova and Bystrova, 2009; Labrecque et al., 2009).

Another major type of permafrost degradation is thermal erosion, i.e. the erosion of ice-rich permafrost by the combined mechanical and thermal action of moving water (van Everdingen, 2005). This process also interacts with other landscape factors and processes, for example by forming thermo-erosional gullies and valleys that may change surface runoff systems, increase sediment and nutrient delivery to rivers, lakes, and the sea or drain thermokarst lakes (Marsh and Neumann, 2001; Bowden et al., 2008; Toniolo et al., 2009; Rowland et al., 2010).

1.1.2 Siberian Ice Complex

In Siberia, vast areas are underlain by late Pleistocene ice-rich permafrost deposits of the Yedoma-type Ice Complex (Figure 1-2). These syngenetically frozen, fine-grained deposits contain large amounts of ground ice in the form of segregated ice and huge ice wedges (Figure 1-3), which make them particularly sensitive to climate warming and prone to degradation (Schirrmeister et al., 2010, 2013). They also contain considerable amounts of fossil organic carbon that might become accessible due to permafrost thaw (Khvorostyanov et al., 2008; Schirrmeister et al., 2011b). The highest methane emissions from arctic lakes are indeed reported from lakes in Yedoma or Yedoma-like sediments (Walter et al., 2006).

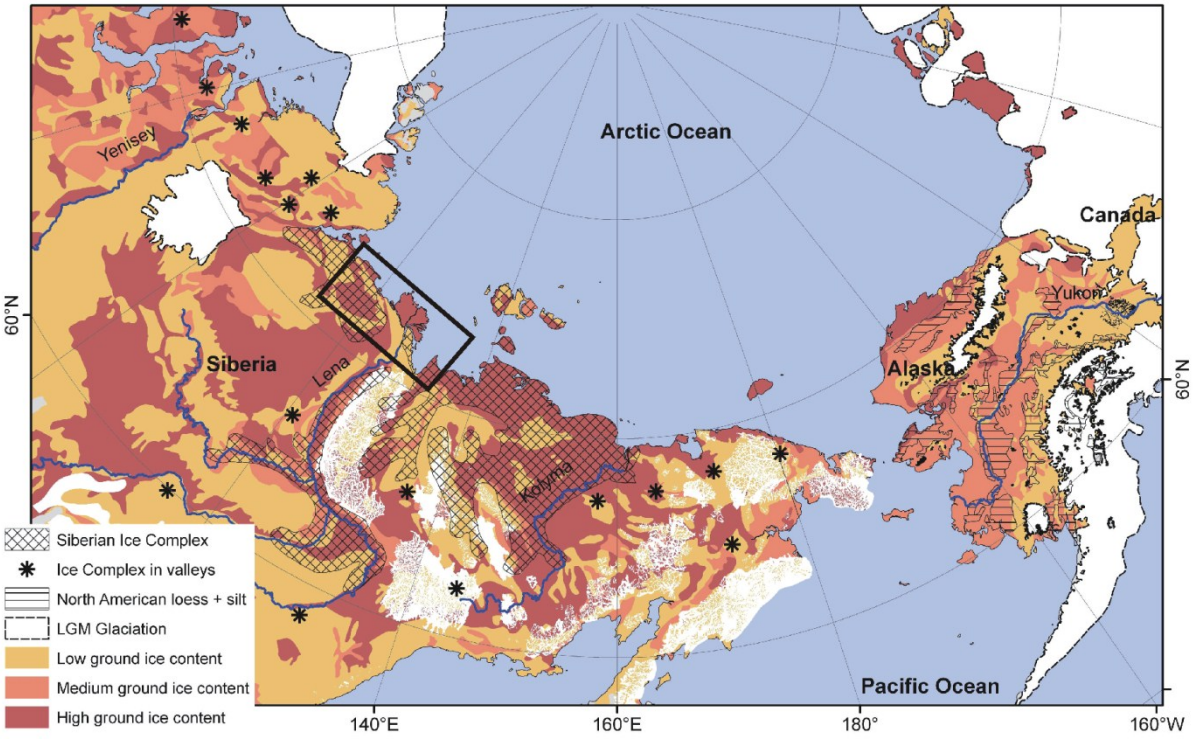

Figure 1-2. Distribution of Ice Complex deposits and location of the study region (black rectangle). Map compiled by G. Grosse, University of Alaska Fairbanks.

Figure 1-3. Exposure of Ice Complex deposits at the Laptev Sea coast of the Cape Mamontov Klyk area. Ice wedges appear in light grey, sediment patches in darker colors. Persons for scale (Photo by G. Grosse, 2003).

The degradation of these ice-rich deposits is not only a modern phenomenon, but has already extensively occurred due to global warming during the transition from late Pleistocene to Holocene (Romanovskii et al., 2004; Kaplina, 2009). Several studies have conducted general areal quantifications of past permafrost degradation by thermokarst and thermal erosion and show that up to >75 % of certain Ice Complex areas have been degraded during the Holocene (Kaplina et al., 1986; Grosse et al., 2005, 2006; Veremeeva and Gubin, 2009). However, detailed knowledge about the evolution of different types of degradational landforms and their interactions is still scarce.

1.2 Aims and approaches

Thermokarst and thermal erosion are two major types of permafrost degradation that are likely to increase under a continuing arctic warming, especially in the sensitive Siberian arctic lowlands underlain by Ice Complex deposits. However, both processes have already affected these regions during previous warm periods and have formed characteristic landscapes that constitute some of the boundary conditions for future changes. The key research questions to be addressed in this thesis are therefore:

How have thermokarst and thermal erosion affected Siberian ice-rich permafrost in the past, and what potential do they have for its future degradation under a continuing arctic warming?

To answer these questions the specific objectives are to:

- quantify existing thermokarst and thermo-erosional landforms in a key region,
- determine the morphometric characteristics and spatial distribution of thermokarst and thermo-erosional landforms in different relief and cryolithological settings,
- distinguish different types and developmental stages of thermokarst and thermo-erosional landforms,
- assess the interaction between thermokarst and thermal erosion,
- deduce the potential extent of future development of thermokarst and thermal erosion.

The methodology applied throughout the thesis is a combination of remote sensing (RS), Geographical Information Systems (GIS), and field investigations. The mapping and characterization of the degradational landforms over the large study region was conducted by means of RS, using medium to high resolution optical satellite imagery (Landsat-7 ETM+, ALOS AVNIR-2, ALOS PRISM, RapidEye, Hexagon, Corona). Relief analyses were performed using Digital Elevation Models (DEMs), and detailed morphometric and process studies were based on field investigations. The integration of all data acquired on the different scales and their spatial analyses were realized in the frame of a GIS. In addition, data derived during field investigations were used for ground truth and validation of RS and GIS data.

1.3 Study region

The East Siberian study region consists of three study areas underlain by Ice Complex deposits, the Cape Mamontov Klyk area, the third terrace of the Lena River Delta, and the Buor Khaya Peninsula (Figure 1-4). These areas are part of the coastal lowlands of the Laptev Sea that are framed by small mountain ridges of 200 to 500 m height to the south, the Pronchishchev Ridge, the Chekanovsky Ridge, and the Kharaulakh Range. The region is situated in the continuous permafrost zone (Figure 1-1) with permafrost depths between 200 and 700 m and mean annual ground temperatures between -9 and -11 °C (Yershov, 2004). The active layer thickness reaches 20 to 60 cm in July-August. The permafrost aggradation over large areas of the coastal plain and the arctic shelf, which was exposed during the regression of the sea in the late Pleistocene, was facilitated by a strongly continental climate that has persisted for several thousand years and prevented glaciation at least since the late Saalian (Hubberten et al., 2004; Svendsen et al., 2004). In the study areas, Ice Complex deposits of up to several tens of meters thickness accumulated during the late Pleistocene (Schirrmeister et al., 2003, 2008, 2011c; Schwamborn et al., 2002b; Wetterich et al., 2008, 2011) (Figure 1-2). In the Lena River Delta, they were eroded to small remnants by

fluvial and deltaic activity during the Holocene and now form the third geomorphological main terrace of the Lena Delta (Grigoriev, 1993; Schwamborn et al., 2002b; Schirrmeister et al., 2011a). During the Holocene transgression, the coastline moved hundreds of kilometers to the south before it reached its present position about 5 cal. ka BP (Bauch et al., 2001).

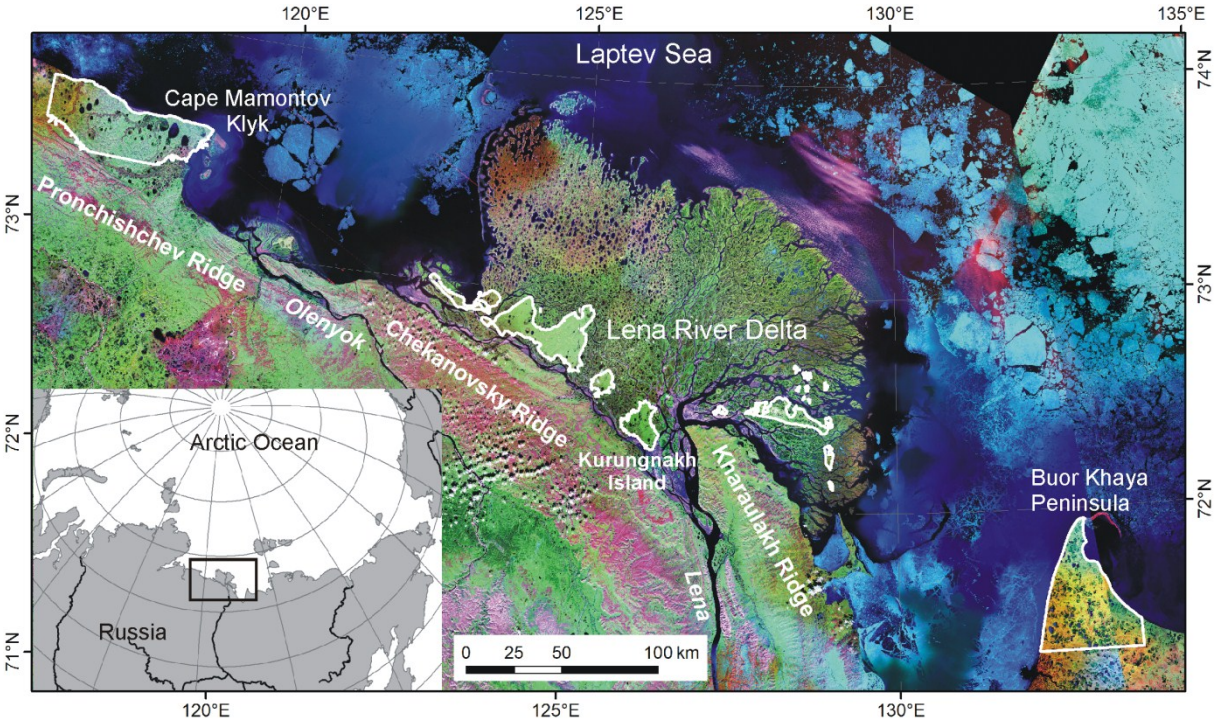

Figure 1-4. Location of the study areas (white outlines).

The Laptev Sea region belongs to the Arctic Rift Zone that is characterized by vertical block tectonics with a high modern seismic activity (Grigoriev et al., 1996; Drachev et al., 1998; Franke et al., 2000). Tectonic movements of significant amplitudes are reported for the Holocene (Galabala, 1987).

The present arctic continental climate is characterized by long severe winters with mean January temperatures between -36 and -32 °C and short cold summers with mean July temperatures between 4 and 8 °C (Treshnikov, 1985). Mean annual precipitation rates are only between 200 and 400 mm. The study region belongs to the arctic tundra zone with vegetation dominated by sedges, mosses, and dwarf shrubs (CAVM team, 2003).

1.4 Thesis outline

This thesis is composed of five chapters, including an introduction, three main chapters, and a synthesis. The main chapters are original research papers that have been published or prepared for publication in international peer-reviewed journals (Table 1-1).

Table 1-1. Overview of publications presented within this thesis.

Publication	Chapter
Morgenstern, A., Grosse, G., Günther, F., Fedorova, I., Schirrmeister, L., 2011. Spatial analyses of thermokarst lakes and basins in Yedoma landscapes of the Lena Delta. The Cryosphere 5, 849-867, doi:10.5194/tc-5-849-2011.	Chapter 2
Morgenstern, A., Ulrich, M., Günther, F., Roessler, S., Fedorova, I. V., Rudaya, N. A., Wetterich, S., Boike, J., Schirrmeister, L., 2012b. Evolution of thermokarst in East-Siberian ice-rich permafrost: A case study. Geomorphology, under review.	Chapter 3
Morgenstern, A., Grosse, G., Arcos, D. R., Günther, F., Overduin, P. P., Schirrmeister, L., 2012a. The role of thermal erosion in the degradation of Siberian ice-rich permafrost. In preparation for Journal of Geophysical Research – Earth Surface.	Chapter 4

Chapter 2 investigates different stages of thermokarst lakes and basins in Ice Complex deposits of the Lena River Delta, their impact on and their future potential for the degradation of ice-rich permafrost (Morgenstern et al., 2011). Chapter 3 reconstructs the evolution of an individual alas on Kurungnakh Island, Lena Delta (Morgenstern et al., 2012b). Chapter 4 provides an inventory of thermo-erosional landforms in three lowland areas adjacent to the Laptev Sea (Morgenstern et al., 2012a). Chapter 5 gives a synthesis of the results presented in all three papers of the thesis. It also highlights the accomplished scientific advances and offers avenues for future research.

Due to the given structure of the three individual papers, overlapping sections and repetition of general information is partly unavoidable within the thesis.

1.5 Authors' contributions

As a result of the multidisciplinary character of the investigations, several co-authors contributed to the three papers with their specific expertise (Table 1-1). As first author, A. Morgenstern designed the studies, reviewed the relevant literature, contributed to the data collection, conducted all analyses and interpretation of the data unless otherwise stated, wrote and coordinated the publications, and created most of the figures.

Further contributions to the papers presented in the three main chapters are as follows and include the results of the diploma theses of F. Günther and S. Roessler that were supervised by A. Morgenstern:

Chapter 2: A. Morgenstern performed the entire mapping of the data, their morphometric and statistical analyses and interpretation. F. Günther constructed the ALOS PRISM DEM and contributed to the DEM analyses. I. Fedorova jointly with A. Morgenstern conducted the bathymetric measurements of the lakes on Kurungnakh Island and their analyses. L. Schirrmeister and G. Grosse provided guidance and help throughout the study and valuable reviews at various stages of the manuscript.

Chapter 3: A. Morgenstern conducted the field work and data acquisition together with M. Ulrich, F. Günther, S. Roessler, I. Fedorova, and J. Boike. A. Morgenstern and M. Ulrich conducted lab analyses of the sediment samples. M. Ulrich and F. Günther constructed the Alas DEM, F. Günther processed the ALOS PRISM data and derived the PRISM DEM. S. Roessler performed the multispectral classification of the ALOS AVNIR-2 data. N. Rudaya and S. Wetterich performed the bioindicator analyses and interpretation. A. Morgenstern performed the entire GIS analysis and integrated all data and their interpretation. All co-authors critically reviewed and discussed interpretation and earlier versions of the manuscript, M. Ulrich and S. Wetterich contributed to some of the figures. L. Schirrmeister helped in designing the study and developing subsequent ideas and provided guidance throughout the whole process.

Chapter 4: A. Morgenstern, G. Grosse, D. Arcos, and F. Günther contributed to the GIS mapping, A. Morgenstern performed all subsequent GIS analyses. A. Morgenstern, G. Grosse, F. Günther, P. Overduin, and L. Schirrmeister participated in the field observations and critically reviewed and discussed interpretation and earlier versions of the manuscript. L. Schirrmeister, G. Grosse, and P. Overduin provided guidance and help throughout the study.

2 Spatial analyses of thermokarst lakes and basins in Yedoma landscapes of the Lena Delta

A. Morgenstern[1], G. Grosse[2], F. Günther[1], I. Fedorova[3], L. Schirrmeister[1]

[1] Alfred Wegener Institute for Polar and Marine Research, Research Unit Potsdam, Potsdam, Germany
[2] Geophysical Institute, University of Alaska Fairbanks, Fairbanks, USA
[3] Arctic and Antarctic Research Institute, Otto Schmidt Laboratory for Polar and Marine Research, St. Petersburg, Russia

The Cryosphere 5, 849-867, 2011, doi:10.5194/tc-5-849-2011.

2.1 Abstract

Distinctive periglacial landscapes have formed in late-Pleistocene ice-rich permafrost deposits (Ice Complex) of northern Yakutia, Siberia. Thermokarst lakes and thermokarst basins alternate with ice-rich Yedoma uplands. We investigate different thermokarst stages in Ice Complex deposits of the Lena River Delta using remote sensing and geoinformation techniques. The morphometry and spatial distribution of thermokarst lakes on Yedoma uplands, thermokarst lakes in basins, and thermokarst basins are analyzed, and possible dependence upon relief position and cryolithological context is considered. Of these thermokarst stages, developing thermokarst lakes on Yedoma uplands alter ice-rich permafrost the most, but occupy only 2.2 % of the study area compared to 20.0 % occupied by thermokarst basins. The future potential for developing large areas of thermokarst on Yedoma uplands is limited due to shrinking distances to degradational features and delta channels that foster lake drainage. Further thermokarst development in existing basins is restricted to underlying deposits that have already undergone thaw, compaction, and old carbon mobilization, and to deposits formed after initial lake drainage. Future thermokarst lake expansion is similarly limited in most of Siberia's Yedoma regions covering about 10^6 km², which has to be considered for water, energy, and carbon balances under warming climate scenarios.

2.2 Introduction

Climate warming in most northern high-latitude permafrost regions (ACIA, 2004) has resulted in widespread warming of permafrost, and also, in some cases, permafrost degradation during the last few decades (Romanovsky et al., 2010). Thawing of permafrost soils and sediments is often accompanied by the release of old organic carbon (Anisimov and

Reneva, 2006; Zimov et al., 2006b; Schuur et al., 2008; Grosse et al., 2011) and changes in water and land surface energy balances (Osterkamp et al., 2009), which may influence atmospheric processes via feedback mechanisms (Chapin et al., 2005; Walter et al., 2006; Schuur et al., 2009).

Thermokarst is one of the most obvious forms of permafrost degradation in arctic landscapes. Thermokarst is defined as the process by which characteristic landforms result from the thawing of ice-rich permafrost or the melting of massive ice (van Everdingen, 2005). During a phase of global warming about ten to twelve thousand years ago, thermokarst affected large areas in arctic lowlands with ice-rich permafrost (Romanovskii et al., 2000; Walter et al., 2007). In the late Pleistocene, such ice-rich deposits (Ice Complex) of the Yedoma Suite were deposited in northern Siberia (Sher et al., 1987; Schirrmeister et al., 2011c). Today, thermokarst lakes and basins alternate with ice-rich Yedoma uplands in this region. Thermokarst has important effects on the ecology, geomorphology, hydrology, and local climate of affected landscapes (Osterkamp et al., 2000; Grosse et al., 2011). Various recent studies have investigated thermokarst lakes as sources of carbon release to the atmosphere (Zimov et al., 1997; Walter et al., 2006, 2007; Schuur et al., 2009; Zona et al., 2009; Karlsson et al., 2010) or as indicators of a changing water balance in permafrost regions by analyzing changes in lake area using remote-sensing methods (Payette et al., 2004; Smith et al., 2005; Riordan et al., 2006; Kravtsova and Bystrova, 2009). The highest methane emissions from arctic lakes are reported for lakes in Yedoma or Yedoma-like sediments (Walter et al., 2006). Drained thermokarst lake basins have been investigated on a broad scale using satellite remote sensing on the North Slope of Alaska (Frohn et al., 2005).

The classical works of Soloviev (1959, 1962) and Czudek and Demek (1970) describe the development of thermokarst in Ice Complex deposits in Central Yakutia (Siberia). In this region with a continental climate, thermokarst starts to develop under subaerial conditions. Only after initial ground subsidence does water accumulate in the evolving thermokarst basins that are termed “alasses” at a more developed stage. In the wet polygonal tundra of the north Siberian lowlands, evolving thermokarst in ice-rich deposits is represented by ponds and circular lakes that completely fill their basins. As these thermokarst lakes grow, they eventually coalesce with neighboring lakes or drain partially or completely. The remaining basins feature steep slopes, flat bottoms, and smaller remnant thermokarst lakes. Repeated cycles of permafrost degradation under thermokarst lakes and subsequent permafrost aggradation after full or partial lake drainage can lead to multiple cycles of secondary thermokarst within basins accompanied by modifications of initial basin-and-lake morphometry and the growth of hydrostatic pingos in the basin (Katasonov, 1960;

Romanovskii, 1961; Soloviev, 1962). Recent studies of modern thermokarst activity in Yedoma landscapes have focused on thermokarst lakes by detecting broad-scale changes in thermokarst lake area (e.g., Kravtsova and Bystrova, 2009). However, thus far they have not distinguished between thermokarst lakes on Yedoma uplands and thermokarst lakes in basins of older-generation thermokarst, and have not addressed these complex thermokarst basins. A broad review of hydrogeomorphological aspects of thermokarst lakes, drainage, and drained lake basins is provided by Grosse et al. (2012).

To estimate future carbon release from Yedoma areas due to thermokarst it is necessary to assess the impact of thermokarst processes on the evolution of permafrost landscapes under climate scenarios that predict significant Arctic warming. In this study we provide a basis for quantifying potential thermokarst evolution in Siberian ice-rich permafrost by answering the question of where and to what extent thermokarst may develop in the study area, an area which comprises the third Lena River Delta terrace with its Ice Complex deposits. The specific objectives are: 1) to assess different stages in lake and basin development based on remote sensing and geoinformation techniques, 2) to analyze the spatial distribution of these lakes and basins, and elucidate any effects of relief position and cryolithological context, and 3) to deduce the potential extent of future thermokarst evolution in the study area.

2.3 Study area and regional setting

The north Siberian Lena River Delta (73°N; 126°E) is situated in the continuous permafrost and tundra zone. It features Ice Complex deposits on insular remnants of a late-Pleistocene accumulation plain in the foreland of the Chekanovsky and Kharaulakh ridges, which now form the third Lena Delta terrace (Grigoriev, 1993) (Figure 2-1). These insular remnants of Ice Complex deposits will be termed islands in the following and named after the delta island they belong to. The stratigraphical composition of the third terrace can be divided into two late-Pleistocene main units and a Holocene unit (Schwamborn et al., 2002b; Schirrmeister et al., 2003, 2011a; Wetterich et al., 2008) (Figure 2-2). The lowest unit consists of fluvial, interbedded medium-to-fine-grained and silty sands deposited by a meandering paleo-Lena River during the early Weichselian period (between 100 and 50 ka). In some lower parts the sands include plant remains and alternate with peaty layers. The cryostructure of the sandy section is mostly massive with some small ice wedges. Gravimetric ice content is between 20 and 40 wt% and total organic carbon (TOC) content is between 1.0 and 5.4 wt%. The upper Pleistocene unit is formed by polygenetic Ice Complex deposits that accumulated during the

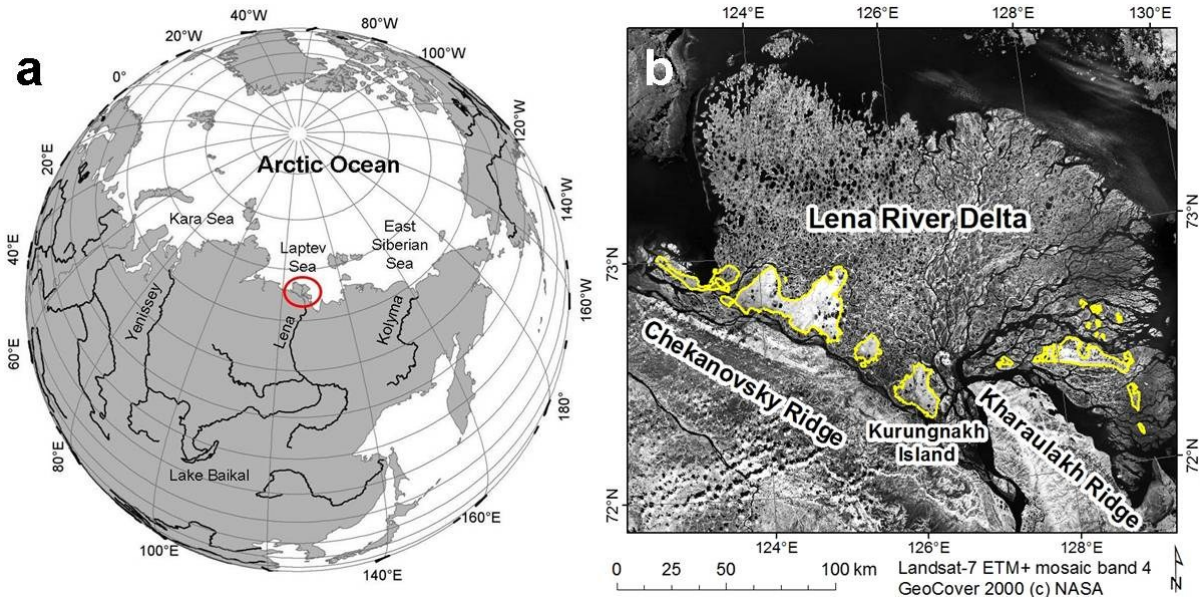

Figure 2-1. Location of the study area in the Lena River Delta, North Siberia.

Figure 2-2. Typical stratigraphical composition of the study area with lower fluvial sand unit, upper Ice Complex unit, and Holocene cover. Ice wedges in the Ice Complex appear in light grey colors. Person for scale (Photo by M. Ulrich, 26 Aug 2008).

middle and late Weichselian (between 44.5 and 17 ka). It consists of peat, silty sand, and peaty paleosoil layers with a high gravimetric ice content (38 to 133 wt%). The ground ice occurs as segregated ice in the form of ice bands, veins, and small ice lenses. Very large syngenetic ice wedges can be several meters wide and up to 20 m tall. TOC content exhibits a wide range in Ice Complex deposits (1.1 to 32.5 wt%). The vertical position of the sharp boundary between the lower and upper units varies within the study area by up to several tens of meters, likely due to neotectonic block movements affecting the Lena Delta

(Schwamborn et al., 2002b). In the western Lena Delta this boundary is found in the height range of 15-25 m above river level (a. r. l.), whereas in the eastern Lena Delta the boundary is located below the river level (Grigoriev, 1993). The Holocene unit is represented by deposits covering the Ice Complex and deposits of thermokarst depressions. Deposits of the Holocene cover exposed on top of the Ice Complex unit consist of brownish-black, cryoturbated silty sand with numerous small peat inclusions and are characterized by smaller ice wedges. Deposits of thermokarst depressions are composed of cryoturbated silty sands, numerous plant remains, and peat inclusions, and contain syngenetic ice wedges about 3 to 5 m wide (Schirrmeister et al., 2003).

The modern outlines and surface patterns of the third terrace are the result of ca. 12,000 years of permafrost degradation and of deltaic processes that have been ongoing since the mid-Holocene (Schwamborn et al., 2002b). Thermokarst processes have greatly influenced the landscapes in this region since the Bølling-Allerød and during the early Holocene (Kaplina and Lozhkin, 1979; Romanovskii et al., 2000; Kaplina, 2009). Thermokarst lakes and basins are depressed into the flat Yedoma uplands of the study area. Individual and sometimes networked thermo-erosional channels drain the islands. Thermal erosion is fostered by high ice contents in the Yedoma and the high relief gradient of the third terrace; these small islands (a few tens of kilometers in diameter) are strongly dissected by delta channels and reach elevations of more than 60 m above the adjacent river level. Yedoma uplands are characterized by polygonal microrelief with small ponds. Thermokarst lakes can reach diameters of several kilometers. If their water table is below the surrounding Yedoma surface, their rims are often dissected by small thermo-erosional gullies (Figure 2-3). Basin diameters range from several hundreds of meters for single forms to tens of kilometers for coalesced forms. Basin floors are mainly flat with ice-wedge polygons, polygon ponds, and thermokarst lakes that are mostly remnants of the initial large thermokarst lake that formed the basin. Pingos have formed in some of the basins, with heights up to 30 m above the basin surface and diameters of up to 150 m (Grigoriev, 1993).

Within the study area, Kurungnakh Island (72° 23'N; 126° 03'E) (Figure 2-1) serves as a key site for more detailed investigations. This island is the easternmost part of the tectonically uplifted western delta and has elevations of up to 55 m above sea level (a. s. l.).

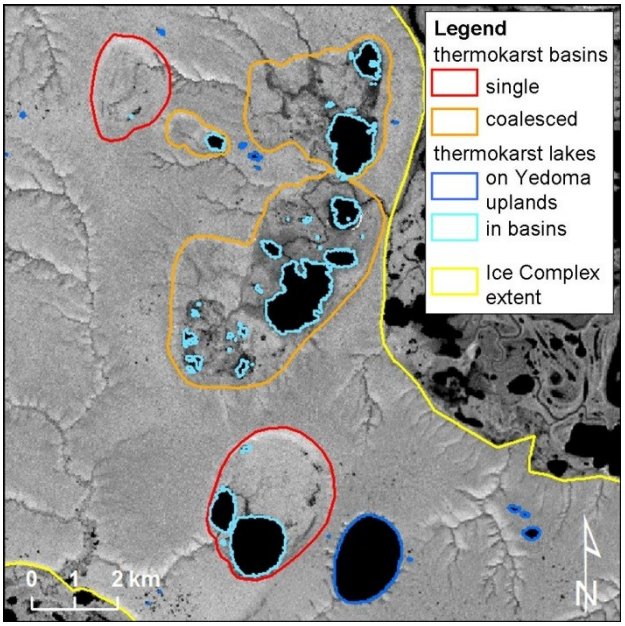

Figure 2-3. Types of thermokarst features distinguished in this study.

2.4 Data and methods

2.4.1 Remote-sensing data and processing

A Landsat-7 ETM+ image mosaic of the Lena River Delta (Schneider et al., 2009) served as the basis for mapping the thermokarst lakes and basins within the extent of the Lena Delta Ice Complex. We defined this extent as all areas of the third geomorphological main terrace, excluding the bedrock outcrops of the Sardakh and Amerika-Khaya islands. We also excluded lakes and basins at the boundary of the Ice Complex whose original morphology has been directly influenced by fluvial-deltaic action. The manual mapping was done using a desktop Geographical Information System (GIS). The resulting vector layer was then modified using our own field knowledge and expert advice given by M. N. Grigoriev (personal communication, 2009).

The Landsat scenes covering the Ice Complex extent show a medium water level situation in summer (26 July 2001 in the western part, 27 July 2000 in the central and eastern part). An Ice Complex area of about 140 km² affected by cloud cover was replaced by a subset of a Landsat scene from 5 August 2000 (path 130, row 9).

To extract all water bodies automatically, we applied a grey-level thresholding on band 5 of the Landsat data using the image processing software ENVI™ 4.6. In these mid-infrared wavelengths water bodies are strong absorbers, easily distinguishable from other land cover types (Morgenstern et al., 2008a). All pixels with top-of-atmosphere reflectance values of 0 to 0.1 were defined as water. We manually removed all water pixels related to drainage

channels, small streams, and river delta channels. The resulting data set was converted into vector polygons. Subsequent data processing and analyses were performed using the GIS software package ArcGIS™ 9.3 and its spatial data analysis toolbox. In the following all extracted water bodies are referred to as lakes for reasons of readability even though smaller water bodies are actually ponds.

Basins were manually digitized along their upper margins at the scale of 1:30,000. The transition between Yedoma surface and basin slopes is visually clearly distinguishable in the Landsat data due to better drainage of slopes. Each basin was assigned to one of two categories: *single* basins are distinct basins formed by local thermokarst activity, whereas *coalesced* basins consist of at least two basins that have merged due to lateral lake expansion in the past. Basins that are located adjacent to each other and connected via narrow drainage channels but have retained their original morphometry were treated as separate features; each was assigned to the category *single*. Each lake was assigned a location attribute that had the value *on Yedoma uplands* or *in basin* (Figure 2-3).

Mapping of all features was performed in the Universal Transverse Mercator (UTM) projection Zone 52N with the geodetic datum WGS 1984 because this was the original projection of the Landsat mosaic. The study area has a large E-W extent of about 250 km and covers the 51N and 52N UTM zones. The UTM meridian is situated in the center of the Lena Delta and crosses Kurungnakh Island. To minimize distortion effects on morphometric calculations the data sets were separated along the UTM meridian into a western and an eastern part. The western part was re-projected to its original UTM Zone 51N. Kurungnakh Island and affiliated data sets were assigned completely to Zone 52N, because the larger areal percentage belongs to this zone.

2.4.2 Morphometric analyses

For all lakes and basins, morphometric variables including *area*, *perimeter*, *circularity index*, *elongation index*, *orientation of major axis*, and the coordinates of centroids were calculated (Table 2-1). The *circularity index* is a measure of how strongly an object's shape deviates from a perfect circle. Values approaching 0 indicate that an object has a) an irregular or complex outline, b) includes islands, or c) is very elongated. A square has a value of 0.785. The calculations of the *elongation index* (major axis/minor axis) and *orientation of major axis* refer to the axes of a best-approximated ellipse with an area equal to that of the object being analyzed.

Table 2-1. Overview of morphometric variables calculated for lakes and basins. Major and minor axes lengths and orientation of major axis for lakes are not shown here, but were calculated the same way as for basins.

illustration	variable	calculation	possible value range
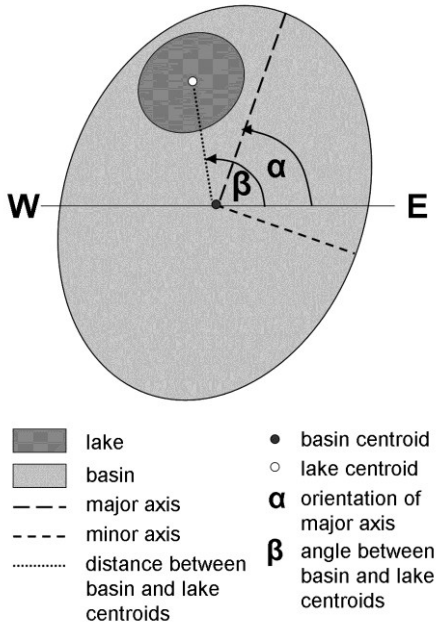	*area*	GIS output	[0; ∞] m²
	perimeter	GIS output	[0; ∞] m
	circularity index	= 4 x π x *area* / *perimeter*²	[0; 1] , 1 = perfect circle
	elongation index	= major axis length / minor axis length	[1; ∞], 1 = equal axes
	orientation of major axis (α)	angle between E-W reference axis and major axis (counter-clockwise)	[0;179.9] °
	normalized centroid distance	= distance between basin and lake centroids / major basin axis length	[0; 1]
	angle between basin and lake centroids (β)	angle between E-W reference axis and the distance between basin and lake centroids (counter-clockwise)	[0;359.9] °

Because the lakes were extracted from raster data and vectorized without smoothing, the 30 m x 30 m spatial resolution of the Landsat data has to be taken into account for morphometric analyses. Star and Estes (1990) recommend using a conservative raster cell size, one sixteenth the size of the minimum mapping unit. Therefore, we set the minimum lake size for analyses of the shape metrics *circularity index*, *elongation index,* and *orientation of main axis* to be 14,400 m² (16 times 30 m x 30 m). The pixel-based outline of the lakes has a strong effect on the *circularity index* because it is based on *area* and *perimeter*. An object with a smooth outline will have a shorter perimeter than an object of the same area with a complex outline. In consequence, the pixel-based lake circularity cannot reach the value of 1 for a perfect circle and will always have lower values than digitized basins of the same shape. Thus, comparisons of *circularity index* between subpopulations of the data set are only legitimate among lakes, but not between lakes and basins, as the basins were manually digitized. The *elongation index* is therefore used as an additional measure and should give meaningful results because visual estimations of the basins (especially in the category *single*) reveal that they generally do not have complex outlines.

For each basin we determined the number of lakes per basin, the sum of lake area, and the percentage of lake area. The distance between basin centroid and lake centroid and the angle formed by moving counter-clockwise from the E-W reference axis to the line between

the centroids were calculated to assess the position of lakes within single basins (Table 2-1). Centroid distances were normalized by dividing the distance by the length of the major basin axis to allow comparison between basins of different sizes. In addition, pingos were mapped as point objects on the basis of Landsat and Corona satellite data and topographic maps. Distances and angles between pingos and basin centroids were calculated in the same way as for lakes in basins.

Statistical analyses of the resulting dataset were performed using the SPSS™ 16.0 software. An explorative data analysis (EDA) and the *Kolmogorov-Smirnov test* revealed non-normal distribution for all variables. Therefore, we used non-parametric tests for subsequent analyses. In order to test for morphometric differences between the subgroups *lakes on Yedoma uplands* versus *lakes in basins* and *lakes on Yedoma uplands* versus *single basins*, we applied the rank-based *Mann-Whitney-U test*.

2.4.3 Relief analyses on Kurungnakh Island

For Kurungnakh Island, a high-resolution Digital Elevation Model (DEM) based on an ALOS PRISM satellite image stereo triplet (acquisition date 21 September 2006) was available (Günther, 2009). The DEM has a horizontal resolution of 5 m and a vertical accuracy of 5.8 m. For the rest of the study area, elevation information was derived from digitized 1:200,000 topographic maps. The spatial resolution of these maps is too coarse to extract terrain information in the detail needed for analyzing the thermokarst relief of the whole Lena Delta Ice Complex.

We used the high-resolution DEM to analyze the relief position of thermokarst features and, in particular, their position in relation to the two sedimentary units. According to Schirrmeister et al. (2003) and Wetterich et al. (2008) we assume that the average boundary between Ice Complex deposits and underlying fluvial sands lies between 15 and 20 m a. r. l. For calculation purposes in the GIS we set the height of the boundary to 17 m a. s. l. All lakes and basins whose floors are partially or completely below the 17 m contour line are considered to have their base in the fluvial sands of the lower stratigraphical unit.

Detailed field observations in combination with DEM analyses in eastern Kurungnakh Island revealed that in areas with a negligible slope of 0 to 2° ice-wedge polygons occur, whereas in areas with slope ≥ 2° usually no polygons exist, but hummocks are prevalent. We also interpret this threshold as the relief condition for thermokarst initiation, i.e. at slopes ≥ 2° better drainage would prevent water accumulation and restrict lake formation. To calculate the area prone to potential new thermokarst lake development within the limits of the remaining Ice Complex on Kurungnakh Island, and assuming that new lakes would

predominantly form on poorly drained, flat Yedoma upland surfaces, we subtracted all areas with a slope of ≥ 2° and existing thermokarst lakes and basins from the area above the 17 m reference plane. The resulting binary raster was target-oriented filtered using a combination of the morphological Erode and Dilate filters of ENVI^{TM} 4.8 with a kernel size of 5 x 5 to correct for the influence of the systematic undulating surfaces of the DEM, which occurred mainly on the flat Yedoma uplands.

During a field campaign in summer 2008, the relief characteristics and lake bathymetries were investigated in detail in one thermokarst basin with three large lakes located in the south of Kurungnakh Island (Morgenstern et al., 2008b; Ulrich et al., 2010).

2.5 Results

2.5.1 Area calculations and morphometric characteristics

The study area, i.e. the mapped Ice Complex, covers an area of 1,688.1 km², which is 5.8 % of the Lena Delta area (29,000 km²) and 98.6 % of the third terrace area (1,711.6 km²); the remaining areas consist of exposed bedrock (Morgenstern et al., 2008a). We detected 2,327 water bodies (minimum one pixel, 900 m²) with a total area of 88.3 km² within the study area (Table 2-2). Thus, at a 30 m pixel resolution 5.2 % of the Ice Complex extent is covered with open water. Of the total water body population, 1,509 water bodies are situated on Yedoma uplands and 818 are in basins. Even though they are much more abundant, lakes on Yedoma uplands cover a smaller total area than lakes in basins (37.4 and 50.9 km², respectively). Figure 2-4 shows the study area with all thermokarst lakes and basins mapped.

Table 2-2. Area calculations for water bodies on the third Lena Delta terrace (except bedrock islands).

	All lakes minimum one pixel (900 m^2)	Lakes on Yedoma uplands	Lakes in basins	All lakes ≥ 14,400 m²
N	2,327	1,509	818	514
Area (km²)	88.3	37.4	50.9	82.8
Percentage of study area	5.2	2.2	3.0	4.9

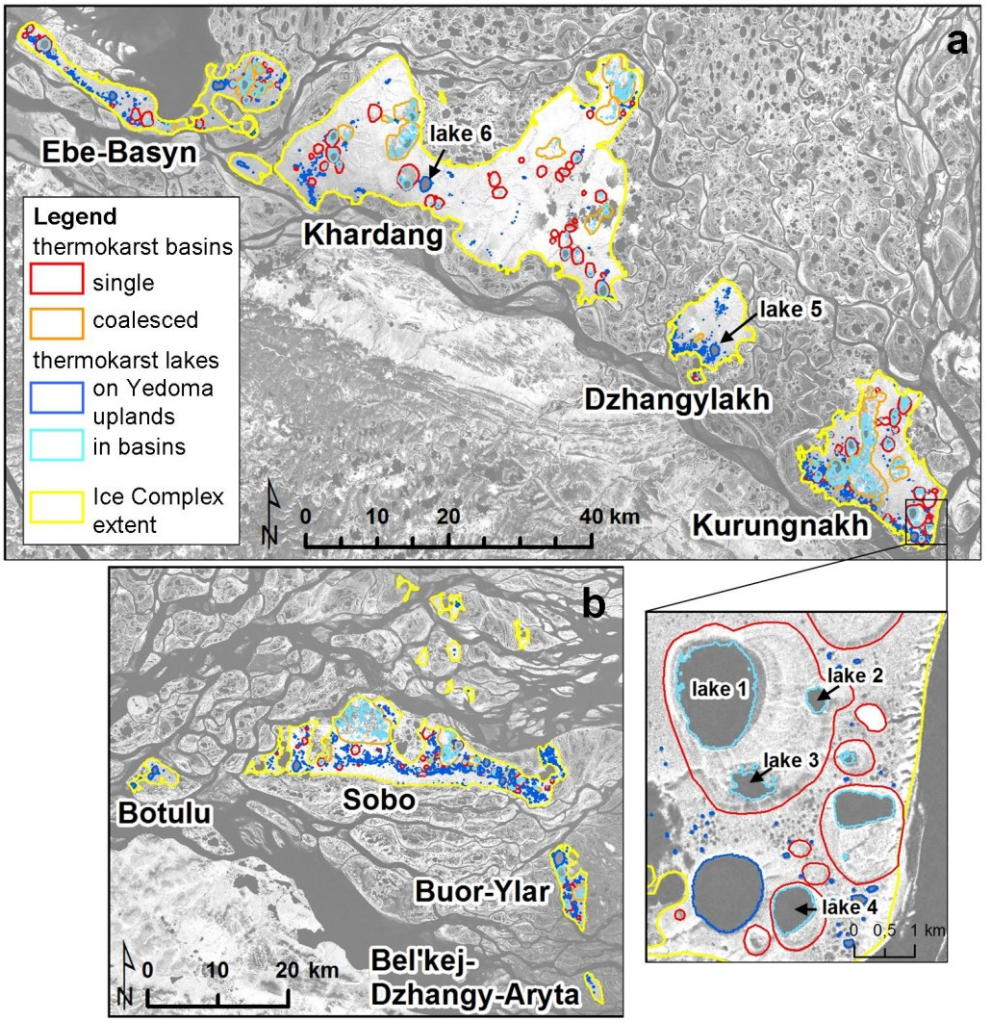

Figure 2-4. Overview of study area with all thermokarst features investigated: a) western part, b) eastern part. Landsat-7 ETM+ mosaic, band 4, GeoCover 2000 © NASA.

Thermokarst basins cover a total area of 337.7 km² or 20.0 % of the study area (Table 2-3). Of the 169 basins mapped, the majority (n = 144) was categorized as *single. Single* basins cover a much smaller areal extent, but show a higher lake area percentage than do *coalesced* basins (20.2 % and 11.7 %, respectively). Finally, 22.2 % of the study area is affected by thermokarst. Lakes on Yedoma uplands account for a much lower proportion of total area than do thermokarst basins (2.2 % and 20.0 %, respectively).

Table 2-3. Area calculations for thermokarst basins on the third Lena Delta terrace (except bedrock islands).

	All basins	Single basins	Coalesced basins
N	169	144	25
Area (km²)	337.7	133.0	204.7
Percentage of study area	20.0	7.9	12.1
Total lake number	818	263	555
Sum of lake area (km²)	50.9	26.9	24.0
Total lake area as a percentage of total basin area	15.1	20.2	11.7

Frequency distributions of *area* values for all water bodies in the study area show strong skewness towards lower values, because small water bodies are much more abundant than large lakes (Figure 2-5). However, lakes ≥ 14,400 m² that are considered for morphometric analyses still cover 93.8 % of the whole lake area, because even though their number is small (514 versus 2,327 for the whole water body population) they account for most of the lake area. This is consistent with the specific patterns of the relationship between lake surface area and areal frequencies found in various Ice Complex regions (Grosse et al., 2008) or in more general patterns throughout other environments (Downing et al., 2006).

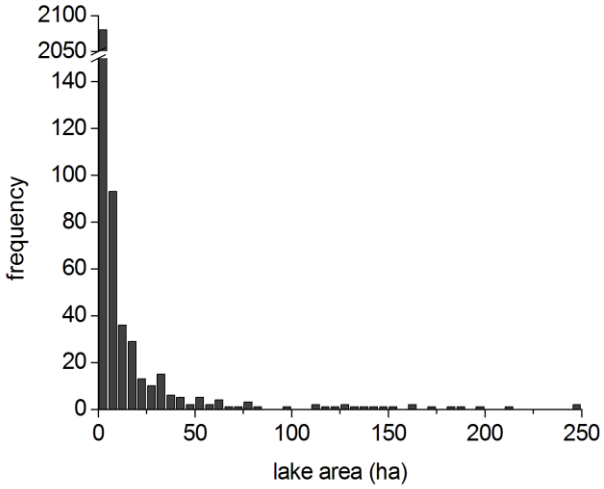

Figure 2-5. Histogram of area of all water bodies in the study area (1 ha = 10,000 m²).

Lakes on Yedoma uplands (n = 296) differ significantly from lakes in basins (n = 218) in their morphometric characteristics except for the *elongation index* (Table 2-4). Lakes on Yedoma uplands are, on average, smaller than lakes in basins (median = 35,000 m² and 67,900 m², respectively) and have a smoother shoreline (Table 2-5). Frequency distributions of lake orientation on Yedoma uplands show a major peak in the WNW direction and a minor peak in the NNE direction (Figure 2-6). Lakes in basins show a slightly different picture with a more pronounced NNE direction, but also two peaks directed to the WNW and NW.

Table 2-4. Results of the rank-based *Mann-Whitney-U test* for morphometric differences between *lakes on Yedoma uplands* and *lakes in basins*. Significant differences between the two lake subgroups were found for *area*, *circularity index*, and *orientation of major axis*.

	Area	*Circularity index*	*Elongation index*	*Orientation of major axis*
Mann-Whitney-U	23,916	23,654	31,059	26,657
Z	-5.017	-5.176	-.724	-3.369
Asymptotic significance (two-sided)	**.000**	**.000**	.469	**.001**

Table 2-5. Comparison of morphometric characteristics of thermokarst lakes ≥ 14,400 m² and single basins. Area values for all lakes including lakes < 14,400 m² are shown in brackets.

	Lakes on Yedoma uplands		Lakes in basins		Single basins
N	296	(1509)	218	(818)	144
Area					
Total (km²)	33.7	(37.4)	49.1	(50.9)	133.0
Median (m²)	35,000	(2,700)	67,900	(2,700)	362,300
Interquartile range (m²)	65,800	(8,100)	210,300	(16,200)	1,096,200
Minimum (m²)	14,400	(900)	14,600	(900)	20,400
Maximum (m²)	2,482,200	(2,482,200)	2,112,300	(2,112,300)	7,706,600
Circularity index					
Median	0.48		0.41		0.93
Interquartile range	0.17		0.21		0.05
Minimum	0.12		0.07		0.74
Maximum	0.70		0.70		0.98
Elongation index					
Median	1.55		1.58		1.29
Interquartile range	0.60		0.82		0.24
Minimum	1.03		1.04		1.02
Maximum	6.19		8.07		2.02
Outlines	smooth shorelines		more complicated shorelines		smooth, circular outlines
Main orientation	WNW		NNE		NNE
Depth	10 m and more		up to 4 m		up to 35 m

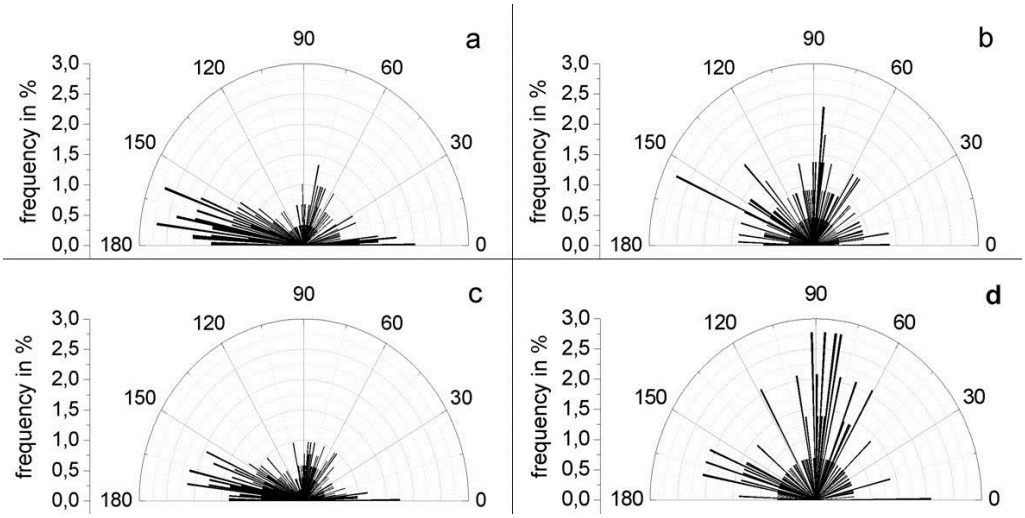

Figure 2-6. Frequency distribution of major axis orientation for a) lakes ≥ 14,400 m² on Yedoma uplands, b) lakes ≥ 14,400 m² in basins, c) all lakes ≥ 14,400 m², and d) single basins. Intervals = 1°, 0° = East, 90° = North, 180° = West.

Tests between lakes on Yedoma uplands (n = 296) and single basins (n = 144) reveal significant differences for all morphometric variables (Table 2-6). Lakes on Yedoma uplands are, on average, much smaller than single basins (by about one order of magnitude; the *area* median equals 35,000 m² and 362,300 m², respectively), and more elongated. Orientation shows the same major peaks for both groups, one in the NNE and one in the WNW direction,

but with differing frequencies (Figure 2-6). Lakes on Yedoma uplands have a much stronger prevailing orientation in the WNW direction; in contrast, single basins are more frequently oriented in the NNE direction. Table 2-5 shows a comparison of the morphometric characteristics between lakes on Yedoma uplands, lakes in basins, and single basins.

Table 2-6. Results of the rank-based *Mann-Whitney-U test* for morphometric differences between *lakes on Yedoma uplands* and *single basins*. Significant differences between the two subgroups were found for all three morphometric variables.

	Area	*Elongation index*	*Orientation of major axis*
Mann-Whitney-U	4,724	9,823	17,742
Z	-13.254	-9.180	-2.852
Asymptotic significance (two-sided)	**.000**	**.000**	**.004**

Frequency distributions of the major axis orientations for all lakes ≥ 14,400 m² show a major orientation peak in the WNW direction and a minor peak in the NNE direction (Figure 2-6). In a previous study, all lakes ≥ 200,000 m² on the third Lena Delta terrace were found to exhibit a major NNE orientation (Morgenstern et al., 2008a). A selected distribution of major axis orientations for lakes with areas between 14,400 m² and 200,000 m² (n = 425) shows a peak in the WNW direction. This indicates an approximately 90° difference between the major orientation of smaller (14,400 m² to 200,000 m²) and of larger (≥ 200,000 m²) lakes. The frequency distributions of the major axis orientation of single basins show a major peak in the NNE and a minor peak in the WNW direction, opposite the orientation of all lakes ≥ 14,400 m².

Basins have a low lake area percentage (median = 3.9 and 2.3, interquartile range = 19.0 and 22.1 for all basins and for single basins, respectively). Correlation between basin area and lake area percentage was found to be slightly positive ($r = .453$, $p \leq .01$ for all basins and $r = .212$, $p \leq .01$ for single basins). Lakes in basins are not regularly situated in basin centers, but are shifted towards basin margins, mostly in northern and southern directions (Figure 2-7).

Bathymetric data from six lakes in the study area suggest that lakes on Yedoma uplands are deeper than lakes in basins (Figure 2-8). Lakes 1, 2, and 3 are situated in a 30 m deep thermokarst basin. Maximum recorded depth is 3.6 m for lake 1, 4.2 m for lake 2, and 4.0 m for lake 3. Lake 4 is also located in a thermokarst basin, but it covers a large part of the basin floor. Its maximum recorded depth is 8.1 m. Lakes 5 and 6 are situated on Yedoma uplands and reach depths of 12.5 and 9.0 m, respectively (Pavlova and Dorozhkina, 2000).

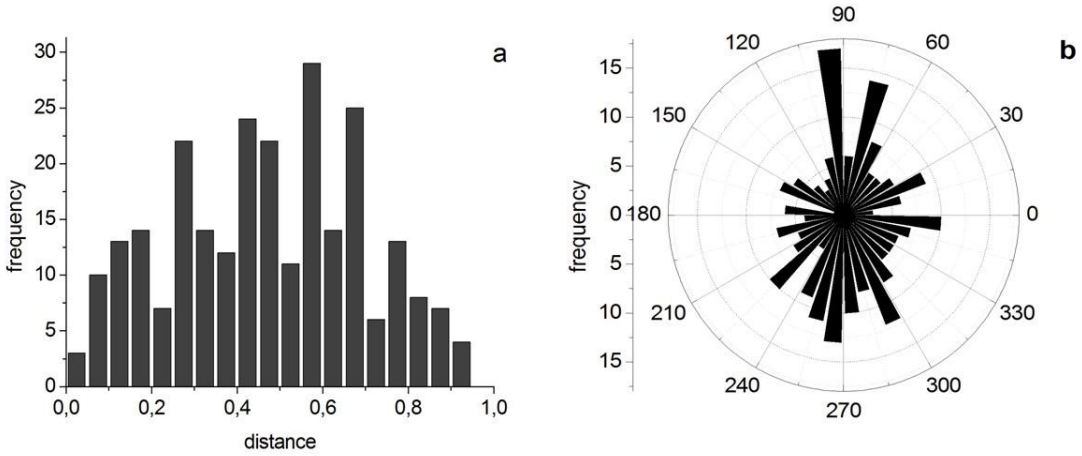

Figure 2-7. Position of lakes within single basins: a) frequency distribution of normalized distances between lake and basin centroids, b) frequency distribution of angles (in °) between basin and lake centroids. 0° = East, 90° = North, 180° = West, 270° = South.

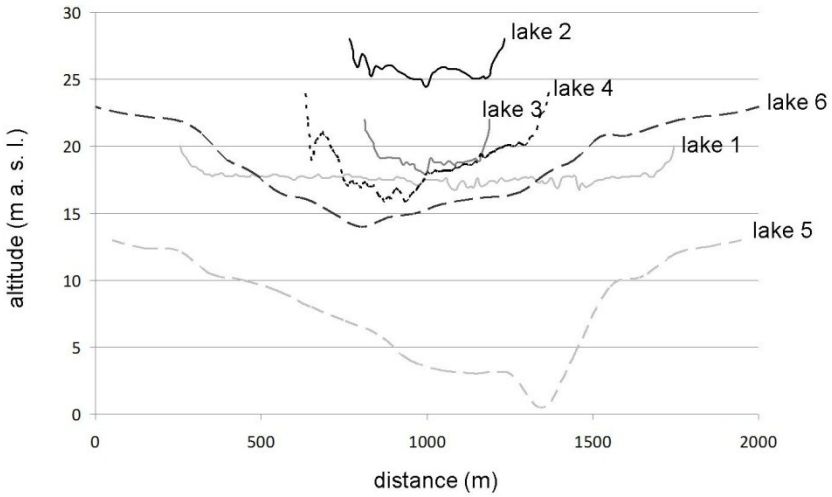

Figure 2-8. Bathymetric profiles of lakes in relation to relief position. For lake locations see Figure 2-4. Lake areas and profile directions are as follows: lake 1 = 1,841,400 m², from N to SE; lake 2 = 104,400 m², from N to S; lake 3 = 221,400 m², from N to S; lake 4 = 421,200 m², from N to S; lake 5 = 1,636,790 m², from NW to SE; lake 6 = 2,460,134 m², from N to S. Bathymetric data from lakes 5 and 6 from Pavlova and Dorozhkina (2000).

Table 2-7 compares the characteristics of permafrost relief, thermokarst lakes, and basins between major islands of the study area. Islands of the tectonically-uplifted western part of the study area show higher maximum relief heights, especially Khardang Island, which experienced separate block uplift (Grigoriev, 1993). Maximum Ice Complex thickness varies greatly between the islands, but shows similar ranges in the western and eastern parts of the study area. Maximum basin depths as inferred from topographic maps are lower in the eastern part, but do not seem proportional to maximum Ice Complex thickness. Khardang Island has a very low lake area percentage while featuring the largest basin sizes by far.

Table 2-7. Comparison of thermokarst features and permafrost characteristics between major islands of the study area.

		Ebe-Basyn	Khardang	Dzhangylakh	Kurungnakh	Botulu	Sobo	Buor-Ylar	Bel'kej-Dzhangy-Aryta
Island	Area (km²)	160.7	826.7	93.9	259.5	14.5	262.1	32.2	5.6
	Max. relief height (m a. s. l.) [a]	51	66	43	55	36	42	21	30
	Max. Ice Complex thickness (m) [b]	33	48	16	38	36 [c]	42 [c]	21 [c]	30 [c]
Lakes	N	205	375	227	549	14	841	92	11
	(N ≥ 14,400 m²)	(57)	(93)	(23)	(116)	(5)	(185)	(27)	(4)
	Area								
	Total (m²)	13,003,200	22,835,900	3,566,900	19,425,600	674,900	20,781,600	6,111,900	126,000
	Median (m²)	4,500	2,700	1,800	2,700	8,600	2,400	4,500	8,100
	Percentage of island area	8.1	2.8	3.8	7.5	4.7	7.9	19.0	2.3
Basins	N	25	46	5	44	0	42	7	0
	Area								
	Total (m²)	28,098,200	128,906,600	1,811,200	99,235,100	-	71,386,400	8,425,000	-
	Median (m²)	553,100	1,451,100	351,600	329,900	-	323,300	278,900	-
	Median of single basins (m²)	380,000	1,211,300	224,700	228,700		248,300	247,000	
	Percentage of island area	17.5	15.6	1.9	38.2	-	27.2	26.2	-
	Total lake area as a percentage of total basin area	26.3	13.7	7.3	16.0	-	10.7	27.0	-
	Median lake area percentage	13.4	1.7	3.7	2.3	-	4.2	3.8	-
	Max. depth (m) [a]	15	30	15	35	-	10	10	-
Lakes on Yedoma uplands and basins	Total area (m²)	33,725,400	134,137,200	5,246,700	102,766,700	674,900	84,509,600	12,266,200	126,000
	Percentage of island area	21.0	16.2	5.6	39.6	4.7	32.2	38.1	2.3

[a] Inferred from 1:200,000 topographical maps.

[b] Estimated from outcrop studies (Grigoriev, 1993) and maximum relief height.

[c] Values indicate the "visible" thickness above the river water level because the Ice Complex base is situated below the sea level here.

In the study area 34 pingos were mapped, the majority situated in coalesced thermokarst basins (24 versus ten in single basins). In single basins, pingos are situated at distances of several hundreds of meters from the basin centers (min = 224 m, max = 598 m; normalized distances: min = 0.24, max = 0.57), mostly in the NNE and SSW directions (Figure 2-9).

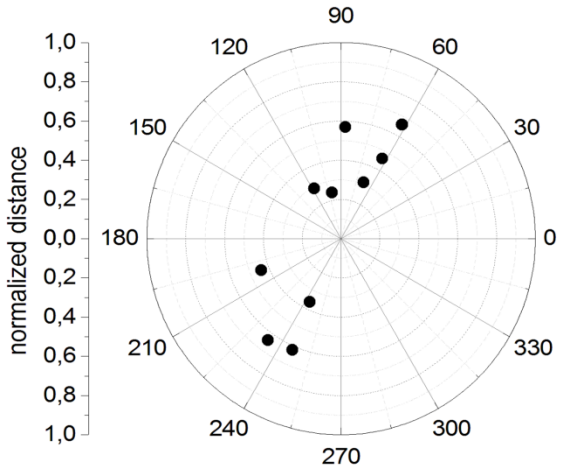

Figure 2-9. Position of pingos within single basins. Normalized distances and angles (in °) were calculated between basin centroids and pingos. 0° = East, 90° = North, 180° = West, 270° = South.

2.5.2 Relief analyses of Kurungnakh Island

The mapped extent of the key study area on Kurungnakh Island is 259.5 km². The total area of thermokarst (i.e., all thermokarst basins and lakes on Yedoma uplands) on Kurungnakh Island is 102.8 km², or 39.6 % of the key study area. Thermokarst lakes and basins that intersect or are situated below the 17 m isoline cover 71 % of the total thermokarst area. This amounts to 73 km², or 28.1 % of the Kurungnakh Island area (Figure 2-10). The surfaces of these thermokarst features (lake water level and basin bottoms) have subsided to the base of the Ice Complex deposits or lower. This areal calculation is very conservative because it does not take into account lakes and basins with surfaces above the 17 m contour line that should have formed taliks (bodies of unfrozen ground) that also reached the boundary between Ice Complex deposits and fluvial sands. This is illustrated in Figure 2-11, which shows a profile line derived from the ALOS PRISM DEM that is situated above 17 m a. s. l. while the lake floors reach the 17 m level.

Based on the ALOS PRISM DEM, the deposits above the 17 m reference plane approximately represent the remaining Ice Complex deposits; the volume of these deposits was calculated to be 2.9 km³. The TOC reservoir of this volume amounts to 70 Mt (= 0.07 Pg) as calculated following the method described in Strauss et al. (2012), and corresponds to an average organic carbon inventory of 24 kg C m^{-3}.

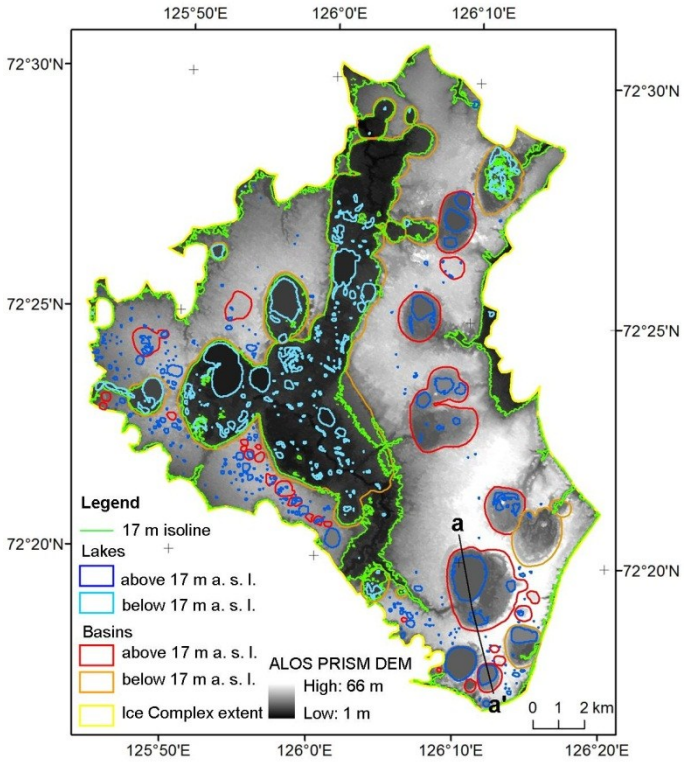

Figure 2-10. DEM of Kurungnakh Island indicating the position of thermokarst features above and below the Ice Complex boundary at 17 m a. s. l. Of the total Kurungnakh Island area, 28.1% is covered by features under which the Ice Complex deposits should have already completely degraded. The line between a and a' indicates a profile section across a Yedoma and thermokarst basin assemblage (see Figure 2-11).

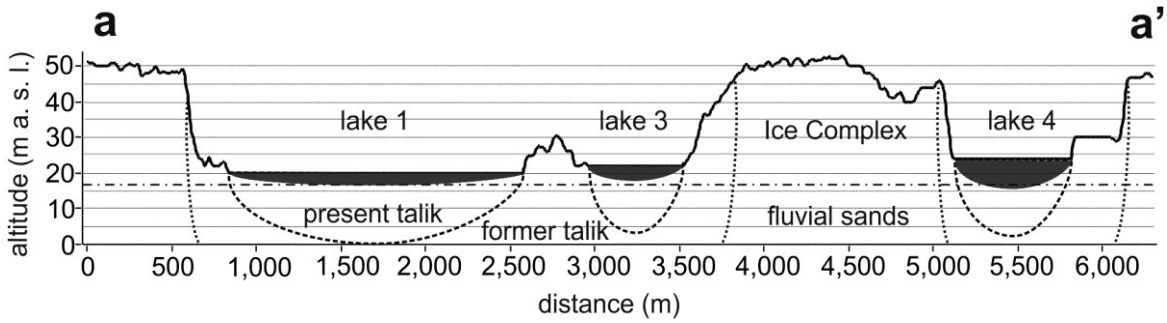

Figure 2-11. Profile section across a Yedoma and thermokarst basin assemblage on Kurungnakh Island (for position see Figure 2-10) showing topographic positions of investigated features. The thaw potential of thermokarst is much greater on Yedoma uplands than in basins. The profile line was derived from the ALOS PRISM DEM, the depths of lakes from bathymetric measurements, and the approximate position of the Ice Complex base from outcrop studies (Schirrmeister et al., 2003; Wetterich et al., 2008). Positions of taliks are hypothetical, based on modeling studies of similar environments in other regions (West and Plug, 2008).

The area of Kurungnakh Island above 17 m a. s. l. with slopes of 0 to 2° that is not included in the thermokarst features amounts to 87.4 km² (Figure 2-12). This means that only 33.7 % of the area within the limits of Ice Complex deposits represents flat Yedoma uplands unaffected by thermokarst or thermal erosion where new thermokarst could potentially

start to develop. However, we are aware that lateral thermokarst expansion of existing lakes close to slopes may result in reworking of Ice Complex deposits along these slopes as well.

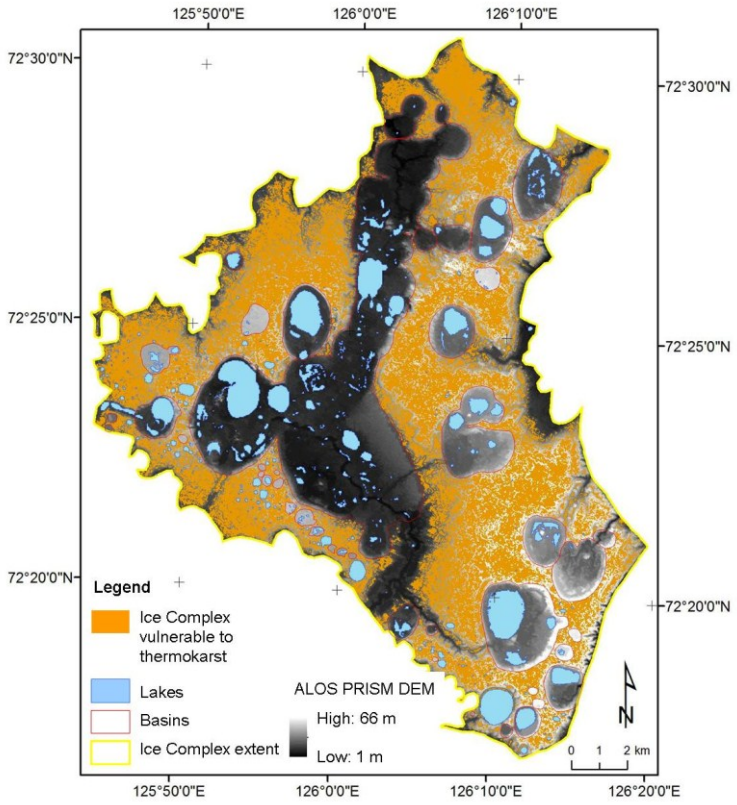

Figure 2-12. Yedoma uplands of Kurungnakh Island unaffected by thermokarst or thermal erosion with slopes < 2°. This area (33.7 % of Kurungnakh Island) is vulnerable to future thermokarst.

2.6 Discussion

2.6.1 Thermokarst extent in the study area

Lakes cover 5.2 % of the study area; this coverage is low compared to other arctic tundra regions like the western arctic coastal plain of Alaska with about 20 % lake coverage (Hinkel et al., 2005) or the Tuktoyaktuk Peninsula in arctic Canada with 30 % lake coverage (Côté and Burn, 2002). Within the Lena River Delta, the third terrace features the lowest lake area percentage (Morgenstern et al., 2008a). The Landsat resolution of 30 m per pixel did not allow small ponds to be detected. Grosse et al. (2008) showed that small ponds significantly contribute to the lake coverage of Ice Complex areas. For their OLE study site, which is part of the westernmost portion of our study area, they calculated 13.3 % lake coverage including all standing water bodies of ≥ 30 m². This is still a small percentage of the whole study area. An assessment of the area available for potential thermokarst evolution in Ice Complex deposits that is solely based on detecting thermokarst lakes by remote-sensing methods

would therefore deduce a high thermokarst potential for this study area. However, the total basin area mapped in our study area exceeds the total current lake area by a substantial factor of four, according to our calculations. This adds a high percentage to the area of Ice Complex degradation due to thermokarst, which is 22.2 % of the study area. In Alaska, on the North Slope thermokarst lakes and drained basins cover a combined area of 46.1 % (Frohn et al., 2005), and on the Barrow Peninsula 72 % (Hinkel et al., 2003). The remaining 77.8 % of our study area cannot be considered undisturbed Yedoma surfaces as thermal erosion also plays an important role in Ice Complex degradation. The results from Kurungnakh Island show that only 33.7 % of the island area is undisturbed flat Yedoma surface. This is in the same range as results of previous remote-sensing-based studies that cover other portions of the Ice Complex accumulation plain in the Laptev Sea region. For the Bykovsky Peninsula east of the Lena Delta, Grosse et al. (2005) calculated the area affected by thermokarst and thermal erosion to be more than 50 %; for the area of Cape Mamontov Klyk west of the Lena Delta, Grosse et al. (2006) calculated the affected area to be 78 %.

2.6.2 Areal constraints on thermokarst development

Modern lakes on Yedoma uplands are, on average, much smaller than single basins (by about one order of magnitude). Taken together with the fact that total basin area exceeds total lake area, this suggests that thermokarst lakes have reached much greater sizes in the past. After drainage, basins can undergo expansion through lateral erosion mainly by secondary thermokarst lakes in the basins. The smoothness of single basin boundaries indicates that this process cannot account for substantial area increase after drainage of the initial lake, which suggests that the size of these basins is indeed largely a result of the first lake that formed. We therefore conclude that conditions for large-area thermokarst lake development were more suitable in the past. During the massive thermokarst development in this region about 12 ka ago the coastline was situated hundreds of kilometers to the north of its present location (Bauch et al., 2001; Kaplina, 2009). The study area was not part of a river delta, but of a broad accumulation plain where Ice Complex deposits were distributed widely (Schirrmeister et al., 2011a). The terrain presumably was not as affected by fluvial erosion as it is nowadays in the delta context (Schwamborn et al., 2002b), and thermo-erosional gullies probably started to form simultaneously with the development of an increasing relief gradient between Yedoma uplands, thermokarst basins, and delta channels. Consequently, the area of thermokarst lake formation was little limited by the hydrological networks that forced growing lakes to drain; hence, large thermokarst lakes with diameters of several kilometers each were able to form.

In contrast, in the present situation small remnants of the former coherent Ice Complex plain have been elevated above a dynamic river delta environment, fostering the development of thermal erosion and the connection of Yedoma uplands to the hydrological network. The limiting effect of thermal erosion on the areal extent of thermokarst is also reflected in a lower lake area percentage in regions of higher relief energy, especially in the uplifted western part of the study area (Table 2-7). On Khardang Island, which has experienced an additional block uplift (Grigoriev, 1993), the discrepancy between the largest basins and the smallest lake area percentage suggests that there has been an abrupt change in thermokarst conditions, from large-scale to very limited, a change resulting from better drainage and thermal erosion.

Bosikov (1991) suggested that the lake area percentage of basins is an indicator of the evolutionary stage of thermokarst basins in central Yakutia. Younger thermokarst basins would have a higher lake area percentage than old basins. Assuming that smaller basins are younger, they should tend to have a higher lake area percentage than larger basins. In our study area we found an opposite correlation. However, *single* basins exhibit a higher lake area percentage compared to *coalesced* basins. This fact results from a better connection of *coalesced* basins to the hydrological network; these basins have often coalesced into broad valleys, which drained through thermo-erosional channels. The water accumulation that is required for renewed lake growth is, therefore, less probable in *coalesced* than in *single* basins. The total number of pingos in *coalesced* basins (24) is much higher than in *single* basins (10). The occurrence of pingos, therefore, might also indicate the evolutionary stage of thermokarst basins. However, it is beyond the scope of this study to further investigate this hypothesis. The more irregular shapes of lakes in basins compared to lakes on Yedoma uplands reflect the complex basin floor morphology with drainage channels, pingos, lake terraces, different areas of permafrost aggradation and subsidence, etc.

2.6.3 Stratigraphical constraints on thermokarst development

The low lake area percentage in basins indicates that if drainage of lakes on Yedoma uplands occurs, lake level falls to the elevation of the drainage sill. Further water supply to the basin cannot lead to further water level rise or to the infilling of the basin to its margins. Subsequent thermokarst evolution in the basins does not seem likely to result in the substantial further subsidence of the lake or basin floor that would be required for large secondary thermokarst lakes to develop in existing basins. This can be explained by the stratigraphy of the study area, in particular the relatively ice-poor and thus thermokarst-resistant sand unit below the Ice Complex.

Figure 2-13 illustrates thermokarst evolution in the specific stratigraphical context of the study area. The maximum Ice Complex thickness observed at coastal bluffs is about 30 m (Grigoriev, 1993) and possibly reaches about 48 m on Khardang Island (Table 2-7). Basin depths of up to 30 m are common, so the majority of first-generation thermokarst lakes have already completely thawed the Ice Complex deposits within their basin footprint (stage 3 in Figure 2-13).

In our study area, the sediments underlying the Ice Complex are fluvial sands with a gravimetric ice content of 20 to 40 %, which is too low to allow for continuing significant thermokarst subsidence below the Ice Complex base. Even if the floor of a first-generation thermokarst lake has not yet reached the Ice Complex base, its talik naturally will expand below it. A thermokarst lake a few meters deep will develop a talik several tens of meters deep in cold, ice-rich permafrost over several hundred to a few thousand years (Anisimova, 1962; Schwamborn et al., 2002a; West and Plug, 2008). Consequently, Ice Complex deposits underneath first-generation thermokarst lakes have undergone taberal development, including ice loss, organic carbon depletion, and compaction, resulting in a diagenetically altered, thawed sediment which may refreeze again after lake drainage. Portions of Ice Complex deposits, including ground ice, are possibly conserved underneath smaller lake basins that drained at a stage corresponding to stage 2 in Figure 2-13, before they reached full thermokarst maturity and developed a deep talik (Kaplina, 2009). However, only a small number of such basins exist in the study area as inferred from basin sizes.

After first-generation thermokarst lakes drained the taliks and basin deposits gradually refroze, permafrost formed accompanied by ground ice aggradation. The renewed ground ice content, however, does not reach the amount included in initial Ice Complex deposits which accumulated over several tens of thousands of years. Permafrost sediments that have developed in thermokarst basins can be divided into three main horizons with varying ground ice content (Kaplina, 2009; Wetterich et al., 2009) (stages 4 and 5 in Figure 2-13). The lowest horizon represents the former Ice Complex sediments, which were thawed, compacted, partly deformed, and refrozen. These so-called taberites have a much lower ice content than did the original Ice Complex (between 20 to 40 wt%), and can be several meters thick. Refrozen lake sediments overlaying the taberites have similar ground ice contents (20 to 40 wt%). The top horizon (i.e., alas deposits) is formed by silt and peat layers with very high ground ice content similar to that of the Ice Complex (up to 200 wt%), and can reach thicknesses of 5 to 7 m. A system of ice veins and wedges penetrates these horizons of basin sediments, which are epigenetic in the taberal and lake sediments and syngenetic, due to peat accumulation, in the alas deposits (Kaplina, 2009; Wetterich et al., 2009). Favourable

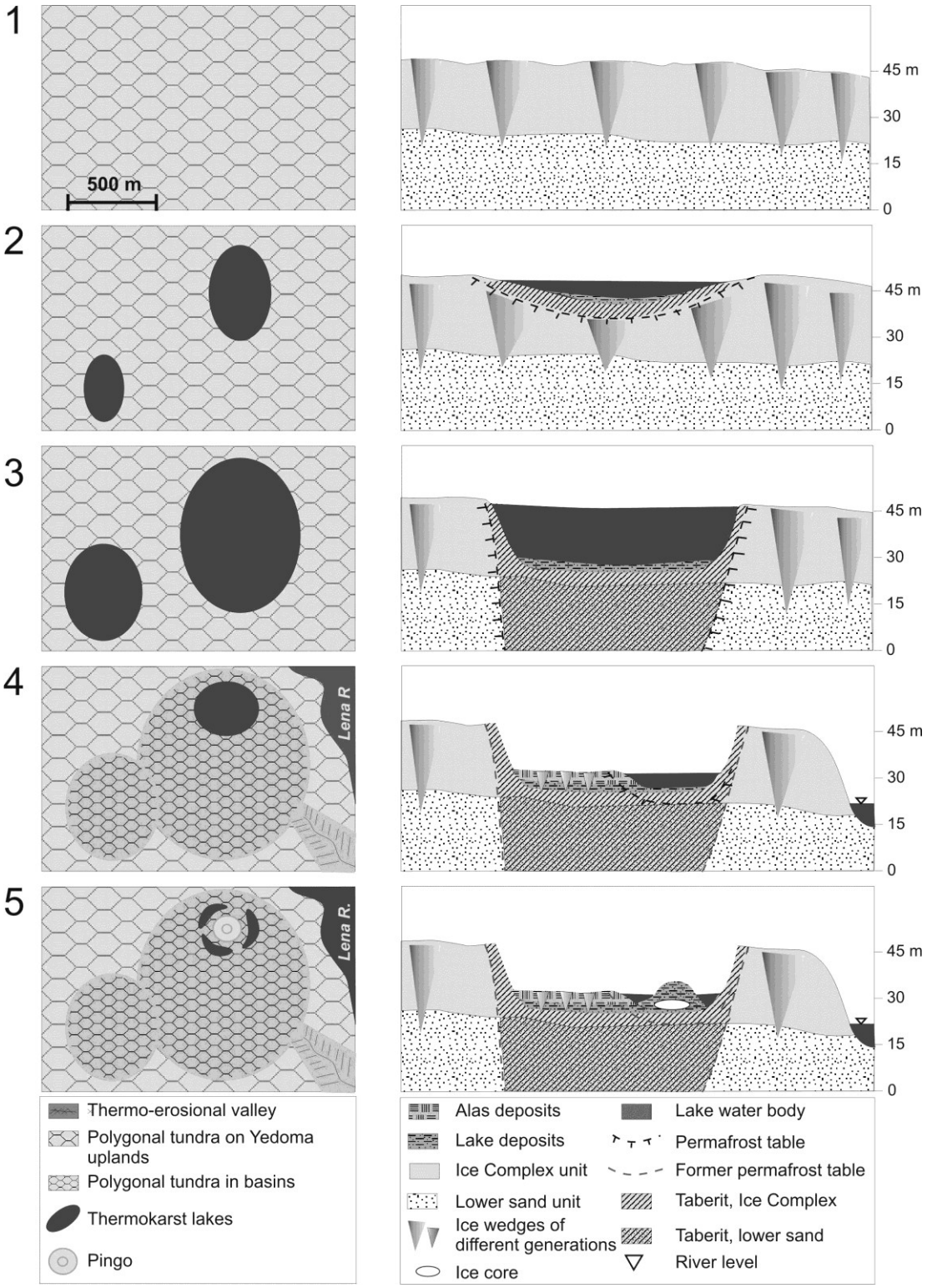

Figure 2-13. Scheme of thermokarst development in Yedoma landscapes of the Lena River Delta in plane view (left) and cross section (right). 1: Flat, undisturbed Yedoma uplands with polygonal tundra. 2: Thermokarst lakes on Yedoma uplands - initial stage with lateral and vertical thermokarst development, lake sedimentation, talik in non-steady state. 3: Thermokarst lakes on Yedoma uplands - mature stage with lateral expansion only, lake sedimentation, talik fully developed. 4: Partially drained, coalesced thermokarst basin with remaining or second-generation thermokarst lake - partial refreezing of former talik, taberites, and lake sediments with ice aggradation and peat accumulation. 5: Partially drained coalesced thermokarst basin with pingo.

conditions for considerable second-generation thermokarst, therefore, are provided only in the top horizon; the lower two resemble the underlying fluvial sands in terms of low ground ice content.

The different potential for ground subsidence due to thermokarst is also supported by the different depths of lakes on Yedoma uplands versus lakes in basins (Figure 2-8). While the former (lakes 5 and 6) reach depths of 12 m, the latter (lakes 1 to 3) are no more than 4 m deep. Lake 4 illustrates an intermediate stage. It partly drained before thermokarst was fully developed. The exposed basin floor is situated at 30 m a. s. l., which is well above the Ice Complex base (Figure 2-11). The remaining lake continued the thermokarst process and reached its present depth of 8 m. The present lake floor is situated directly at the 17 m level, which we defined as the generalized Ice Complex base. In fact, the Ice Complex base should be situated a few meters lower here, because a layer of taberites necessarily exists underneath the lake bottoms. Its thickness depends on the original ice content of the Ice Complex; the lower the ice content, the thicker the taberal layer.

Figure 2-11 shows lake bottoms situated at the assumed Ice Complex base and lake surfaces and basin floors located only a few meters higher. This suggests that the taberal layer is only a few meters thick and the original ice content was very high. For the large thermokarst basin with lakes 1 to 3, taberites have been calculated to be 2.3 m thick, assuming a total ice content of 90 vol% in the original Ice Complex (Ulrich et al., 2010). Soloviev (1962) also describes central Yakutian basin floors situated just above the Ice Complex base. Therefore, basin depths can be used as indicators of ice content and total thickness of Ice Complex deposits.

2.6.4 Impact of future thermokarst development

These findings emphasize that the effect of thermokarst development varies depending on whether it takes place on undisturbed plain surfaces or in existing basins of older-generation thermokarst. Newly developing thermokarst lakes on Yedoma uplands have a stronger transformative impact on permafrost sediments, landscape character, and environmental processes than thermokarst lakes in existing basins. Taliks forming underneath thermokarst lakes on Yedoma uplands enable the activation of physical and biochemical processes in the Ice Complex deposits, altering their structure and the composition of organic matter that had been conserved for thousands of years. The sediments in basins, however, have already been reworked and do not possess the characteristics of the very ice-rich permafrost of the surrounding Yedoma uplands. These differences between thermokarst on Yedoma uplands and thermokarst in basins also have implications for the carbon cycle. Walter et al. (2007) report that refrozen taberal Ice Complex deposits beneath drained Holocene thermokarst

lakes contain ~33 % less carbon than those Ice Complex deposits that never thawed. Ice Complex on Yedoma uplands has a high ground ice content; therefore, it is very sensitive to potential thermokarst development in a warming climate. Thermokarst lakes developing on Yedoma uplands thus have a higher potential to mobilize older, and more labile, carbon than do second-generation thermokarst lakes in existing basins. At the same time the potential for the development of new thermokarst lakes, especially large lakes that are able to form extensive taliks before they drain, is very limited. A well-established connection of the basins to the drainage system also allows for the erosion of basin sediments. Taberites, lake sediments, and Holocene peat horizons together with ground ice that aggraded during refreezing can be removed from the basin floor, thus eliminating the basis for future thermokarst development. In this case, the organic matter of the basin sediments is transported to the fluvial system.

On Kurungnakh Island, at least 71 % of all thermokarst lakes and basins have subsided to the Ice Complex base. Here, the Ice Complex deposits have thawed completely and have been exposed to biogeochemical processes such as the decomposition of old organic matter. If we assume that fully-developed taliks have existed underneath most of the remaining 29 % of thermokarst lakes and basins, thermokarst has completely degraded Ice Complex deposits in up to 39.6 % of the area of Kurungnakh Island. Areas outside existing thermokarst lakes and basins above the Ice Complex base with slopes of up to 2° are available for the initiation of new thermokarst lakes because these areas allow ponding of water and ground subsidence. The areas with slopes of more than 2° can also be affected by thermokarst, mainly by lateral growth of existing thermokarst lakes. In some cases ponding of water can also occur on upper slopes of Yedoma uplands. However, extensive thermokarst activity is not possible here, because lateral growth will lead to drainage when the lake reaches the lower parts of the slope. Many of the steeper slopes (5 to 20°) surround large thermokarst lakes or belong to thermo-erosional valleys that cut across the surface of Kurungnakh Island, indicating that lateral sediment transport and mass wasting processes are also important contributors to the degradation of Ice Complex deposits. Key processes are thermal abrasion of lake shores and thermal erosion in retrogressive valleys or gullies. Mobilization, transport, and transformation of organic matter differ between *in situ* thawing and ground subsidence in local thermokarst lakes and the lateral dynamics involving slope processes and flowing water. It will thus be of interest in future work to investigate the extent to which the remaining Ice Complex is degraded by newly developing thermokarst, or by thermal abrasion due to the expansion of thermokarst lakes in existing basins, or by thermal erosion.

The implications of significantly reduced thermokarst potential in large parts of the study area are also highly relevant for most other Yedoma landscapes in Siberia, which are estimated to occupy an area of 10^6 km² (Zimov et al., 2006a). Environmental changes at the transition between Pleistocene and Holocene led to extensive thermokarst activity in Siberian Ice Complex deposits (Kaplina, 2009). The percentage of thermokarst affected terrain as well as the morphology of thermokarst lakes and basins varies between different Yedoma regions. Precise calculations of Yedoma and thermokarst area percentages are rare, but old thermokarst basins generally exist in nearly all Yedoma regions and restrict future thermokarst lake expansion. In the Kolyma lowlands, for example, Kaplina et al. (1986) report different degrees of Yedoma dissection by thermokarst basins from weak (<25 %) to very high (>75 %). In a subset of this area, Veremeeva and Gubin (2009) calculated that 65 % are covered by thermokarst basins and only 26 % represent Yedoma uplands. For the Yedoma region of the Bykovsky Peninsula, Grosse et al. (2005) found that about 53 % of the area is affected by thermokarst. For the Lena-Anabar lowland, which is similar in geological composition to the Lena Delta study area with Ice Complex deposits underlain by fluvial sands, about 49 % of the area is covered with thermokarst landforms (Grosse et al., 2006). Kaplina (2009) points out two types of Yedoma territories in north Yakutian lowlands, where thermokarst has no potential to develop. The first type corresponds to the situation in our study area representing drained Yedoma massifs and remnants where water accumulation is impeded. The second type are areas, where coalesced thermokarst basins form extensive alas plains underneath which the former Ice Complex almost completely underwent taberal reworking. This shows that investigations of modern and possible future thermokarst lake development in Siberian Yedoma regions in the context of changes in landscape, hydrology, climate, carbon cycle, etc. always have to consider the history of former thermokarst evolution and permafrost degradation.

2.6.5 Oriented thermokarst development

The lateral growth of thermokarst lakes and the spatial development of second-generation thermokarst in existing basins did not proceed uniformly, as can be seen from morphometric and orientation analyses. Even though lakes and basins in the study area are not as elongated as the oriented lakes of the second Lena Delta terrace (Morgenstern et al., 2008a), the descriptive statistics of circularity and elongation indicate a general deviation from round and regular forms. Smaller lakes (14,400 to 200,000 m²) are oriented mainly in the WNW direction whereas larger lakes (≥ 200,000 m²) and single basins have major orientation peaks to the NNE. Several hypotheses can be proposed to explain this 90° shift in orientation from smaller to larger forms. First, if it is true that smaller thermokarst lakes have not existed as long as larger lakes and single basins, the external orienting forces may

have changed their direction by 90° at some time during the Holocene. Second, the strength of the orienting forces may have changed with growing lake size. Third, smaller lakes may be dominated by different orientation-driving forces than are larger lakes. Despite several decades of research, there is still a debate about which factors control thermokarst lake orientation in areas where lake orientation does not follow underlying relief structures. On the North American Arctic Coastal Plain, preferential erosion of the lake shores at right angles to prevailing summer wind directions due to wind-driven currents and wave activity has been proposed and agrees well with current main wind directions (e.g., Carson and Hussey, 1962; Côté and Burn, 2002; Hinkel et al., 2005); however, authors investigating orientation and directed evolution of thermokarst lakes and basins in Siberian Ice Complex deposits discuss solar insolation (e.g., Soloviev, 1962; Boytsov, 1965; Ulrich et al., 2010) and erosion due to wave activity in the direction of prevailing summer winds (e.g., Kuznetsova, 1961). The first of our three hypotheses would rule out solar insolation as the main factor for lake orientation. A possible explanation could be a change in major summer wind direction during the Holocene. Under our second hypothesis an important effect of solar insolation is also implausible. However, if main summer wind direction remained stable, a change in its effect from wave-induced erosion (abrasion) in the wind direction to the establishment of wind-driven currents at right angles to the main wind direction or *vice versa* might be possible. Our third hypothesis implies that in smaller lakes wind has a stronger effect on orientation than does solar insolation, while in larger lakes and in basins the effect of solar insolation dominates that of wind effects. This is physically not plausible, as wind effects should intensify with growing lake area.

A change detection study for all lakes ≥10,000 m² on Kurungnakh Island revealed the directional growth of lakes in the NNW direction during the investigated time period of about 40 years (Günther, 2009). Following the solar radiation hypothesis, the NNE (SSW-facing) slopes of the lakes and basins should receive maximum energy shortly after noon and therefore be preferentially eroded. The results of modeling solar radiation rates for a thermokarst basin on Kurungnakh Island showed the highest values for south-facing basin slopes. Rates for west-facing slopes exceeded rates for east-facing slopes (Ulrich et al., 2010). Solar insolation as the single orienting factor is thus only acceptable if a summer cloud-cover regime with consistently higher cloudiness in the afternoon were to be observed on Kurungnakh Island. Wind data from the meteorological station on Stolb Island near Kurungnakh Island (72.4°E 126.5°N, data from 1955–1991) show pronounced southern wind directions for the whole observation period and three peaks for the period of positive temperatures, one from the S, one from the ESE, and one from the NNW (Morgenstern et

al., 2008a). This would support the hypothesis of orientation due to prevailing winds in the direction of major axes for the lakes of Kurungnakh Island over the last 40 years.

Lakes in basins are not situated in the centers of the basins, but are shifted mainly towards northern and southern margins (Figure 2-7), indicating that asymmetrical basin profiles result from directional basin evolution. Thermokarst lakes are often deeper at the sides of active thermokarst development (Romanovskii, 1961). After partial drainage, residual lakes in basins remain at the sides of recent thermokarst activity. If thermokarst development proceeded unidirectionally over the whole study area, as has been observed for Kurungnakh Island over the last 40 years, lakes in basins should be situated predominantly in one direction only from the basin center. The bi-directionally clustered distribution of lakes in basins therefore does not support hypotheses of unidirectional factors such as solar insolation and prevailing summer winds in the direction of the main axes. It is interesting to note that the position of pingos in single basins is similar to the position of lakes in basins; pingos are also shifted in northern and southern directions from the basin centers (Figure 2-9). However, the low number of pingos in single basins in the study area does not permit using pingo position to derive robust conclusions about oriented thermokarst development.

The inconsistencies of lake and basin orientation patterns in the study area over space and time, as described above, do not allow the cause of oriented thermokarst development in the Yedoma landscapes of the Lena River Delta to be clearly elucidated at present.

2.7 Conclusions

Large parts of the study area are affected by thermokarst, and total thermokarst basin area exceeds total thermokarst lake area by a factor of four. Three developmental stages of thermokarst complexity have been distinguished in this study: 1) lakes on Yedoma uplands, 2) single basins with residual and second-generation lakes, and 3) coalesced basins with residual and second-generation lakes. The morphometric characteristics of lakes on Yedoma uplands differ significantly from those of lakes in basins or single basins, reflecting different evolutionary conditions. However, the differences between the two lake types are not clear-cut and do not allow for automatically classifying lakes on Yedoma uplands and lakes in basins based on morphometric indicators in a GIS. Thermokarst lakes and single basins show oriented morphometries, but the factors and processes responsible for oriented thermokarst development in the study area remain unclear. Conditions more suitable to the development of large-area thermokarst in the Ice Complex deposits of our study area have existed in the past; such development will be further limited in area and depth in the future.

The proximity of newly-developing thermokarst to existing degradational features like thermokarst basins and thermo-erosional valleys as well as to delta channels reduces the potential for considerable thermokarst activity on Yedoma uplands before drainage occurs. On Kurungnakh Island, 33.7 % of the total area is vulnerable to future thermokarst on Yedoma uplands. Further thermokarst processes in existing basins are limited due to the underlying ice-poor fluvial sands and, in the case of basins where permafrost has aggraded during the Holocene, due to the thin layers of ice-rich alas sediments and peat horizons. No old organic carbon will be directly mobilized from these areas. Developing thermokarst lakes on undisturbed Yedoma uplands have the highest impact on the alteration of Ice Complex deposits and Yedoma landscapes. However, past thermokarst activity and erosion have severely diminished original Yedoma surfaces, not only in the study area, but in Siberian Yedoma regions in general, so future thermokarst lake expansion in these landscapes may be considerably restricted. Therefore, it is necessary to differentiate between the various developmental stages of thermokarst and landscape units in order to assess the degradation of very ice-rich permafrost due to thermokarst, for example to quantify organic carbon inventories and the potential for future carbon fluxes.

Acknowledgements

We thank M. N. Grigoriev for his advice on enhancing the map of the Ice Complex in the Lena Delta, as well as for discussions of the broader context of the study. We also thank U. Herzschuh for discussions of statistical methods used to assess lake and basin morphologies and J. Strauss for calculating the total organic carbon inventory of the Kurungnakh Island Ice Complex. We greatly appreciate the efforts of all German and Russian colleagues in organizing and supporting the expeditions to the Lena Delta, and especially the field assistance of M. Ulrich, S. Rößler, and P. Ivlev. ALOS PRISM data used for DEM compilation were kindly provided by JAXA and ESA through the LEDAM project (awarded by ESA ADEN, PI H. Lantuit, ID 3616). A. Morgenstern was supported by the German National Academic Foundation and the Christiane Nüsslein-Volhard Foundation. G. Grosse was supported by NASA grant NNX08AJ37G and NSF OPP grant #0732735. C. O'Connor (University of Alaska, Fairbanks) provided careful language revision and constructive comments. The constructive reviews of L. Smith and one anonymous reviewer as well as the personal discussion with T. N. Kaplina helped to enhance the manuscript.

3 Evolution of thermokarst in East Siberian ice-rich permafrost: A case study

A. Morgenstern[1], M. Ulrich[1,2], F. Günther[1], S. Roessler[1,3], I. V. Fedorova[4], N. A. Rudaya[5], S. Wetterich[1], J. Boike[1], L. Schirrmeister[1]

[1] Alfred Wegener Institute for Polar and Marine Research, Research Unit Potsdam, Potsdam, Germany
[2] present address: University of Leipzig, Institute of Geography, Leipzig, Germany
[3] present address: Technical University of Munich, Limnological Station Iffeldorf, Iffeldorf, Germany
[4] Otto Schmidt Laboratory for Polar and Marine Research, Arctic and Antarctic Research Institute, St. Petersburg, Russia
[5] Center of Cenozoic Geochronology, Institute of Archaeology and Ethnography, Russian Academy of Sciences, Siberian Branch, Novosibirsk, Russia

Geomorphology, under review

3.1 Abstract

Thermokarst lakes and basins are major components of ice-rich permafrost landscapes in East Siberian coastal lowlands and are regarded as indicators of regional climatic changes. We investigate the temporal and spatial dynamics of a 7.5 km², partly drained thermokarst basin (alas) using field investigations, remote sensing, Geographic Information System (GIS), and sediment analyses. The evolution of the thermokarst basin proceeded in two phases. The first phase started at the Pleistocene/Holocene transition (13 to 12 ka BP) with the initiation of a primary thermokarst lake on the Ice Complex surface. The lake expanded and persisted throughout the early Holocene before it drained abruptly about 5.7 ka BP, thereby creating a >20 m deep alas with residual lakes. The second phase (5.7 ka BP to present) is characterized by alternating stages of lower and higher thermokarst intensity within the alas that were mainly controlled by local hydrological and relief conditions and accompanied by permafrost aggradation and degradation. It included diverse concurrent processes like lake expansion and stepwise drainage, polygonal ice-wedge growth, and the formation of drainage channels and a pingo, which occurred in different parts of the alas. This more dynamic thermokarst evolution resulted in a complex modern thermokarst landscape. However, on the regional scale, the changes that occurred during the second evolutionary phase after drainage of the initial thermokarst lakes were less intense than the extensive thermokarst development that affected vast areas of East Siberian coastal lowlands during

the early Holocene as a result of a significant regional change to warmer and wetter climate conditions.

3.2 Introduction

Thermokarst lakes and basins are ubiquitous landforms in arctic lowlands. Current research has a particular focus on thermokarst processes in ice-rich permafrost deposits in Siberia and the North American Arctic, because these deposits are highly vulnerable to degradation under a warming climate. The high content of excess ice accounts for their high thawing potential, and the large amount of organic matter (OM), which has been stored in permafrost deposits for several thousand years, has a high potential for the release of greenhouse gases (Jorgenson et al., 2006; Walter et al., 2007; Schuur et al., 2009; Grosse et al., 2011). Thermokarst in East Siberian ice-rich permafrost massively developed at the transition from Pleistocene to Holocene, but after the Boreal period (9-7.5 ka BP), the thermokarst landscapes appeared as they do today and have experienced only minor changes since then (Romanovskii et al., 2004; Kaplina, 2009). Parallel to this concept of unidirectional thermokarst evolution, including initiation, expansion, drainage, and cessation of thermokarst activity leading to stable modern thermokarst landscapes, thermokarst has been regarded as a highly dynamic process, and the concept of a thaw lake cycle which has been repeated several times during the Holocene has been proposed (e.g. Hopkins, 1949; Tomirdiaro, 1965; Billings and Peterson, 1980; Hinkel et al., 2003). This concept describes secondary thermokarst activity in drained basins after sufficient ice aggradation, but substantial evidence is lacking that several complete thaw lake cycles have occurred in arctic tundra landscapes during the Holocene (French, 2007; Jorgenson and Shur, 2007). Many recent studies, which investigate thermokarst lake area changes by means of multitemporal remote sensing, reveal ongoing thermokarst dynamics during the last decades. For different Siberian regions in the continuous permafrost zone, these change detection studies show thermokarst area increase (Smith et al., 2005; Walter et al. 2006; Kravtsova and Bystrova, 2009) as well as decrease resulting from lake drainage (Kravtsova and Bystrova, 2009; Günther et al., 2010), but also areas where no changes occur (Kravtsova and Bystrova, 2009). These studies merely differentiate the settings in which these lake area changes take place, but it has been shown that there are great differences between the potential and impact of developing thermokarst in undisturbed ice-rich late-Pleistocene deposits and that in older-generation thermokarst basins (Morgenstern et al., 2011).

In Yedoma-type Ice Complex deposits of the Laptev Sea region several studies have been conducted regarding the general stratigraphy (e.g., Wetterich et al., 2008; Schirrmeister et al., 2011a, 2011c), the onset of thermokarst (Kaplina and Lozhkin, 1979; Tumskoy, 2002),

recent changes of thermokarst lake area (Günther, 2009; Kravtsova and Bystrova, 2009; Günther et al., 2010), or the potential of future thermokarst evolution (Morgenstern et al., 2011). However, there is a gap in our knowledge about how these permafrost degradation landforms have developed during the Holocene, i.e. whether they experienced several cycles of drainage, permafrost aggradation, and thermokarst formation, or not.

Our investigations aim at the detailed characterization of the temporal and spatial dynamics of thermokarst in ice-rich permafrost. Field investigations of a partly drained thermokarst lake basin (alas) in Ice Complex deposits with three large lakes are combined with remote sensing, Geographic Information System (GIS), and sediment analyses to distinguish different stages of thermokarst dynamics. The specific objectives are: 1) to characterize the modern thermokarst landscape based on morphological and surface properties, 2) to discriminate different phases of thermokarst development, and 3) to reconstruct the landscape dynamics due to permafrost degradation and aggradation during the Holocene.

3.3 Study site and regional setting

The investigated alas is situated on Kurungnakh Island in the south-central Lena River Delta (72°19'N; 126°12'E) (Figure 3-1) in the continuous permafrost and subarctic tundra zone. Kurungnakh Island belongs to the third geomorphological main terrace of the Lena Delta (Grigoriev, 1993), which is distributed in the southern delta as erosional remnants of a late-Pleistocene accumulation plain in the foreland of the Chekanovsky Ridge bordering the Lena Delta to the south. It consists of three stratigraphical main units (Schwamborn et al., 2002b; Schirrmeister et al., 2003, 2011a; Wetterich et al., 2008) (Figure 3-2). The lowest unit is composed of fluvial sands with a gravimetric ice content between 20 and 40 weight percent (wt%), which accumulated between 100 and 50 ka BP. The transition to the overlying Ice Complex unit is very sharp and is situated between 15 and 20 m above river level (arl), corresponding to 16 to 21 m above sea level (asl) at the eastern side of Kurungnakh Island. The Ice Complex unit consists of silty and peaty deposits with high gravimetric ice content (38 to 133 wt%) and huge syngenetic ice wedges. It polygenetically accumulated during the interstadial period between about 50 and 32 ka BP and during the stadial period about 17 ka BP. The Holocene unit (8 to 3 ka BP) occurs as a cover on top of the Ice Complex unit and as infillings of thermokarst depressions and is composed of cryoturbated silty sands with peat inclusions and small ice wedges.

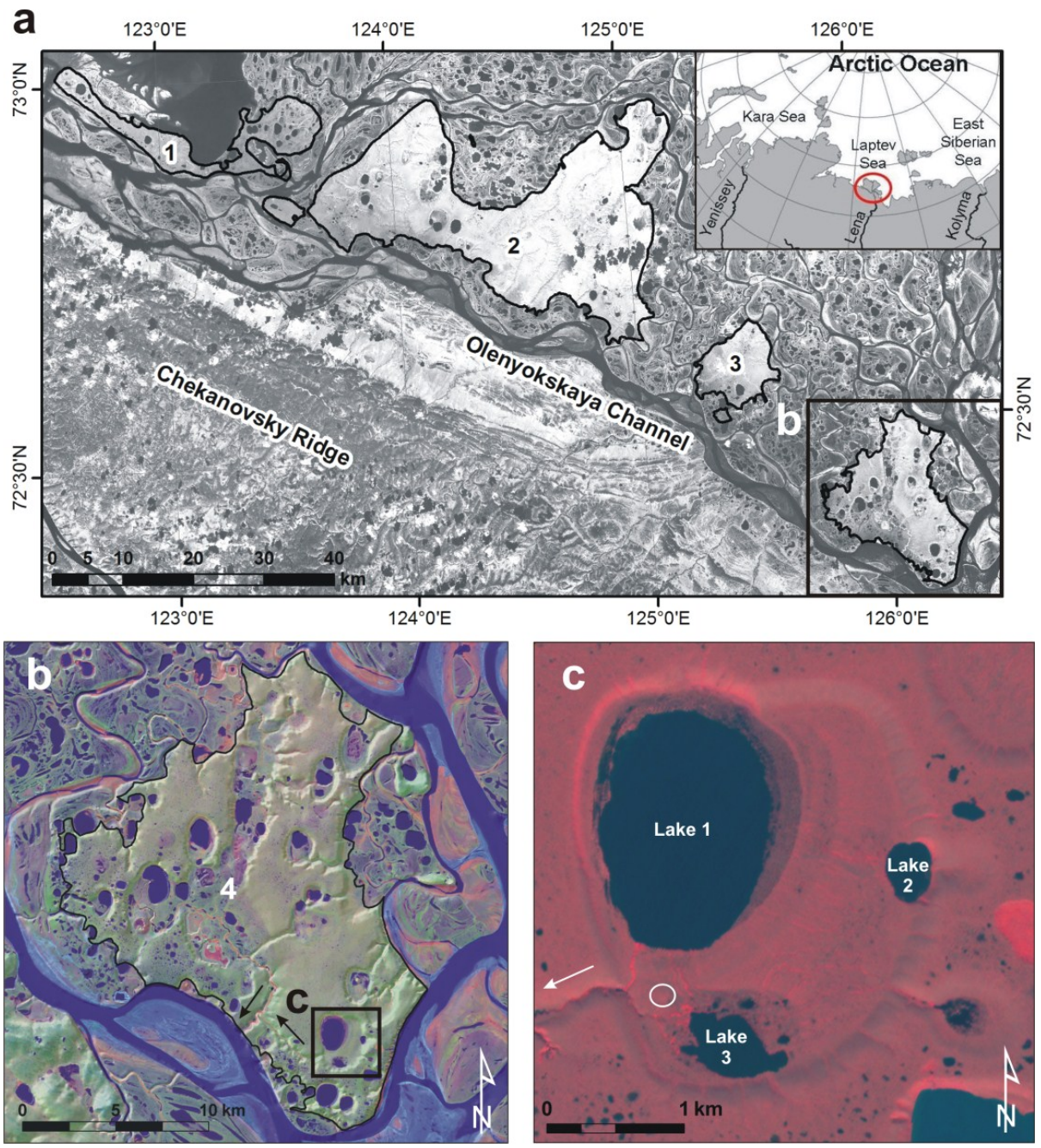

Figure 3-1. Location of the study area**. (a)** Ice Complex remnants (black outlines) in the southwestern Lena River Delta forming the third terrace. 1 – Ebe-Basyn Island, 2 – Khardang Island, 3 – Dzhangylakh Island (Landsat-7 ETM+ mosaic, band 4). **(b)** Kurungnakh Island. Black outline marks the Ice Complex extent; arrows indicate the flow direction of the thermo-erosional valley draining the investigated alas. 4 – Alas valley formed by coalescence of several alasses (Landsat-7 ETM+, RGB 4-5-3, over DEM shaded relief derived from topographic maps). **(c)** Investigated thermokarst depression with three large thermokarst lakes. White circle indicates a small pingo; white arrow shows the flow direction of the draining thermo-erosional valley (ALOS AVNIR-2, RGB 4-3-2, acquisition date: 18 August 2006).

Figure 3-2. Bluff at the eastern side of Kurungnakh Island. This location close to the investigated alas reveals the stratigraphical composition of the island with lower fluvial sands, upper Ice Complex, and Holocene cover. Ice wedges in the Ice Complex appear in light grey colors; border between sands and Ice Complex located at 15 to 20 m height.

The total area of Kurungnakh Island is 350 km², but the described stratigraphy has been eroded in large part at the margins by meandering delta channels. The area with the preserved stratigraphy of fluvial sand, Ice Complex, and Holocene units has an extent of 259.5 km² (black outline in Figure 3-1b), but also shows a highly dissected surface resulting from intensive thermokarst and thermo-erosional activity during the Lateglacial to early Holocene period (Romanovskii et al., 2000; Morgenstern et al., 2011). The thermokarst-affected area within the Ice Complex extent of Kurungnakh Island covers 103 km², with total alas area considerably exceeding total lake area (99 km² and 19 km², respectively). Maximum surface elevation of Kurungnakh Island is 55 m asl in the southeast on the Yedoma surface close to the investigated alas and gradually decreases in the northwestern direction. The flat Yedoma uplands are characterized by polygonal tundra with numerous ponds and small thermokarst lakes.

Alasses on Kurungnakh Island are mostly oval in shape, up to 3.5 km long, 3 km wide, and 30 m deep, with steep slopes and flat floors. They have often coalesced with neighboring depressions, most notably in central Kurungnakh, where a large alas valley dissects the island from north to south (Figure 3-1b). Most alasses contain lakes and ponds and small streams or drainage channels. Many of them drained through thermo-erosional valleys that cut across the island's surface. Pingos have developed on some of the alas floors. The investigated alas is considered to be typical of thermokarst landforms in northeast Siberian coastal lowlands with ice-rich permafrost as they are described, for example, in Romanovskii (1961).

3.4 Material and methods

3.4.1 Remote-sensing data and processing

ALOS PRISM satellite data with a geometric resolution of 2.5 m acquired in triplet OBS1 mode on 21 September 2006 entirely cover Kurungnakh Island and surrounding delta areas. A Digital Elevation Model (DEM) was derived from all stereo pairs of this PRISM triplet. This DEM with a horizontal resolution of 5 m and a vertical accuracy of 5.8 m was then used to orthorectify the PRISM nadir image (Günther, 2009). Both data sets were used in this study for context analyses of the Kurungnakh Island setting and relief.

For high resolution spatial analyses of the 7.5 km² large alas, an alas DEM with 3 m pixel size was produced from detailed tacheometric field measurements (Ulrich et al., 2010, 2011). Its vertical accuracy of 0.28 cm is very high and allows for detailed analyses of the alas terrain. Spatial data processing and analyses were performed using the GIS software package ArcGIS™ 10.0 of ESRI™.

Multispectral ALOS AVNIR-2 satellite data with a geometric resolution of 10 m acquired on 18 August 2006 cover the eastern part of Kurungnakh Island including the investigated alas. The four spectral bands of these data cover the visible (VIS) and near-infrared (NIR) parts of the electromagnetic spectrum and allow for the classification of land cover types, which are characterized by different moisture regimes and vegetation coverage and composition. A supervised maximum-likelihood classification of the AVNIR-2 data was performed using the ENVI™ 4.5 software. Detailed field records of surface characteristics were used for training, and the alas DEM as well as a soil adjusted vegetation index (SAVI) were considered in the classification approach (Roessler, 2009).

3.4.2 Field data and sediment analyses

Field work in August 2008 during the LENA 2008 Expedition within the framework of the Russian-German Cooperation “System Laptev Sea” (Wagner et al., 2012) included detailed surface characterization of the whole study area, lake investigations, and sediment sampling. A detailed tacheometric survey, which included a trigonometric point close to the alas at 55 m asl as a reference, provided for accurate height assignment of different relief features, e.g. lake levels (Ulrich et al., 2010). Bathymetry of the three large alas lakes was measured along several profiles using an echo sounder (Garmin™ GPSmap 178C Sounder) on board a small non-motorized rubber boat. In the deeper parts, one short core per lake was taken from the rubber boat using an UWITEC gravity corer equipped with a 60 cm long and 6 cm wide PVC liner (Lake Core (LC)-1, LC-2, and LC-3 at 2.4, 4.0, and 3.6 m water depth, respectively). The short cores did not penetrate deeply (max. 31 cm), because the high density of the clastic sediments at the bottom prevented further penetration of the PVC

liner. The cores were kept upright until they reached the shore. After visual examination and description, the cores were cut into approximately 1 cm thick slices that were stored in plastic bags until they reached the lab. Two outcrops were studied for stratigraphical reconstructions, one at a 1.5 m high bluff at the southeastern shore of Lake 3 (OC-A) and one in a neighboring alas to the southeast, where a thermo-erosional valley exposed deposits of the alas floor (OC-B) (Morgenstern et al., 2008b; Wagner et al., 2012) (Figure 3-3).

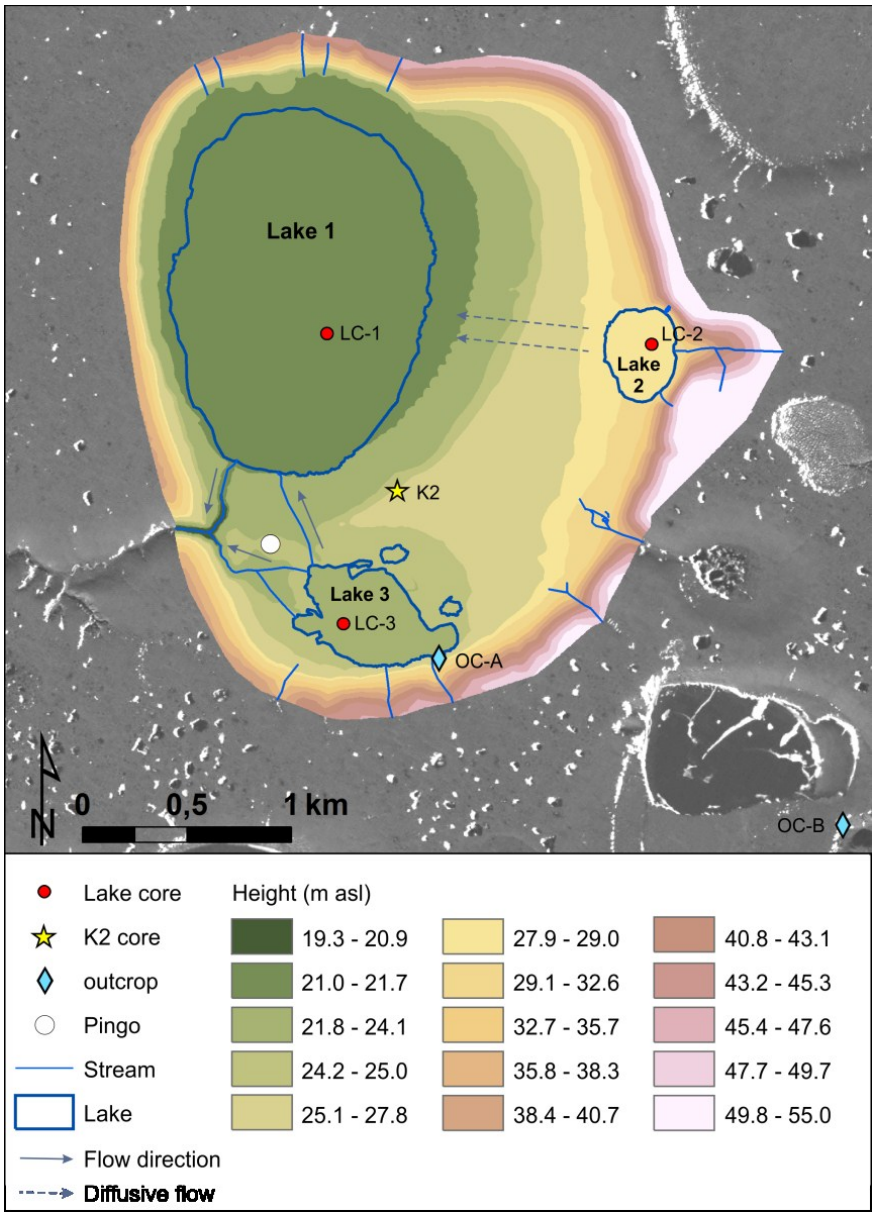

Figure 3-3. Elevation zones of the alas derived from the alas DEM and location of sampling sites. Background image: ALOS PRISM, acquisition date: 21 September 2006.

In 2009, a 4 m deep permafrost core (K2) was drilled into the alas floor between Lake 1 and Lake 3 (72°19'12.6''N, 126°11'35.7''E) (Figure 3-3) and the removed core was kept frozen (Boike et al., 2009). An unfrozen peat cover of 20 cm depth was removed before coring and is not included in subsequent laboratory analyses. The core was already split in the field into 5 to 10 cm long segments. Because of the warm air temperatures during the sampling process, the core sections thawed superficially and subsequently refroze, so that primary sediment and ice structures could not be clearly distinguished during subsequent inspection in the lab.

All sediment samples were analyzed for sediment parameters (magnetic susceptibility (MS), grain size mean, grain size distribution, and sorting degree after Trask (1932)) and OM characteristics (total organic carbon (TOC), total carbon (TC), and total nitrogen (TN) contents, and stable carbon isotopes (δ^{13}C of TOC)) at AWI Potsdam using the institute's standard procedures as described in Wetterich et al. (2009). MS was determined using a Bartington MS2 MS meter, sensor type MS2B. Grain size distribution was measured with a laser diffraction particle analyzer (Coulter LS 200), TOC, TC, and TN contents with the CNS analyzer Elementar Vario EL III, and stable carbon isotopes (δ^{13}C) of TOC with a Finnigan DELTA S mass spectrometer. δ^{13}C analyses of the K2 permafrost core were conducted at the German Research Center for Geosciences (GFZ), Potsdam using a Finnigan DELTAplusXL mass spectrometer. The accelerator mass spectrometry (AMS) ^{14}C dating of selected samples was performed at the Poznan Radiocarbon Laboratory, Poland (Goslar et al., 2004). Plant remains for dating were hand-picked under a microscope; only in some cases, where no plant fragments were visible under the microscope, bulk samples were used. Calibrated ages were calculated using CALIB rev. 6.0.0 (data set: IntCal09; Reimer et al., 2009) (Table 3-1). Throughout the paper, uncalibrated ages are given. Some samples of the K2 permafrost core produced modern ages. These were excluded from calibration and further interpretation, because they most probably result from contamination of the samples with fresh plant material.

Table 3-1. Results of the AMS ^{14}C dating of samples from different alas sections. Ages in brackets were excluded from calibration and further geochronological interpretation.

section	No.	Sample ID	Lab no.	mean depth (cm)	dated material	Uncal. AMS ages (a BP)	Cal. AMS ages, minimum (ka BP)	Cal. AMS ages, maximum (ka BP)
K2 permafrost core	1	K2-2	Poz-37315	59	plant remains	(modern)	-	-
	2	K2-5	Poz-41118	93.5	bulk	3620 ± 35	3.84	3.99
	3	K2-9	Poz-37316	154	plant remains	(modern)	-	-
	4	K2-9	Poz-41119	154	plant remains	5660 ± 50	6.31	6.56
	5	K2-13	Poz-37318	184	plant remains	(1775 ± 35)	-	-
	6	K2-19	Poz-41120	241.5	bulk	17390 ± 100	20.33	21.2
	7	K2-22	Poz-37319	287.5	plant remains	(modern)	-	-
	8	K2-26	Poz-41121	346	plant remains	12640 ± 80	14.42	15.25
	9	K2-27	Poz-41122	354.5	plant remains	(260 ± 80)	-	-
	10	K2-28	Poz-37320	367.5	plant remains	(modern)	-	-
	11	K2-28	Poz-41124	367.5	plant remains	(modern)	-	-
	12	K2-29	Poz-41125	379.5	plant remains	(590 ± 50)	-	-
	13	K2-30	Poz-41126	399	bulk	17340 ± 100	20.28	21.16
LC-1	14	LC-1-12	Poz-30237	13.9	plant remains	795 ± 30	0.673	0.744
	15	LC-1-23	Poz-30238	25.4	plant remains	1515 ± 35	1.33	1.448
LC-2	16	LC-2-15	Poz-30239	14.4	plant remains	1280 ± 30	1.171	1.288
	17	LC-2-29	Poz-30240	30.5	plant remains	1645 ± 30	1.485	1.617
LC-3	18	LC-3-11	Poz-30241	12.4	plant remains	1230 ± 30	1.068	1.189
	19	LC-3-22	Poz-30243	25.4	plant remains	1660 ± 30	1.514	1.628
OC-A	20	OC-A-4	Poz-42943	55	plant remains	4240 ± 30	4.81	4.86
	21	OC-A-8	Poz-42944	113	plant remains	5015 ± 35	5.66	5.77
	22	OC-A-12	Poz-42945	149	plant remains	5440 ± 50	6.18	6.32
OC-B	23	OC-B 64-67	Poz-30244	65.5	plant remains	635 ± 39	0.551	0.666
	24	OC-B 129-145	Poz-30245	137	plant remains	9980 ± 50	11.25	11.63
	25	OC-B 162-183	Poz-30247	167.5	plant remains	6570 ± 40	7.42	7.52
	26	OC-B 225-238	Poz-30248	231.5	plant remains	9930 ± 50	11.23	11.42

3.4.3 Pollen analyses

Twelve samples of the K2 permafrost core were analyzed for pollen. Each sample of two grams of dry sediment was treated for pollen analysis using standard methods of Faegri and Iversen (1989). In total, 51 pollen, spore, and non-pollen palynomorph (NPP) taxa were identified. The microscopic analysis revealed moderately high pollen concentration and good preservation of pollen grains allowing an easy counting of up to 300 terrestrial pollen grains per sample. Percentages of all taxa were calculated based on the total sum of all pollen and spore taxa of higher vascular plants taken as 100 %. A pollen diagram was produced with the Tilia/TiliaGraph software (Grimm, 1991). In the diagram, visual definition of the local pollen zones was supported by CONISS (Grimm, 1987).

3.5 Results

3.5.1 Relief and morphometry

The investigated alas is a single, closed basin of oval shape surrounded by Yedoma uplands (Figure 3-1c). It is about 3.3 km long (N-S) and 2.5 km wide (E-W). One drainage outlet in the southwest discharges the alas via a thermo-erosional valley into the Olenyokskaya Channel. The relief height of the alas as derived from the alas DEM ranges from 19.3 m asl at the drainage valley in the southwest to about 50 m asl at the upper alas slope in the east (Figure 3-3). Mean alas depth is 21.5 m. Elevations of the alas floor, slopes, and surrounding Yedoma uplands are generally lower in the west than in the east. The height difference between the Yedoma uplands adjacent to the eastern and western alas slopes are up to 15 m with maximal heights of about 53 and 38 m asl in the east and west, respectively. This pattern follows the general elevation decline of the surface of Kurungnakh Island as evident from the PRISM DEM derivatives, where the mean slope over the whole Ice Complex extent of Kurungnakh Island (Figure 3-1b) from east to west is 0.05° and the slope around the investigated alas is 0.18° in the WNW direction. The highest elevation of the island, 55 m asl, is located on the Yedoma upland just east of the alas (Figure 3-3).

Three large lakes are situated on the alas floor close to the alas margins in the northwest (Lake 1), east (Lake 2), and south (Lake 3), with areas of 1.7, 0.1, and 0.2 km², respectively (Table 3-2). The lake levels were measured in August 2008 at 21.0, 28.4, and 24.0 m asl, respectively. Lake 1 and Lake 2 have a regular, oval shape with their major axes oriented in N-S directions and an elongation index (major axis / minor axis) of 1.4 and 1.3, respectively. Lake 3 has an irregular shoreline with several small bays and is elongated in the WNW-ESE direction with an elongation index of 1.7. Maximum recorded depth was 3.6 m for Lake 1, 4.2 m for Lake 2, and 4.0 m for Lake 3. These depths exceed the thickness of the maximum ice cover, which can be up to 2 m thick in arctic regions (Jeffries et al., 1996), so the lakes do not freeze to the bottom in winter. The bathymetric profiles revealed differences between the lakes in subaqueous relief. In Lake 1 and Lake 3, a water depth of 1.5 m and more is reached at 40 and 28 m distance from the shore, respectively, except in the small western and eastern bays of Lake 3 where water depth is less than 1.5 m. In Lake 2, these shallow depths occur as far as 130 m from the shoreline. Lake 2 is the smallest and the deepest of the three lakes; its deepest parts (more than 3 m) occur along the major axis and close to the retrogressive thaw slump. The deepest parts of Lake 1 and Lake 3 were recorded in the central part and in the western half, respectively. Direct hydrological connections via distinct beaded streams (i.e. a stream characterized by narrow reaches linking pools or small lakes (van Everdingen, 2005)) exist between Lake 1 and Lake 3 and between each of these lakes and the discharging drainage valley (Figure 3-3). Outflow from Lake 2 into Lake 1 occurs

diffusively over the alas floor through widened polygonal troughs as observed during the field work in 2008. The surrounding Yedoma uplands drain into the alas via several small thermo-erosional gullies that are indented into the alas slopes, except at the steep slope sections without gullies in the west, where the adjacent Yedoma uplands are inclined away from the alas.

Table 3-2. Comparison of morphometric characteristics of the three alas lakes.

	Lake 1	Lake 2	Lake 3
Area (m²)	1,737,357	122,203	239,482
Perimeter (m)	5,168	1,343	2,872
Elongation index (major axis / minor axis)	1.37	1.31	1.69
Orientation (angle between E-W reference axis and major axis, counter-clockwise) (°)	83	92	155
Lake level in August 2008 (m asl)	21.0	28.4	24.0
Maximum recorded depth (m)	3.6	4.2	4.0
Deepest position of lake floor (m asl)	17.4	24.2	20.0

Around Lake 1, two lake terraces exist with their upper borders at 21.7 and 24.1 m asl (Figure 3-3). The lower terrace narrows from north to south and is completely absent at the southernmost part of Lake 1. The upper terrace is broader in the east and south of Lake 1, where it was not restricted by the alas slopes. Lake 3 has one lake terrace with its upper border at 25.0 m asl. The outline of this border is more regular than that of Lake 3 itself. The lake terrace is very narrow in the south, where the shoreline of Lake 3 lies almost at the foot of the alas slope, and merges with the upper terrace of Lake 1 in the area between the two lakes. There, a circular area with a diameter of about 50 m, which is elevated up to 1 m above the surrounding terrace and features distinct vegetation and moisture, is assumed to be an initial pingo. The rest of the alas floor, i.e. the alas floor above the lake terraces, increases in relief height from 25.0 m asl in the west to 32.6 m asl in the east.

The shores of Lake 1 are very flat. In some places a zone of brown, peaty sediments occurs between the lake and the vegetated polygons of the alas floor. On the eastern shore, this material was built up in mounds of up to 40 cm height in summer 2008 (Figure 3-4a). These mounds were probably created from lake ice pushing against the shore. At the beginning of the field campaign, the shoreline was situated within a few meters of the peat mounds. Frequent heavy rain events at the end of August (Muster et al., 2012) obviously contributed a substantial water supply to the lake and led to its areal increase, so that the shoreline approached the peat mounds by the end of the field campaign. At the southern shore of Lake 1, eroding polygons with surfaces well above the lake level are building a small cliff. Here, the lake floor in the littoral zone is characterized by peat mats which are dissected by large cracks (Figure 3-4b). The cracks are about 10 to 20 cm deep and in some places reveal

light-colored, fine-grained sand underneath the peat mats. The lower lake terrace at the western shore is partially submerged, thereby forming several small islands at the lake shore, which makes it hard to clearly define the shoreline (Figure 3-4c).

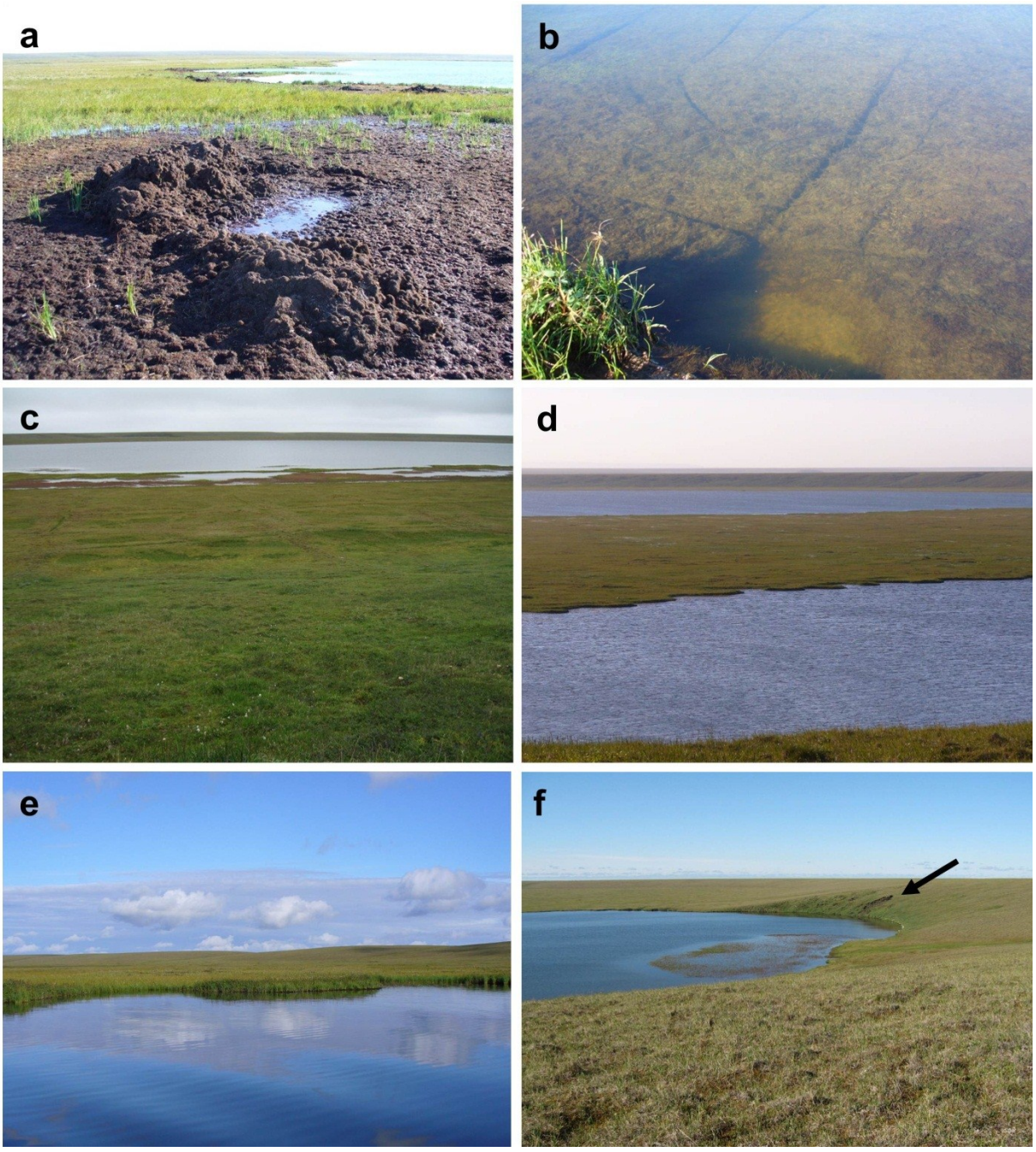

Figure 3-4. Surface characteristics of selected alas elements. **(a**) Peat mounds at the eastern shore of Lake 1 resulting from ice push. View to the south. **(b)** Littoral zone of Lake 1 (southern shore) displays peat mats dissected by large cracks. **(c)** View from the Yedoma uplands west of Lake 1 shows western alas slope, lake terraces with rectangular low-center polygons, and irregular western shoreline of Lake 1. View to the east. **(d)** Eroding polygons at the western shoreline of Lake 2. View from the Yedoma uplands east of Lake 2 to the west; Lake 1 is in the background. **(e)** Northern shoreline of Lake 3 with prominent polygon centers. View to the northeast. **(f)** View from the Yedoma uplands east of Lake 2 to the northwest reveals alluvial fan with belt of aquatic plants and steep slope section with retrogressive thaw slump (black arrow), where the lake cuts into the alas slope.

At the western shore of Lake 2 and around Lake 3 the shoreline traces degrading polygons (Figure 3-4d, e), indicating that these lake shores are not stable and the lakes are expanding. At the location of the OC-A outcrop at the southern shore of Lake 3 close to the southern alas slope, parts of the polygons that are being eroded have slumped into the lake, creating a small cliff with disturbed vegetation cover, which made the deposits accessible for sediment investigations. The lake floor at this location exposes mineral sediments without submerged vegetation or peat.

Lake 1 and Lake 2 prograded into the adjacent alas slopes, thereby interrupting the initial oval alas outline. The angles of the alas slopes are much steeper in these interrupted areas (Figure 3-5a). The slope north of Lake 2 features a retrogressive thaw slump indicating its instability (Figure 3-4f). In August 2008, the thaw slump was about 15 m wide and 50 m long with a headwall of about 2.50 m height. East of Lake 2, the alas slope appears to bulge to the east. A horseshoe-shaped depression segues into a short valley and drains the Yedoma surface into Lake 2. At the valley termination, an alluvial fan is prograding into Lake 2, leading to a displacement of the Lake 2 eastern shoreline by about 10 m over a length of about 60 m. In front of this alluvial fan, a belt of aquatic plants with their upper parts above the water table is visible (Figure 3-4f).

On the southeastern alas side a small lake basin drains into the alas via a broad U-shaped valley. Visual comparison of satellite data from different years and seasons shows that the small basin is sometimes filled with one large lake and sometimes several smaller residual lakes are scattered on the basin floor. In 2008, the small basin contained two irregular, residual lakes, and four ponds were lined up along the valley (beaded drainage). At the termination of the drainage valley, the alas floor is elevated by about 1 m relative to the surrounding surface, which points to the aggradation of an alluvial fan in front of the valley.

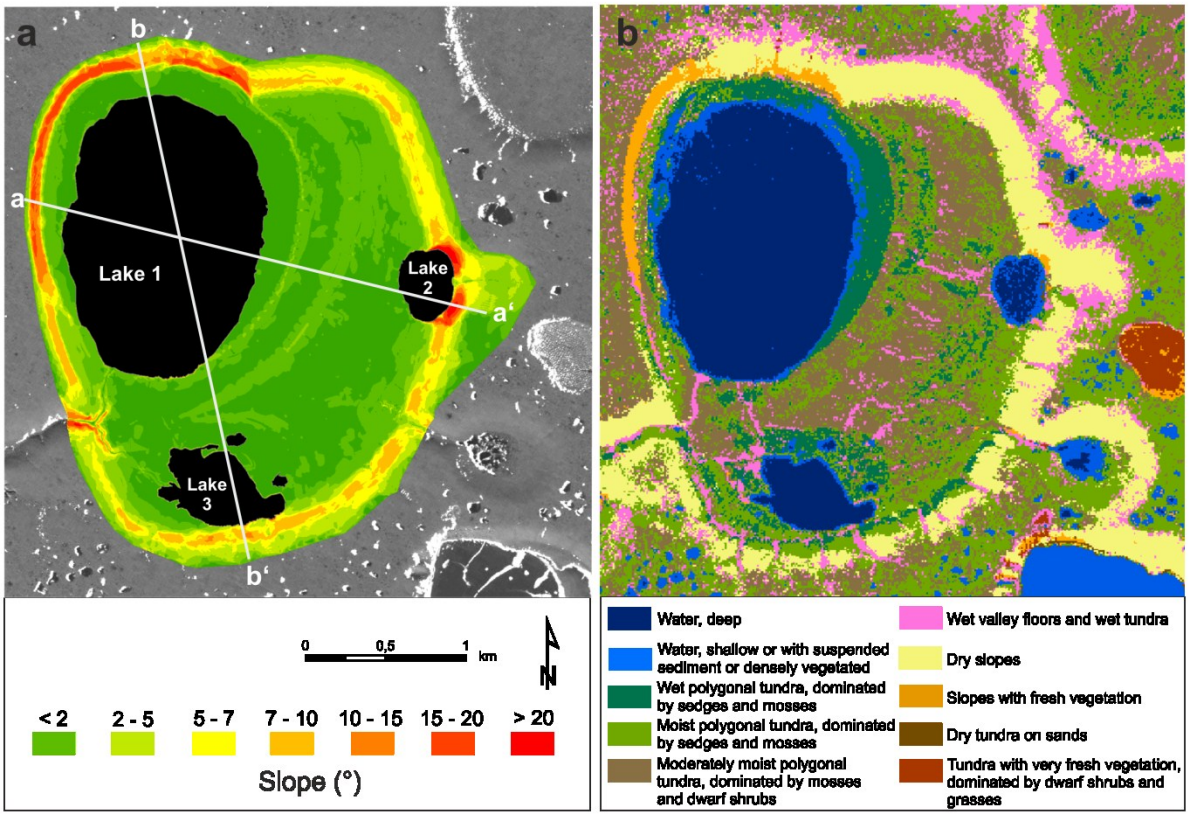

Figure 3-5. Surface characteristics of the alas. **(a)** Slope map derived from the alas DEM. The steepest slope sections indicate unstable slopes after the progradation of Lake 1 and Lake 2 into the initial alas outline. Background image: ALOS PRISM, acquisition date: 21 September 2006. Lines a-a' and b-b' show position of profiles in Figure 3-9. **(b)** Results of the multispectral classification of ALOS AVNIR-2 data (acquisition date: 18 August 2006) adopted from Roessler (2009).

3.5.2 Land cover

Figure 3-5b shows the result of the land cover classification. The shore regions of Lake 1, Lake 2, and Lake 3 are classified as shallow water areas, either loaded with a large amount of sediment or overgrown with *Carex stans* or *Arctophila fulva*. The terrace of Lake 3 and the lower terrace of Lake 1 were assigned to "Wet polygonal tundra, dominated by sedges and mosses". The polygon walls are built by *Sphagnum* sp., and the centers are covered with *Carex stans* (coverage 10 to 50 %). At the shore of Lake 2, this class is completely absent. The upper terrace of Lake 1 and the alas floor are composed of the classes "Moist polygonal tundra, dominated by sedges and mosses" and "Moderately moist polygonal tundra, dominated by mosses and dwarf shrubs". They are intersected by drainage channels of the class "Wet valley floors and wet tundra". The moist polygonal tundra class is characterized by a strong differentiation between the well-drained concave polygonal rims, which are covered by mosses and dwarf shrubs, and the water-filled centers, which are densely covered with sedges. Such wet centers are absent in the class "Moderately moist polygonal tundra …"; only the polygonal troughs are water-filled. The flat or convex polygon surfaces

are covered with mosses and dwarf shrubs (*Salix* sp.). There is a smooth transition between the classes “Moderately moist polygonal tundra …” and “Wet valley floors and wet tundra”, depending on the proportion of wet polygonal troughs and ponds and drainage channels to drier polygon parts; this proportion determines the amount of moisture present, which defines the class. Tall and dense growths of *Eriophorum scheuchzeri* are characteristic of the class „Wet valley floors and wet tundra“. Clearly visible in Figure 3-5b is the class differentiation of the alas floor with increasing distance to the slope. Drainage concentration in polygonal troughs leads to clearly drier surfaces.

The alas slopes and the thermo-erosional valley appear drier than the flat surrounding Yedoma uplands and alas floors, but the steepest slope sections adjacent to Lake 1 and Lake 3 are distinguishable by fresher vegetation, which is dominated by dwarf shrubs, mostly *Salix* sp. The slopes are characterized by hummocks of different heights, mostly covered with *Eriophorum vaginatum*. The numerous thermo-erosional gullies that intersect the slopes are much wetter and were therefore classified as “Wet valley floors and wet tundra”.

The Yedoma surface contains classes similar to those of the alas floor, but shows a larger amount of small overgrown ponds, especially south and east of the alas. The Yedoma surface west of the alas is drier and dominated by the class “Moderately moist polygonal tundra …”. A special feature is the basin of a thermokarst lake on the Yedoma surface east of the alas, which drained a few decades ago (Ulrich et al., 2009) and is characterized by thermokarst mounds and very fresh, dense and tall growths of grasses and dwarf shrubs.

It becomes obvious that some of the distinctive relief units described in chapter 3.5.1 are also characterized by discrete land cover types. The lower terrace around Lake 1 and the terrace of Lake 3 as well as the discharge paths and drainage channels are clearly distinguishable from the rest of the alas floor due to higher surface moisture. The slopes of the thermokarst basins and the thermo-erosional valley appear drier than the flat surrounding Yedoma uplands and alas floors, but the steepest slope sections adjacent to Lake 1 and Lake 3 are distinguishable by fresher vegetation.

Table 3-3 summarizes all morphological elements which compose the investigated thermo-karst landscape in ice-rich permafrost. Their quantitative and qualitative characteristics are described on the basis of field observations and remote sensing and GIS analyses.

Table 3-3. Quantitative and qualitative characteristics of morphological elements of the investigated alas.

Relief element	Areal percentage of study area[a]	Spatial range of individual features	Relief height (m asl)	Microrelief and micromorphology	Vegetation	Spectral characteristics[b]
Lakes	26.7	See Table 3-2	See Table 3-2	-	Hydrophytes, peat mats in littoral zone	Low reflectance, slightly higher in green region, very low in NIR
Lake terraces	53.3	Up to 350 m wide; 0.7 to 2.3 m relief difference	21 to 25	Low center polygons with large polygonal ponds on flat parts, hummocky on gentle slopes	Sedges dominate in low centers, sphagnum on polygon walls	Low reflectance due to open water bodies, very low SAVI values
Alas floor	17.3	-	25 to 32.6	Flat to slightly inclined; moist to wet polygonal tundra	Sedges in polygonal ponds	Moist polygons with highest reflection in VIS; slightly lower reflectance of wet polygons
Pingo	0.7	50 m in perimeter, 1 m high	24.5 to 25.5	Slightly convex elevation with circular base	Dense moss cover with salix shrubs and few grasses	High reflections, high SAVI values due to clearly drier surface on elevated part; wet margin around the base with lower reflectance
Stable alas slopes	22.7	2 to 9°	22 to 50	Low profile curvature, flat and more rectilinear	Dense moss and dwarf shrub coverage, hummocks with *Eriophorum*	Driest surfaces, high reflectance and high SAVI values
Unstable alas slopes	2.5	9 to 29°	24 to 50	Very convex upper slope sections, very concave lower slope sections, end sharply on alas floor	Tall growths of dwarf shrubs and grasses, very fresh vegetation	Dry surfaces, densely vegetated, highest SAVI values

Continuation of **Table 3-3.** Quantitative and qualitative characteristics of morphological elements of the investigated alas.

Relief element	Areal percentage of study area[a]	Spatial range of individual features	Relief height (m asl)	Microrelief and micromorphology	Vegetation	Spectral characteristics[b]
Retrogressive thaw slump	0.008	15 m wide, 50 m long, headwall 2.5 m high	29 to 40	Concave profile curvature, slope movement, disturbed vegetation cover	-	Not distinguishable as individual feature in ALOS AVNIR-2 data
Thermo-erosional gullies in the alas slopes	-	120 to 200 m long	21 to 50	Higher frequency of deep gullies in stable alas slopes	Tall and densely growing grasses and sedges, moss interspersed	High NIR reflectance, high SAVI values
Inflowing valleys	n.d.	370 to 525 m long, 150 to 300 m wide	28.4 to 53	U-shaped cross profile, slightly concave slopes	Densely vegetated floors (*Eriophorum*, grasses), hummocky slopes with mosses and dwarf shrubs	Dry slopes with high reflectance, floors with high SAVI values
Outflowing valley	n.d.	4.3 km long	19 to 32	V-shaped cross profile	Grasses and salix shrubs	High reflectance
Beaded streams	n.d.	370 to 600 m long	19 to 24	Small streams connecting pools of open water	Densely vegetated channels (*Eriophorum*)	High reflectance, highest SAVI values
Yedoma uplands	2.7	-	38 to 55	Flat or slightly inclined, polygonal tundra	Moist polygons with mosses and dwarf shrubs	high reflectance

[a] The study area reference for this table is the extent of the alas DEM (Figure 3-3), which has an area of 7.5 km².

[b] Based on Roessler (2009).

3.5.3 Core and exposure records

Permafrost core K2

The K2 permafrost core contains three lithological units as inferred from the results of grain size and OM analyses (Figure 3-6a):

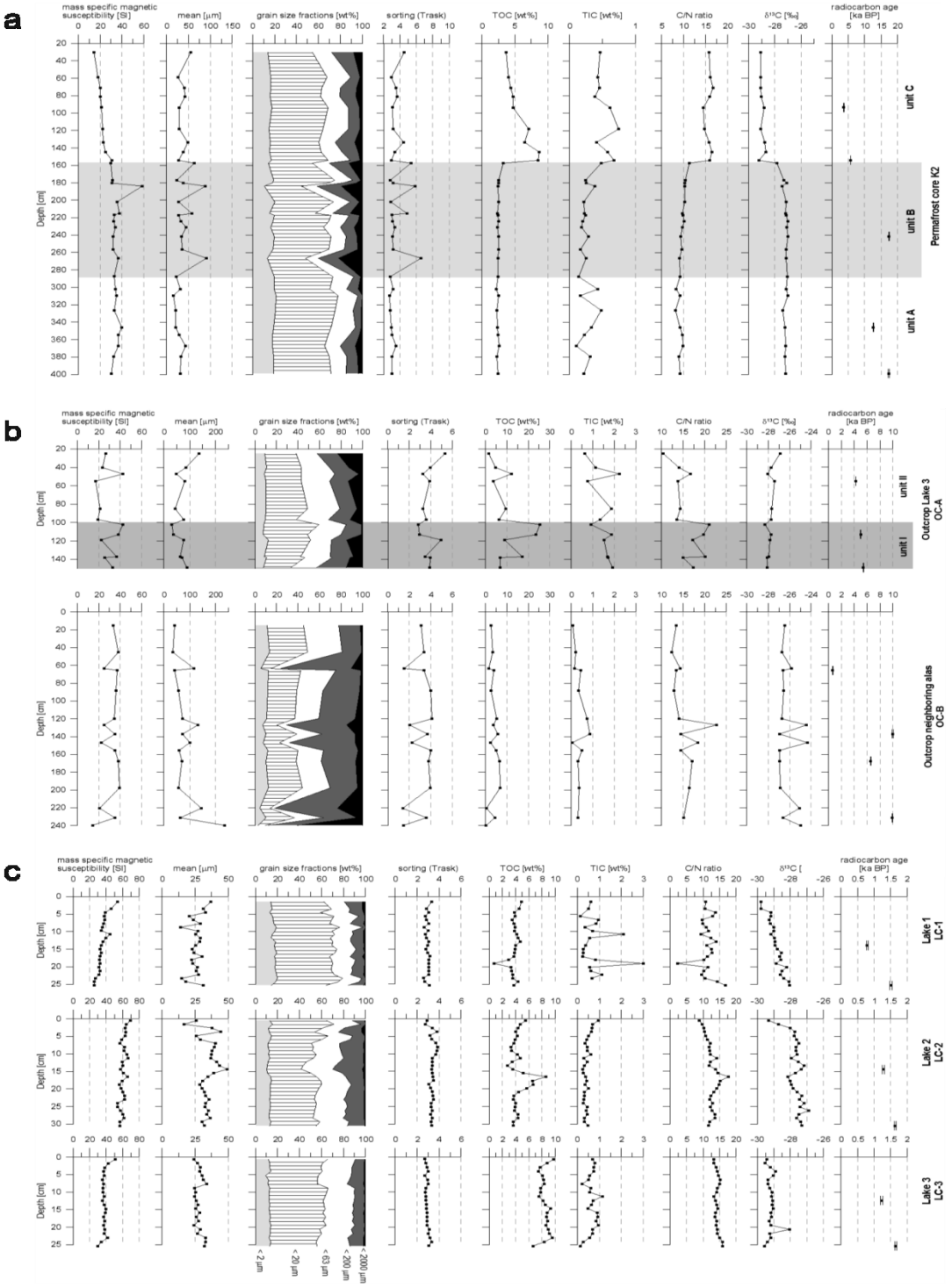

Figure 3-6. Comparison of the sedimentological, biogeochemical, and geochronological records of the study site. **(a)** Permafrost core K2, **(b)** outcrops OC-A and OC-B, **(c)** short cores of Lake 1, Lake 2, and Lake 3. Note changing scale ranges of some of the parameters.

The lower unit A (400 to 285 cm depth) is dominated by consistent fine-sandy silt with a mean grain size between 20 and 43 µm and a sorting degree of 2.7 to 3.5. The OM data are also consistent with TOC contents between 2.2 and 2.6 wt%, C/N ratios of 8.1 to 9.9, and $\delta^{13}C$ values between -27.4 and -27.0 ‰. The total inorganic carbon (TIC) content varies between 0.1 and 0.5 wt%. At a depth of 346 cm, Ephippia (water flea eggs) were found and at a depth of 370 cm, ostracod shells (2 x *Cytherissa lacustris* adult, 1 x *Cytherissa lacustris* juvenile, and some ostracod fragments). This holarctic distributed ostracod species is common in thermokarst deposits of late Quaternary interstadial or interglacial periods. Regionally, it was found in last interglacial and Lateglacial-Holocene permafrost sequences at the Oyogos Yar coast and on Bol'shoy Lyakhovsky Island (Dmitry Laptev Strait) (Wetterich et al., 2009; Kienast et al., 2011). Radiocarbon dates for unit A are of Lateglacial age (17,340 ± 100 a BP at 399 cm depth and 12,640 ± 80 a BP at 346 cm depth) (Table 3-1).

Unit B (285 to 155 cm depth) differs from unit A only in its considerably varying grain size parameters. Mean grain size of the silt and sandy silt varies from 23 to 92 µm and the sorting degree from 2.8 to 6.6. OM is similarly composed as in unit A with TOC contents between 2.4 and 3.2 wt%, C/N ratios of 9.1 to 11.3, and $\delta^{13}C$ values between -27.9 and -27.0 ‰. TIC content varies between 0.2 and 0.5 wt%. One radiocarbon date of 17,390 ± 100 a BP was obtained at 241.5 cm depth (Table 3-1).

There is a distinct change in OM characteristics at about 155 cm depth. Therefore, the upper part of the core (155 to 0 cm depth) is separated as unit C. TOC contents and C/N ratios are higher (3.2 to 8.7 wt% and 14.4 to 16.7, respectively), reflecting less intense OM decomposition, while lower $\delta^{13}C$ values between -29.2 and -28.7 ‰ are probably also caused by changes in the plant community composing the OM. TIC is slightly higher than in units A and B, varying between 0.4 and 0.7 wt%. Grain size parameters show a similar consistent pattern as in unit A with sandy silts having a mean grain size between 27 and 55 µm and a sorting degree of 2.9 to 4.5. Radiocarbon ages in unit C belong to the middle (5660 ± 50 a BP at 154 cm depth) and late Holocene periods (3620 ± 35 a BP at 93.5 cm depth) (Table 3-1).

Changes in pollen and spore taxa composition and abundances led to a subdivision of the K2 permafrost core into three pollen zones (PZs) (Figure 3-7). The border between the upper two PZs coincides with the border between units B and C described above.

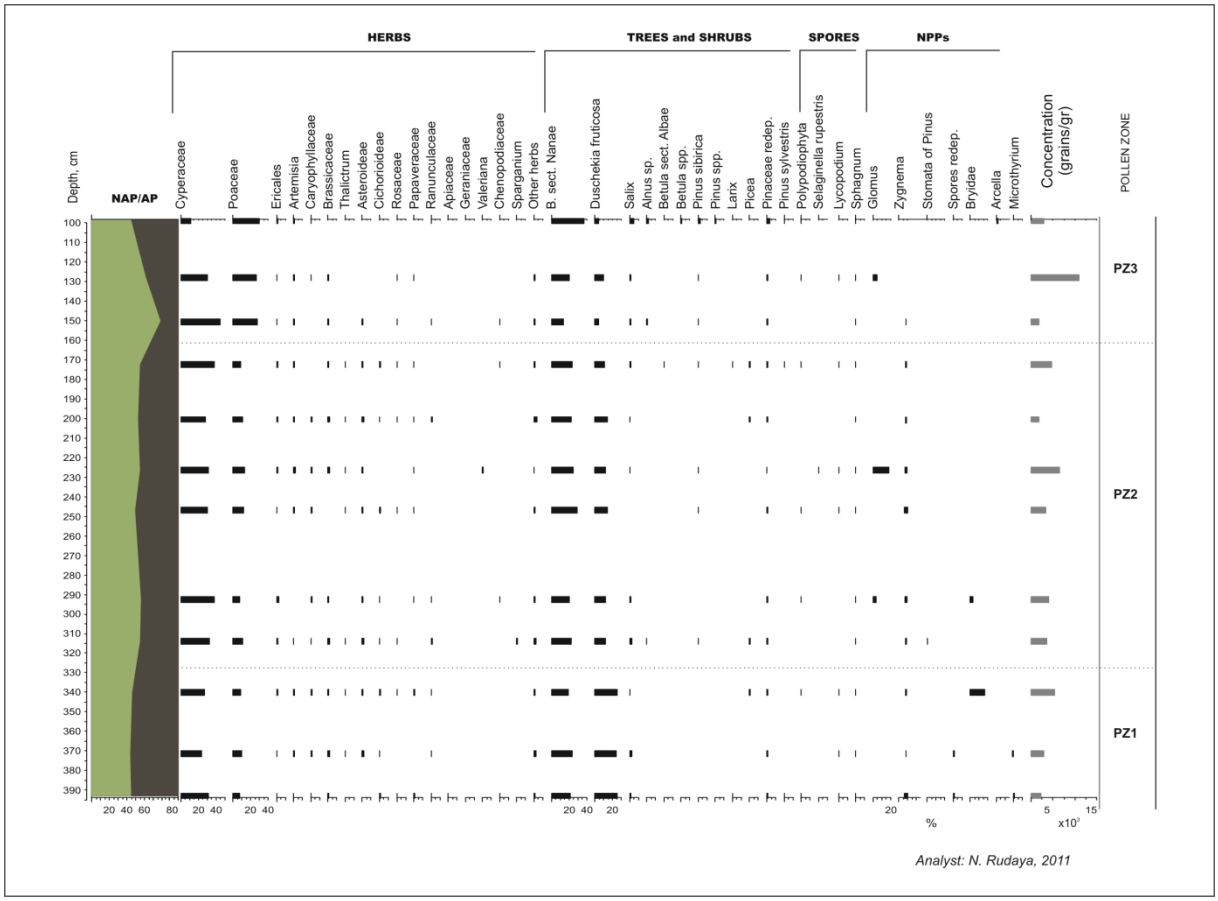

Figure 3-7. Pollen diagram of the K2 permafrost core drilled on the alas floor. Note that the pollen record starts at 100 cm depth (NAP: non-arboreal pollen, AP: arboreal pollen).

PZ 1 (400 to 330 cm) is characterized by the dominance of *Duschekia fruticosa*, *Betula* S. *Nanae,* and Cyperaceae. This zone reveals the highest percentages of arboreal pollen taxa owing to high abundances of dwarf alder and birch pollen. The spectral composition of this pollen zone suggests the spread of shrubby tundra with *Duschekia fruticosa* and *Betula* S. *Nanae* in the region.

PZ 2 (330 to 155 cm) is noticeable for a decrease of *Duschekia fruticosa* pollen. Dominating taxa of PZ 2 are Cyperaceae and *Betula* S. *Nanae*. These changes may reflect a change to colder and drier climate, resulting in the disappearance of dwarf alder.

Distinctive features of PZs 1 and 2 are the continuous presence of the cosmopolitan green algae family Zygnemataceae (*Zygnema*-type) spores. Algae prefer stagnant, shallow, and mesotrophic freshwater habitats (van Geel and van der Hammen, 1978) or fluvial surface sediment (Medeanic, 2006); their presence indicates the occurrence of lacustrine sediments.

PZ 3 (155 to 100 cm) exhibits a significant increase of Poaceae pollen abundances accompanied by a dominance of Cyperaceae and *Betula* S. *Nanae* pollen. Pollen specta of PZ KS3 suggest grass tundra distribution.

Outcrops OC-A and OC-B

The OC-A outcrop at the southeastern shore of Lake 3 revealed 1.6 m of unfrozen deposits (Figure 3-8a). The permafrost table was located at 160 cm and water accumulated at 155 cm depth. The deposits are characterized by sandy silt with a mean grain size between 64 and 137 µm and a sorting degree of 2.8 to 5.3 (Figure 3-6b). A noticeable change occurs in the OM characteristics at 100 cm depth. The profile is therefore divided into the lower unit I and the upper unit II. TOC contents and C/N ratios are considerably higher in unit I (6.8 to 25.4 wt% and 15.0 to 21.1, respectively) than in unit II (1.6 to 12.2 wt% and 10.4 to 16.8, respectively). $\delta^{13}C$ values are slightly more negative in the lower than in the upper part of the profile (-28.3 to -27.8 ‰ and -28.1 to -26.9 ‰, respectively). TIC contents vary throughout the whole profile between 0.6 and 2.2 wt%. Radiocarbon dates show increasing middle to late Holocene ages from 5440 ± 50 to 5015 ± 35 to 4240 ± 30 a BP at 149, 113, and 55 cm depth, respectively.

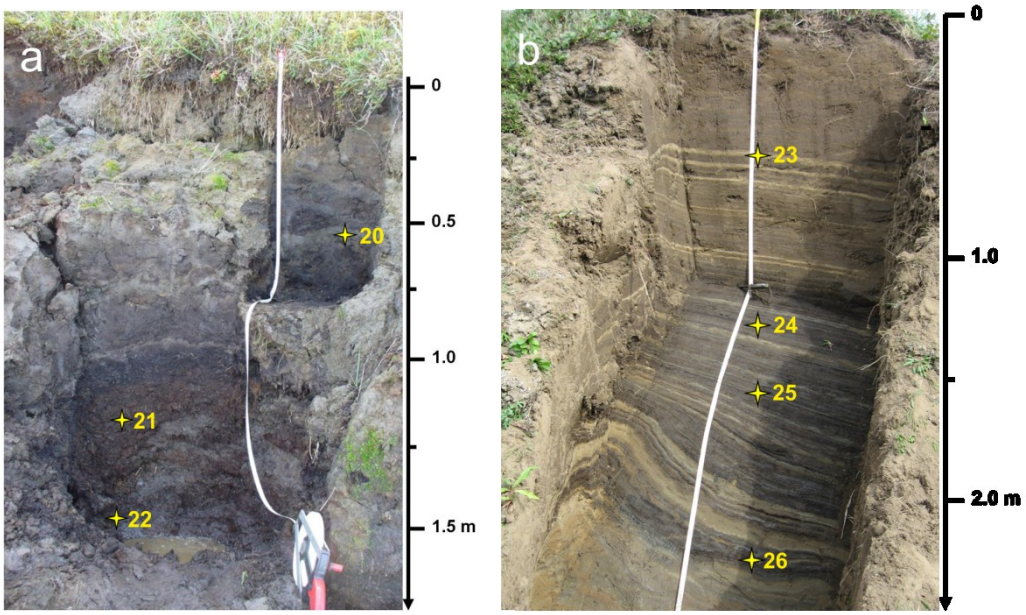

Figure 3-8. Outcrops studied for stratigraphical reconstructions. **(a)** Outcrop OC-A at the southern shore of Lake 3. The 160 cm deep profile is composed of two overlapping sections and was accessible from the shallow water. **(b)** Outcrop OC-B in the neighboring alas. The 320 cm deep profile is located at the upper slope of a thermo-erosional valley, which cuts about 10 m deep into the alas floor and drains the alas into the Olenyokskaya Channel. The lower part of the profile (115 to 320 cm) was perennially frozen with the permafrost table bending subparallel to the slope angle. Yellow stars indicate the location of samples with AMS dates used for geochronological interpretation, numbers correspond to No. in second column of Table 3-1.

Outcrop OC-B exposed unfrozen deposits in the upper 115 cm, while the lower section down to 320 cm depth diagonally followed the permafrost table (Figure 3-8b). The fine layering of darker and lighter sediments could not be resolved in the sampling process. Therefore, the results of the laboratory analyses (Figure 3-6b) represent the integral characteristics of

several layers. The deposits consist of sandy silt and silty sand with a mean grain size between 35 and 236 µm and a sorting degree of 1.4 to 4.1. TOC and TIC contents are constantly low (0.2 to 6.9 wt% and 0.1 to 0.9 wt%), but the C/N ratios and $\delta^{13}C$ values vary greatly (between 12.4 and 22.8 and between -26.9 and -24.3 ‰, respectively). Radiocarbon dating results show Lateglacial/early-Holocene ages at the 231.5 and 137 cm depths (9930 ± 50 and 9980 ± 50 a BP, respectively), a mid-Holocene age at the 167.5 cm depth (6570 ± 40 a BP), and a late-Holocene age at the 65.5 cm depth (635 ± 39 a BP) (Table 3-1). The fine layering of the deposits and the position of the outcrop at the slope of a valley cutting into the alas floor indicate the lacustrine origin of the deposits.

Short lake cores LC-1, LC-2, and LC-3

The sediments of Lake 1 are characterized by silt and fine sandy silt with a mean grain size between 14 and 37 µm and a sorting degree of 2.6 to 3.3 (Figure 3-6c). MS increases from 25 SI at the bottom to 37 SI at the top of the short core. TOC content and the C/N ratio vary between 0.7 and 4.9 wt% and 2.3 and 16.9, respectively. TIC content shows a high variability between 0.1 and 3.0 wt%. $\delta^{13}C$ values gradually decrease from -28.1 ‰ at the bottom to -29.8 ‰ at the top. Radiocarbon dates reveal a late Holocene age of the deposits (1515 ± 35 and 795 ± 30 a BP at the 25.4 and 13.9 cm depths, respectively) (Table 3-1).

The short core of Lake 2 reveals slightly coarser sediments (predominantly sandy coarse silt) with mean grain sizes between 17 and 49 µm and a sorting degree of 2.7 to 3.9 (Figure 3-6c). Magnetic susceptibility is comparatively high (between 54 and 70 SI). TOC contents and C/N ratios vary between 2.8 and 8.6 wt% and 8.9 and 15.2, respectively. TIC contents are constantly low (0.2 to 0.9 wt%). $\delta^{13}C$ values are higher than in Lake 1 (between -29.3 and -26.9 ‰). Radiocarbon ages are late Holocene (1645 ± 30 and 1280 ± 30 a BP at the 30.5 and 14.4 cm depths, respectively) (Table 3-1).

Sediments of Lake 3 are composed of sandy silt with mean grain sizes between 24 and 34 µm and a sorting degree of 2.7 to 3.3 (Figure 3-6c). MS shows little variation and ranges from 30 to 51 SI. TOC contents and C/N ratios are the highest among all three lake cores (6.6 to 9.7 wt% and 13.2 to 16.0, respectively) and $\delta^{13}C$ values are constantly low (-29.6 to -28.1 ‰). TIC contents are between 0.1 and 1.1 wt%. Radiocarbon datings at the 25.4 and 12.4 cm depths show similar late Holocene ages (1660 ± 30 and 1230 ± 30 a BP) as retrieved from Lake 2 (Table 3-1).

3.6 Discussion

3.6.1 Morphostratigraphy

The different relief levels with their specific surface characteristics and periglacial morphostructures (chapters 3.5.1 and 3.5.2, Table 3-3) provide the basis for a morphostratigraphical classification of the considered thermokarst landscape (Figure 3-9).

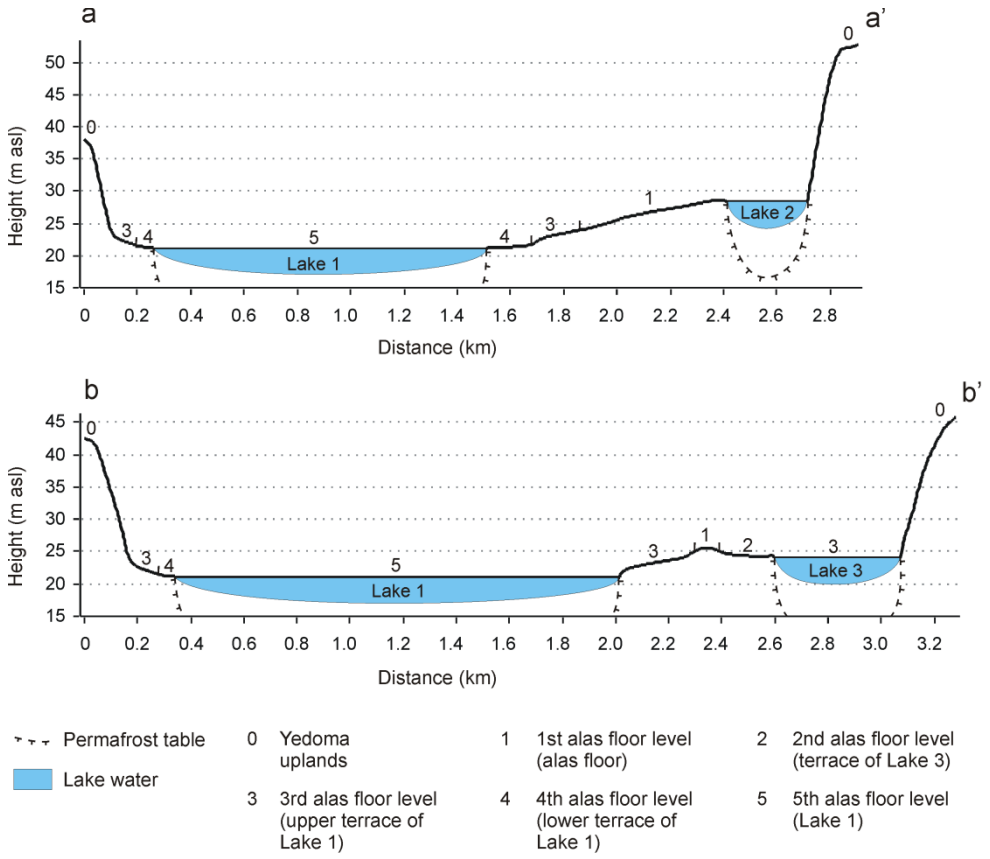

Figure 3-9. Morphostratigraphical levels of the thermokarst landscape on the basis of relief profiles through the alas (for position see Figure 3-5a). The surface profile lines were derived from the alas DEM. Lake profiles are schematic with maximum depths from bathymetric measurements. The position of the permafrost table is hypothetical, based on modeling studies in similar thermokarst lake environments (West and Plug, 2008).

The highest and oldest level is the surface of the Yedoma uplands, which has elevations between 36 and 55 m asl around the alas, but declines down to 20 m asl at the western and northern margins of the Ice Complex extent on Kurungnakh Island. This level represents the erosional remnants of a former accumulation plain in front of the Chekanovsky Ridge (Schirrmeister et al., 2011a). This slightly inclined plain is considered to be the initial situation of the regional thermokarst history. The next morphostratigraphical level is the alas floor at about 25 to 32 m asl outside the lake terraces (Figure 3-3). It represents the lake bottom of the initial thermokarst lake, which resulted from thawing and subsidence of the Ice Complex surface and created a uniform closed basin. Lake 2 is also located on this level. The terraces around Lake 1 and Lake 3 as well as the current Lake 1, Lake 2, and Lake 3 with

their lake floors reflect further thermokarst stages that proceeded on the initial alas floor and led to a stronger differentiation of the thermokarst basin. Each terrace is indicative of a separate thermokarst lake stage. Therefore, the terrace around Lake 3 (24.2 to 25.0 m asl), the upper terrace of Lake 1 (21.8 to 24.1 m asl), the lower terrace of Lake 1 (21.0 to 21.7 m asl), and Lake 1 itself (21.0 m asl) can be considered the second, third, fourth, and fifth alas floor levels, respectively. Lake 3 (24.0 m asl), its drainage channels, and the lower areas adjacent to these channels are located at the same level as the upper terrace of Lake 1 (Figure 3-3) and can thus be assigned to the third alas floor level.

Further morphostratigraphical relief forms concern the stronger dissection of the alas floor levels as well as the wide dry alas slope zone along the southern and eastern alas rim by drainage pathways and thermo-erosional gullies. They are easily distinguishable by their wet floors (Figure 3-5b). The degrading lake shorelines and the active retrogressive thaw slump north of Lake 2 (Figure 3-4f) also belong to the modern morphostratigraphical class, which reflects local permafrost degradation. Micro-relief structures like ice-wedge polygon systems on each terrace level as well as the small pingo elevation on the lake terrace of Lake 3 represent the youngest structures that are connected with modern permafrost aggradation.

3.6.2 Lithostratigraphy

A general stratigraphy including source deposits and thermokarst derivatives will be established using core records and exposure studies on Kurungnakh Island inside and outside of the alas area (Figure 3-3). The records from the K2 permafrost core, two outcrop sequences (OC-A, OC-B), and three short cores of lake deposits (LC-1, LC-2, LC-3) (chapter 3.5.3) completed by published data sets cover several stages of thermokarst history.

The late Pleistocene Ice Complex unit with its high ice content provided the preconditions for the extensive thermokarst processes that led to the formation of the large and deep alasses on Kurungnakh Island. This Ice Complex is still present in the inter-alas areas above heights of 15 to 20 m asl and was investigated in detail at the eastern margin of the Island where it is exposed at a steep cliff (Schwamborn et al., 2002b; Schirrmeister et al., 2003, 2011a, 2011c; Wetterich et al., 2008). The Ice Complex deposits consist of poorly-sorted silt to fine sand, peat, and peaty paleosol layers with a mean grain size between 35 and 175 µm. They have a high gravimetric ice content (38 to 133 wt%) and contain syngenetic ice wedges, which are several meters wide and up to 20 m tall. The deposits show highly varying TOC contents (1.1 to 11.7 wt%), C/N ratios (5.2 to 23.2), and $\delta^{13}C$ values (-29.5 to -25.1 ‰). The wide range in the latter two reflects variable degrees of OM decomposition and changes in vegetation composition. In general, lower C/N ratios in combination with higher $\delta^{13}C$ values are indicative of a higher degree of OM decomposition (Pfeiffer and Janssen, 1994).

Radiocarbon datings from Kurungnakh Island revealed a continuous Ice Complex deposition between about 50 and 32 ka BP (interstadial) and a second accumulation period around 17 ka BP (stadial).

The mineral and organic components of the late Pleistocene Ice Complex unit are the sediment source for the deposits that accumulate in the thermokarst depression. Due to thawing and ground-ice loss during the initial thermokarst development, the Ice Complex sediments were compacted and partly deformed at the bottom of the developing depression and form the lowest lithostratigraphical thermokarst unit (Kaplina, 2009; Wetterich et al., 2009). These so-called taberites can be several meters thick depending on their original ice content and the basin depth (Ulrich et al., 2010). Unfortunately, they are not captured in the records of this study; neither is the base of the overlying lithostratigraphical unit of Lateglacial to early Holocene thermokarst lake deposits.

With the formation of the initial thermokarst lake, lacustrine sediments started to accumulate on the lake floor on top of the taberites. The lacustrine lithostratigraphical unit also incorporates reworked Ice Complex material, because sedimentation in growing thermokarst lakes occurs to a large degree due to the abrasion of lake shores (Romanovskii, 1961). This is reflected in the fine-layered deposits of outcrop OC-B (Figure 3-8b). Despite the fact that they are completely assigned to the lacustrine lithostratigraphical unit, they show highly variable sedimentological and biogeochemical characteristics (chapter 3.5.3, Figure 3-6b) that are partly comparable to those of the Ice Complex deposits. The high sand content of OC-B compared to all other records is consistent with the mean grain-size values found in the lower Ice Complex deposits by Wetterich et al. (2008), but the very high mean grain size and the sand fraction of the lowest OC-B sample is more likely to have originated from the fluvial sand unit below the Ice Complex (chapter 3.3, Figure 2-2). According to DEM analyses, the floor of this alas and the valley with the OC-B outcrop are located at the same relief heights as the boundary between fluvial sands and overlying Ice Complex deposits as reported from a cliff section further north (e.g., Wetterich et al., 2008).

The incorporation of older material from the surrounding Ice Complex into the lake sediments can also lead to biased radiocarbon ages in the lacustrine records. The oldest age for the OC-B section of 9980 ± 50 a BP was obtained for the sample at 137 cm depth and does not fit into the chronology of the profile (Table 3-1, Figure 3-6b). It was sampled from a dark layer with the highest TOC content (Figure 3-6b, 3-8b), which could have originated from peat inclusions in the Ice Complex that would yield older radiocarbon dates than the date of the actual deposition time in the lake profile. However, the early Holocene dates at 231.5 and 167.5 cm depths (9930 ± 50 and 6570 ± 40 a BP) are consistent with other reports

on thermokarst dates in north Siberian coastal lowlands (e.g. Kaplina, 2009). The radiocarbon age at 65.5 cm depth indicates that the lake had existed during the Holocene at least until 635 ± 39 a BP before it rapidly drained into the Olenyokskaya Channel.

For the studied alas basin, the Lateglacial/early Holocene lacustrine lithostratigraphical unit is disclosed in the lower part of the K2 permafrost core. While units A and B (and pollen zones PZ 1 and 2) are interpreted to be lake deposits, probably with changing accumulation conditions in unit B, the organic-rich upper part (unit C, PZ 3) is considered to be subaerial boggy deposits. The strong shift in TOC contents, C/N ratios, and $\delta^{13}C$ values at 155 cm depth points to an abrupt change in depositional conditions, from lacustrine to terrestrial. The radiocarbon age of 5660 ± 50 a BP at 154 cm depth suggests that the change from lacustrine to terrestrial depositional conditions occurred prior to this time. In a terrestrial environment, OM is produced mainly by vascular plants that have high C/N ratios; the presence of nonvascular aquatic plant material with low C/N values lowers the overall C/N signal in the lacustrine sediments (Meyers, 1994). The $\delta^{13}C$ values of terrestrial and aquatic plant material are similar in permafrost regions, because the terrestrial vegetation is composed mainly of C3 plants, which have similar $\delta^{13}C$ values as lacustrine algae (Meyers, 1994). Therefore, a change in $\delta^{13}C$ values in permafrost environments is attributed to a changing amount of decomposition (Pfeiffer and Janssen, 1994). Consistently lower TOC contents and higher $\delta^{13}C$ values in the lower core can be explained by less accumulation of OM in the center of a deep thermokarst lake in relation to terrestrial or littoral environments and more continuous decomposition of the available biomass, because the lake bottom stays unfrozen year-round. Under subaerial conditions, the produced OM is available for decomposition only during the short summer in the active layer. During syngenetic permafrost aggradation on the alas floor and the rising of the permafrost table, the lower parts of the terrestrial deposits also become perennially frozen, thereby preserving the OM from further decomposition. The pollen and non-pollen composition supports this change from a lacustrine to a terrestrial environment, because of the high abundance of green algae in PZ 1 and PZ 2 that are absent above 155 cm depth and which reflect lake conditions. In addition, the high abundances of non-aquatic grass instead of sedge pollen in the upper zone can be indirect evidence of the change from lacustrine to terrestrial conditions. The occurrence of Ephippia and lacustrine ostracods at 346 and 370 cm depth also supports the presence of a large thermokarst lake during the deposition of the lower core sediments. The considerably varying grain-size parameters in the middle part of the core reflect bedded deposits formed by varying sediment input during the lake phase, which could indicate strong variations of hydrological conditions.

The earliest phase of thermokarst initiation in North Siberian coastal lowlands has been assigned to the 13 to 12 ka BP interval (Bølling interstadial) (Romanovskii et al., 2000; Kaplina, 2009). The radiocarbon age from unit A of 12,640 ± 80 a BP fits into this interval. The older ages of units A and B (17,340 ± 100 and 17,390 ± 100 a BP) are interpreted to result from the relocation of older material from the adjacent Ice Complex deposits during active thermokarst development and lateral expansion of the initial lake as described above for outcrop OC-B in the neighboring alas. The thickness of the lake sediments and the size of the alas, which is much larger than the neighboring alas where outcrop OC-B is located and the lowest sample is dated 9930 ±50 a BP, indicate that the onset of the thermokarst process of the main alas falls into the starting phase of the regional thermokarst development at 13 to 12 ka BP.

The stronger variations in the sediment characteristics of the OC-B outcrop compared to the lacustrine part of the K2 permafrost core can be explained not only by higher variation of the surrounding Ice Complex deposits, but also by the position of the sample sites in the corresponding alas. While outcrop OC-B is located very close to the alas margin, the K2 core is situated in the central part of the alas (Figure 3-3). During phases of active abrasion, the deposits surrounding the alas were eroded and accumulated on the lake floor. The high wave activity, which occurs in large lakes, led to the redistribution of the accumulating sediments on the lake floor (Simova, 1964), resulting in a mixing of sediments from different sources, which should be more pronounced in the lake center, thereby leveling strong differences in sediment characteristics.

The next lithostratigraphical unit is made up of mid-to-late-Holocene boggy deposits, and is represented in unit C of the K2 core and in unit II of the OC-A outcrop at the southern shore of Lake 3. In the K2 core, the terrestrial record continues up to the top of the core. This and the covering peat layer indicate that at the position of the core the alas floor has been continuously exposed since at least 5660 ± 50 a BP. In contrast, the profile of the OC-A outcrop is interpreted to reveal boggy deposits in lower unit I and lacustrine sediments in upper unit II. The OM characteristics of unit I (higher TOC contents and C/N ratios and lower $\delta^{13}C$ values) reflect a higher bioproductivity, plant composition with a higher amount of vascular plants, and a lower degree of decomposition of the OM compared to the upper unit II. In analogy to the K2 core, a change from terrestrial in the lower to lacustrine depositional conditions in the upper part of the profile is inferred from the change in OM characteristics at 100 cm depth. The considerable variations of sediment and OM characteristics within both units of OC-A can be explained by the position of the outcrop at the present shore of Lake 3 and very close to the southern alas slope, which suggests a dynamic environment

involving sediment input due to slope processes and possibly a changing moisture regime during boggy conditions. The radiocarbon ages retrieved from the OC-A outcrop are all younger than the drainage time of the alas prior to 5660 ± 50 a BP, which was inferred from the K2 core. Therefore, the two mid-Holocene ages of the terrestrial unit I (5440 ± 50 and 5015 ± 35 a BP) in OC-A show that the drainage of the alas also affected the southern part of the alas basin where the outcrop is located. However, the alas floor was only exposed for several hundred years or a millennium at most here, because the terrestrial deposits are overlain by the lacustrine deposits of unit II, which yielded a late Holocene radiocarbon age of 4240 ± 30 a BP at 55 cm depth.

Late Holocene lake deposits can therefore be distinguished as the youngest lithostratigraphical unit. In addition to unit II in outcrop OC-A, they are also represented in the three short cores of Lake 1, Lake 2 and Lake 3. The short lake cores have a maximum depth of 31 cm and do not reach the base of the lacustrine deposits. However, the similar radiocarbon ages for the lowest core sections of about 1.5 ka BP (Table 3-1) prove the continuous existence of these lakes at least during this time period. The lake phase surrounding the modern Lake 3, which is represented in the lacustrine deposits in outcrop OC-A, must have started between 5015 ± 35 and 4240 ± 30 a BP.

The three lake cores and the lacustrine unit II of outcrop OC-A show large differences in sediment and OM characteristics (Figure 3-6). Unit II reveals much coarser grain sizes than the lake sediment cores, and among the present lakes, Lake 2 shows coarser grain sizes than Lake 1 or Lake 3. This might be explained by the close proximity of the outcrop and Lake 2 to the alas slope and their erosional impact on the Ice Complex deposits, which contain silty sands. The cores of Lake 1 and Lake 3 are situated further away from the alas margins. Coarser grain sizes are not transported as far as fine sediment particles and therefore the coarser material is less represented in the LC-1 and LC-3 cores. The OM characteristics of Lake 3 significantly differ from the other late Holocene lacustrine records. Lake 3 shows consistently higher TOC contents and C/N ratios and lower $\delta^{13}C$ values, which reflect a higher bioproductivity and a lower degree of decomposition of the OM. LC-1 shows decreasing $\delta^{13}C$ values from bottom to top while TOC contents and C/N ratios stay relatively constant throughout the core, which might indicate a shift in the plant association composing the OM. LC-2 reveals the highest $\delta^{13}C$ values of all late Holocene lacustrine records while TOC contents and C/N ratios are in similar ranges as in LC-1. This again could be due to a different plant association compared to the vegetation that composes the OM of the other two lakes.

3.6.3 Thermokarst evolution

The morphostratigraphical levels and lithostratigraphical units reflect different stages of thermokarst development (Figure 3-10).

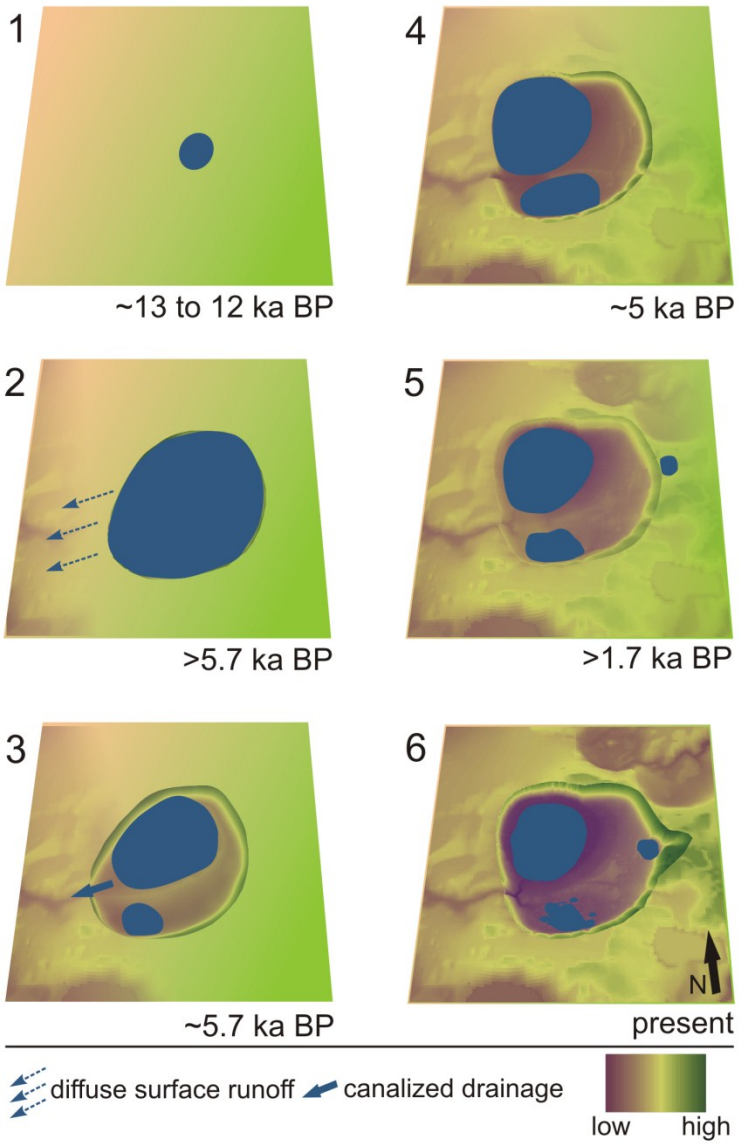

Figure 3-10. Stages of thermokarst lake and basin development (color scale represents relative terrain gradient). **1** Formation of initial thermokarst lake in Ice Complex deposits. **2** Primary thermokarst lake has reached its maximum extent. **3** Partial drainage of the primary thermokarst lake through thermo-erosional valley. Two smaller lakes remain in the western basin part; permafrost starts to aggrade on the alas floor. **4** Expansion of the residual lakes and modification of northwestern alas slope. **5** Partial drainage of residual lakes and formation of lake terraces. **6** The evolved modern alas morphometry resulted from a further modification of the northwestern alas slope, another partial drainage of Lake 1 and the exposure of its lower terrace, and the formation of Lake 2 and the small pingo.

The beginning of thermokarst evolution in the region was triggered by a significant change to warmer and moister climate conditions around the late Pleistocene/Holocene boundary (Kuzmina and Sher, 2006; Kaplina, 2009). This regional change was locally expressed in the formation of a primary thermokarst lake on the Yedoma surface during that time (Figure 3-10.1). This lake expanded in area and depth, and lacustrine sediments started to accumulate on the lake floor. When the lake depth exceeded the thickness of the winter ice cover, a talik developed underneath the lake. The lake floor subsided by more than 20 m into the Ice Complex deposits, because these were thawed completely, and the previous high ice content of the deposits led to a large volume loss. Modeling results showed that Ice Complex deposits of 40 m thickness will completely thaw in 1600, 2050, or 2300 years depending on their volumetric ice content of 60, 80, or 90 %, respectively (Tumskoy, 2002). The lateral expansion of the initial lake was more pronounced in the NNE-SSW direction, which led to its elongation in the N-S extent of the present day alas (Figure 3-10.2).

About 5.7 ka BP the primary thermokarst lake partially drained and thereby formed the alas basin (Figure 3-10.3). The drainage occurred through a large thermo-erosional valley in the southwest that discharges into the Olenyokskaya Channel. The drainage path can be dissected into three valley sections from the alas margin to the Olenyokskaya Channel. The first section is about half a kilometer long and is directed from ENE to WSW (Figure 3-3). The second section is a valley, which is about 3.8 km long and follows a straight course from SE to NW (Figure 3-1b). It encounters the third section at a 90 degree angle. The third section belongs to a large valley, which is directed from NE to SW and drains into the Olenyokskaya Channel. The second section probably evolved independently from the thermokarst lake as a branch of the large valley due to retrogressive erosion of the polygonal Yedoma surface along ice-wedges in the direction of the southern lake margin. The lake itself may have experienced outflow via small outflow bands over the Yedoma surface in the direction of the relief gradient during times of high lake water. Simova (1964) describes outflow through such bands that are only slightly incised into the surface and function mainly during snow melt. One of these bands probably existed at the position of the current first valley section. The drainage of the alas probably happened catastrophically at a time of summer water surplus, when the connection between the lake and the second valley section was established through the outflow band. Warm lake water is reported to be capable of creating deep new outlet channels due to ice-wedge erosion, which can lead to complete lake drainage within a few hours (Marsh and Neumann, 2001). The primary thermokarst lake drained rapidly and transformed the outflow band into the deep thermo-erosional valley which is now the described first section. The drainage supposedly did not occur completely, but a large residual lake remained in the northwest of the alas and a smaller one in the

southwest (Figure 3-10.3). The position of the residual lakes in the western part of the drained basin and the declined exposed alas floor (Figure 3-9a) show that the bathymetric profile of the initial thermokarst lake was asymmetric. The decline of the basin floor from east to west is consistent with the overall inclination of the surface of Kurungnakh Island, which is reflected in higher absolute relief heights of the upper alas slopes in the east compared to the west. The asymmetric basin floor profile suggests that the base of the Ice Complex deposits is also declined in this direction.

After drainage, permafrost started to aggrade in the talik and the lake sediments accompanied by ground-ice accumulation. The refreezing of the talik occurred at a much faster rate than the complete thawing of the initial Ice Complex deposits. Modeling studies showed a complete refreezing within decades depending on talik depth and initial ground temperature conditions (Ling and Zhang, 2004). On the exposed alas floor, ice-rich boggy deposits accumulated and ice-wedge polygons evolved. Terrestrial deposition, peat growth, and ice accumulation led to the elevation of the alas floor.

The residual lake in the northwest of the alas, which is now Lake 1, was situated at the alas margins that still consisted of ice-rich Ice Complex deposits. The lake continued thawing the ice-rich permafrost at this alas slope section, expanded into the alas slope, and thereby modified the initial alas outline (Figure 3-10.4). This lateral lake expansion was supported by two phases of high water availability due to increasing precipitation between 5 and 3 ka BP in the region as inferred from pollen-based climate reconstructions (Andreev et al., 2004). The lakes on the alas floor respond quickly to changes in the hydrological regime with lake area changes, which was also observed during field work (chapter 3.5.1). The wet climate phases are furthermore reflected in the southern part of the alas. The lacustrine deposits of outcrop OC-A were dated to fall into this interval, which indicates that wetter climate conditions also led to the expansion of the southern residual lake to the position of outcrop OC-A after 5 ka BP (Figure 3-10.4). It can therefore be concluded that the upper terrace of Lake 1 and the terrace of Lake 3 were formed due to maximum lake level stands during the late Holocene wet climate phases.

Subsequently, both residual lakes drained partially and exposed first the lake terrace around Lake 3 and then the upper terrace of Lake 1 (Figure 3-10.5). The drainage could have resulted from a lowering of the base level of erosion. This lowering could be caused by thermo-erosional valley sections cutting deeper into the sediments or by the Olenyokskaya Channel eroding the island so that the base of erosion moves inland. On the exposed terraces, permafrost started to aggrade, and between the two lakes a small pingo evolved (Figure 3-10.6). Its present position close to the outflow streams of Lake 1 and Lake 3

prevents the pingo from further growth, because any excess water at that location will promptly be discharged by the streams. Lake 1 continued eroding the adjacent alas slopes in northwestern directions until they reached their present position (Figure 3-10.6). Then it experienced another partial drainage that exposed the modern lower terrace of Lake 1.

In contrast to Lake 1 and Lake 3, Lake 2 is supposed to be a secondary thermokarst lake. Its high relief position, small size, and the absence of lake terraces indicate that it has evolved during the late Holocene on the perennially frozen alas floor. Its thermokarst process was probably initiated by the drainage of a small thermokarst lake, which was situated on the Yedoma surface close to the upper alas slope (Figure 3-10.5). This small lake created the depression east of modern Lake 2. It eventually drained via a thermo-erosional gully into the alas, and the draining water ponded on the ice-rich alas floor very close to the alas slope at least 1.7 ka BP. When the pond expanded laterally, it continued to erode the alas slope north and south of the thermo-erosional gully. The depression on the Yedoma surface thereby deepened and its western margin eroded completely.

The other alas slope sections, which were not being eroded by the lakes in the alas basin, stabilized. Hence, they are characterized by more moderate gradients than the slope sections that are still geomorphologically active today (Figure 3-5a). With the last partial drainage of Lake 1, the Lake 1 shore retreated from the northwestern alas slope and the erosional activity of Lake 1 on this slope section stopped. The currently steep gradient will therefore flatten as it stabilizes, whereas the steep slope sections east of Lake 2 will continue to be eroded by the expanding lake.

The morphometric description of the alas in its present appearance corresponds to the “complex alas” stage in the classification of Soloviev (1962). This stage is characterized by differences in alas floor height with lakes often covering the lower parts. Around the lakes, terraces are slightly expressed and the surface elevates. Because of the directional expansion of the alas basins, the asymmetry of the slopes as well as the elongation of the basin increases.

The reconstructed evolution of the investigated thermokarst basin is characterized by an alternation of stages with high and low thermokarst intensity (Figure 3-11). High thermokarst intensity is connected to thermokarst lake expansion and permafrost degradation, whereas during stages of low thermokarst intensity permafrost can aggrade in drained areas. The first stage of very high thermokarst intensity represents the lake phase of the primary thermokarst lake. It coincides with the phase of intensive thermokarst development in the East Siberian arctic lowlands with lateral and vertical lake expansion,

which lasted until the end of the Boreal period (9-7.5 ka BP) (Romanovskii et al., 2004; Kaplina, 2009). However, the regional cessation of thermokarst activity 7 to 6 ka BP (Romanovskii et al., 2004; Kaplina, 2009) is not to be equated with the local sharply decreasing thermokarst intensity from about 5.7 ka BP (Figure 3-11), which resulted from the drainage of the primary thermokarst lake. The unidirectional two-phased concept of thermokarst evolution with an active thermokarst phase between 13 and 7 ka BP and a stable situation after that (Romanovskii et al., 2004; Kaplina, 2009) has to be understood as a regional concept on a large landscape scale. It means that a fundamental change in climate conditions led to the formation of large thermokarst basins throughout the East Siberian arctic lowlands, which have not changed significantly in their overall areal extent since 7 to 6 ka BP. In contrast, the timing of drainage of the primary thermokarst lakes is controlled by the local topographical and hydrological conditions and can differ throughout the region. After drainage, the thermokarst evolution within the alasses can be more dynamic than during the first phase as is shown by the investigated alas (Figure 3-11), even though the overall areal extent of the primary basins does not change significantly. Furthermore, the impact of thermokarst processes in existing alas basins on the alteration of permafrost deposits is much less intense than the impact of initial thermokarst lake development on the Ice Complex surface (Morgenstern et al., 2011).

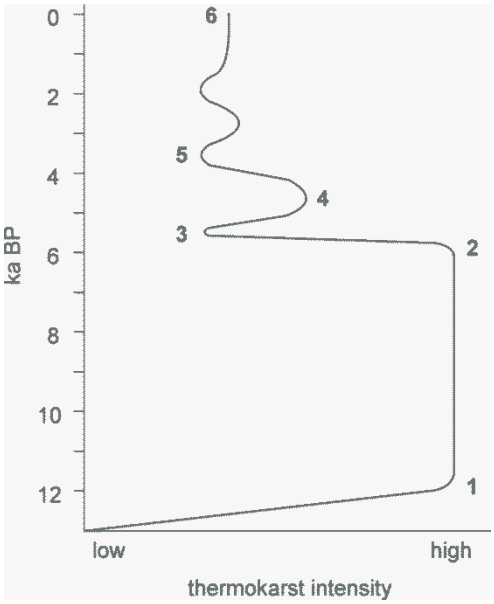

Figure 3-11. Thermokarst intensity of the investigated basin over time. Numbers in the graph correspond to the stages in Figure 3-10.

It is possible that on the floor of the drained initial thermokarst basin cycles of secondary thermokarst lake evolution occur, meaning the repeated formation, growth, and drainage of secondary lakes on the alas floor, and subsequent permafrost aggradation with sufficient

ground-ice content to allow for renewed thermokarst processes. However, a full thaw lake cycle in the strict sense of Jorgenson and Shur (2007), which would require the surface to return to its original conditions, is not possible in Ice Complex deposits because of their high original ice content and the significant subsidence during thermokarst formation. The resulting basins are several meters, sometimes 20 to 30 m, deep. Subsequent syngenetic permafrost aggradation will not lead to an uplifting of the basin floor or an infilling of the basin up to the original Yedoma surface.

3.7 Conclusion

The evolution of the investigated alas proceeded in two phases. The first phase was the continuous development of the primary thermokarst lake. It was initiated on the Ice Complex surface probably at the transition between Pleistocene and Holocene (13 to 12 ka BP) and continued until the drainage of the lake about 5.7 ka BP, which was triggered by the breaching of the formerly closed basin contour by a thermo-erosional valley. The second, late Holocene phase comprised different concurrent processes and events that were connected with stepwise lake drainage and lake expansion within the alas basin, accompanied by permafrost aggradation and degradation. Permafrost aggradation is reflected in polygonal ice-wedge growth and pingo formation on the exposed alas floor and lake terraces. Degradational processes include the expansion of residual and the formation of secondary thermokarst lakes in the alas, the modification of the initial alas contour by lake expansion, and the formation of drainage channels. The interplay between aggradational and degradational processes reflects changes in regional climate as well as local relief conditions and resulted in the strongly differentiated modern thermokarst landscape with five morphostratigraphic levels within the alas.

In contrast to the first phase of thermokarst evolution, which comprised only one continuous stage of high thermokarst intensity, the second phase since about 5.7 ka BP includes several stages of higher and lower thermokarst intensity and can therefore be considered more dynamic on the local scale. However, on the regional scale, the changes that occurred during the second evolutionary phase after drainage of the initial thermokarst lakes are less intense than the extensive thermokarst development that affected vast areas of East-Siberian coastal lowlands during the early Holocene. The massive early Holocene thermokarst activity led to a profound alteration of Ice Complex deposits and permafrost landscapes and formed the setting for smaller scale late Holocene and modern thermokarst dynamics. Future thermokarst activity will be influenced by the existing thermokarst terrain and will occur mainly in basins of older-generation thermokarst rather than affecting large portions of undisturbed late Pleistocene Ice Complex deposits.

Acknowledgements

Partial support of this work was provided by the German National Academic Foundation, Christiane Nüsslein-Volhard-Foundation and the Faculty of Mathematics and Natural Science of the University of Potsdam to A. Morgenstern and by the Helmholtz Association through the ‘‘Planetary Evolution and Life’’ research alliance to M. Ulrich. ALOS PRISM data were kindly provided by JAXA and ESA through the LEDAM project (awarded by ESA ADEN, PI H. Lantuit, ID 3616). We greatly appreciate the efforts of all German and Russian colleagues in organizing and supporting the expeditions to the Lena Delta. We thank J. Stapel, U. Bastian, C. Sawallisch, M. Lamottke, C. Springer, L. Schönicke (all AWI Potsdam) and B. Plessen (GFZ Potsdam) for their support with lab analyses. We also thank G. Schwamborn, H. Meyer, M. N. Grigoriev, V. E. Tumskoy and T. N. Kaplina for critical discussions. C. O’Connor (University of Alaska, Fairbanks) provided careful language revision.

4 The role of thermal erosion in the degradation of Siberian ice-rich permafrost

A. Morgenstern[1], G. Grosse[2], D. R. Arcos[1], F. Günther[1], P. P. Overduin[1], L. Schirrmeister[1]

[1] Alfred Wegener Institute for Polar and Marine Research, Research Unit Potsdam, Potsdam, Germany

[2] Geophysical Institute, University of Alaska Fairbanks, Fairbanks, USA

In preparation for Journal of Geophysical Research – Earth Surface

4.1 Abstract

Siberian coastal lowlands underlain by ice-rich permafrost often feature streams, valleys, and valley networks that have formed under the influence of thermal erosion. This study conducts an inventory of streams and valleys in three ice-rich lowland areas adjacent to the Laptev Sea using remote sensing, GIS, and field investigations. The calculated total stream length is 4,153 km in the Cape Mamontov Klyk area, 1,541 km in the Lena River Delta area, and 2,047 km in the Buor Khaya Peninsula area; valley densities are 1.8, 0.9, and 1.0 km/km², respectively. Strong variations in the morphology and spatial distribution of streams and valleys are observed and can be attributed to differences in the size, relief characteristics, and previous degradation of the study areas by thermokarst. Based on the results, the evolution of different valley types is discussed. The current valley pattern is the result of the late Holocene evolution of the hydrological system that is strongly connected to the degradation of ice-rich permafrost by thermal erosion.

4.2 Introduction

Climate warming in the Arctic is occurring at a much faster rate than the global average (AMAP, 2011), which has a significant impact on polar permafrost regions. Permafrost warming and permafrost degradation have been reported throughout the northern high-latitudes (AMAP, 2011; Romanovsky et al., 2010). Thermokarst and thermal erosion are two major types of permafrost degradation in periglacial landscapes. They are capable of releasing fossil organic carbon pools to the atmosphere and the hydrological system (Zimov et al., 1996; Walter et al., 2006; Schuur et al., 2008; Grosse et al., 2011) and may substantially alter the water and energy balances of affected regions (Chapin et al., 2005; Osterkamp et al., 2009).

Thermokarst is defined as the process by which characteristic landforms result from the thawing of ice-rich permafrost or the melting of massive ice. Thermal erosion means the erosion of ice-bearing permafrost by the combined thermal and mechanical action of moving water (van Everdingen, 2005). While thermokarst is an in situ process including thermal melting of ground ice followed by surface subsidence but without hydraulic transport of earth materials, thermal erosion is a dynamic process involving the wearing away by thermal means (i.e., the melting of ice), and by mechanical means (i.e., hydraulic transport). Two types of thermal erosion can be distinguished: linear thermal erosion, which acts into depth, and lateral thermal erosion, which acts sideways (Czudek and Demek, 1973; Yershov, 2004).

Thermokarst processes occur mostly in flat lowland relief with inhibited drainage; resulting landforms are thermokarst lakes, thermokarst depressions (alasses), and thermokarst mounds. Thermal erosion can take place at river banks and coastlines (Costard et al., 2003; Gavrilov et al., 2003; Dupeyrat et al., 2011), at the shores of lakes with significant wave activity (Jones et al., 2011), but also in ice-rich lowlands with sufficient relief gradients to allow for significant surface water flow. Here, it can result in the formation of thermo-erosional gullies (Fortier et al., 2007; Godin and Fortier, 2012) or even large thermo-erosional valleys and valley systems. Both processes and landforms interact with each other, because thermo-erosional gullies and valleys can supply water to thermokarst lakes and basins (Grosse et al., 2006, 2007) and enlarge thermokarst depressions (Toniolo et al., 2009) as well as inhibit thermokarst activity by drainage of thermokarst lakes (Marsh and Neumann, 2001; Morgenstern et al., 2011, 2012b).

While thermokarst lakes have been investigated in numerous studies, for example as sources of carbon release to the atmosphere (Zimov et al., 1997; Walter et al., 2006) or as indicators of a changing water balance in permafrost regions by analyzing changes in thermokarst lake area using remote-sensing methods (Smith et al., 2005; Kravtsova and Bystrova, 2009), there is very few literature available on thermo-erosional gullies and valleys in ice-rich permafrost landscapes. Thermo-erosional valleys have been described for example in the Lena River Delta (Grigoriev, 1993) and mapped in two regions of East Siberian coastal lowlands in the context of an overall quantification of thermokarst-affected terrain types (Grosse et al. 2005, 2006). Other studies reveal local increasing and rapid formations of thermo-erosional gullies due to thawing permafrost (Fortier et al., 2007; Bowden et al., 2008; Godin and Fortier, 2012). Thermo-erosional gullies and valleys can deeply erode ice-rich deposits, increase sediment and nutrient delivery to rivers, lakes, and the sea (Bowden et al., 2008; Toniolo et al., 2009), and restructure arctic drainage networks, thereby leading to greatly changing runoff volumes and timings (Rowland et al., 2010). Thermo-erosional gullies and valleys extend over vast parts of the arctic landscape, act as important snow

accumulation areas, and have been proven to significantly alter the water, sediment, and organic matter transport from permafrost to coastal waters at the local scale. However, there is no systematic study available to quantify these impacts at the artic scale. As a first step to fill this gap, this study provides a comprehensive inventory of thermo-erosional valleys in one of the most sensitive ice-rich permafrost lowland regions of the eastern Siberian Arctic. It will answer the key question how important is thermal erosion for the degradation of ice-rich permafrost. The specific objectives of this study are: 1) to analyze patterns of thermo-erosional gullies and valleys using remote sensing data and geoinformation techniques, 2) to characterize their morphometry and spatial distribution, and 3) to relate the identified spatial patterns to topographical and cryolithological settings.

4.3 Regional setting

This study focuses on three lowland sites underlain by ice-rich permafrost of the Yedoma-type Ice Complex at the Siberian Laptev Sea coast (Figure 4-1). The western site, Cape Mamontov Klyk, belongs to the Lena-Anabar coastal lowland. It is bordered by the Pronchishchev Ridge to the south and slightly declines from this hill range in NNE direction towards the Laptev Sea (Grosse et al., 2006). The central site, the third geomorphological main terrace of the Lena River Delta, is composed of insular remnants of Ice Complex

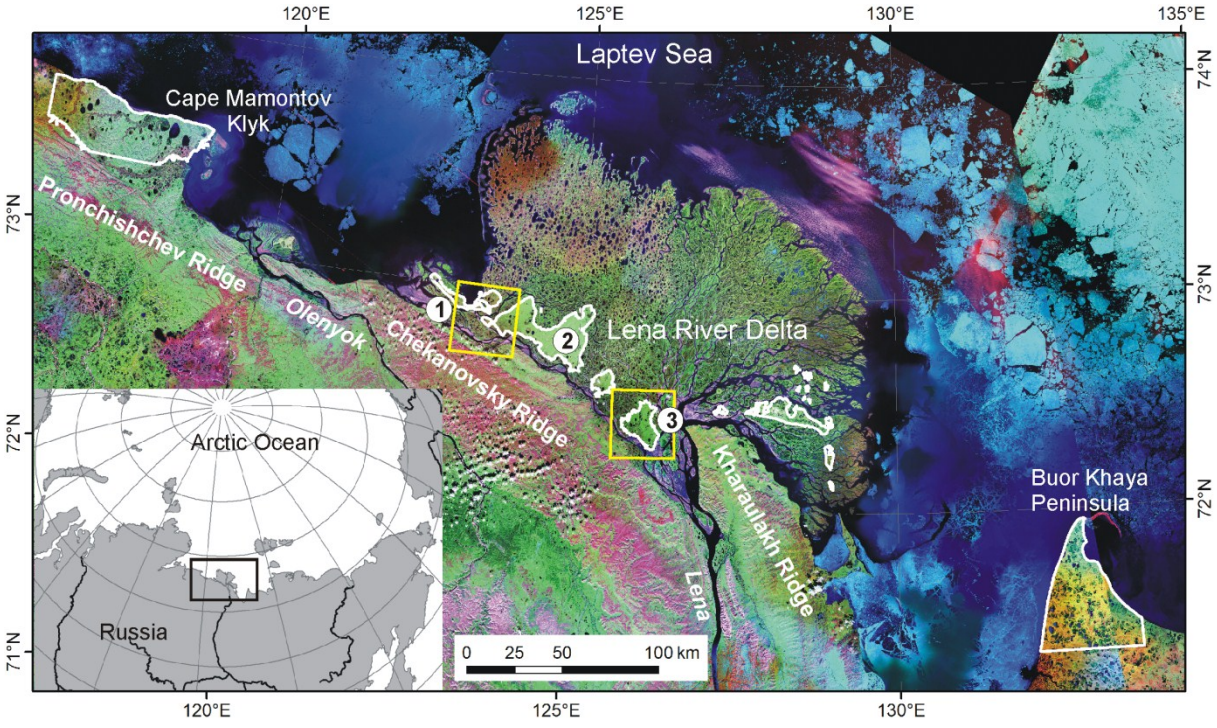

Figure 4-1. Regional setting of the study areas (Landsat-7 ETM+ mosaic; GeoCover™ 2000). White outlines mark the spatial extent of individual study areas, yellow outlines the location of the Lena Delta DEMs. 1 – Ebe-Basyn Island, 2 – Khardang Island, 3 – Kurungnakh Island.

deposits (Grigoriev, 1993; Schwamborn et al., 2002b; Morgenstern et al., 2011). The eastern site, the Buor Khaya Pensinula, is the westernmost part of the Yana-Indigirka coastal lowland. All three sites are situated in the continuous permafrost zone with several hundreds of meters permafrost depths and mean annual ground temperatures from -9 to < -11 °C (Yershov, 2004) and in the arctic tundra zone (Walker et al., 2005).

The stratigraphical composition of exposed frozen deposits in the three study areas is comparable, consisting of Ice Complex deposits of up to several tens of meters thickness underlain by fluvial sandy deposits and covered by Holocene deposits (Schirrmeister et al., 2003, 2008, 2011c; Schwamborn et al., 2002b; Wetterich et al., 2008, 2011). On the Buor Khaya Pensinsula, the base of the Ice Complex deposits and underlying deposits have not been revealed, but during a coring campaign about 500 m off the western shore sands were reached in the depth of 30 m below sea level (P. Overduin, unpublished data, 2012). The lowest sandy deposits in the Cape Mamontov Klyk and the Lena Delta study areas are of middle to late Pleistocene age. Ice Complex deposits of all sites were polygenetically formed during the late Pleistocene (Schirrmeister et al., 2003, 2008, 2011a, 2011c; Schwamborn et al., 2002b; Wetterich et al., 2008, 2011). The Ice Complex deposits consist of ice-supersaturated silty to sandy sediments and buried cryosols with large syngenetic ice wedges. The total ice volume in the Ice Complex deposits can therefore reach up to 80 %. Thin Holocene deposits cover the Ice Complex deposits and are also found in thermokarst depressions and river and thermo-erosional valleys. They consist of peat as well as silty to sandy sediments with high organic matter and ice content (Schirrmeister et al., 2011b).

The high ice content of the Ice Complex deposits provided the conditions for widespread terrain subsidence and surface changes due to thermokarst and thermal erosion since the Pleistocene/Holocene transition about 12 to 10 ka BP. For all study sites, high areal percentages of permafrost degradation landforms have been reported. Of the Cape Mamontov Klyk area, 78 % was estimated to be affected by permafrost degradation (Grosse et al., 2006). This percentage is composed of slopes (29 %) and flat surfaces of thermokarst lakes and alasses and valley floors (48.7 %). The coverage of degradation landforms increases from north to south. Of the Lena Delta site, 22.2 % is covered by thermokarst lakes and alasses (Morgenstern et al., 2011). The total area affected by permafrost degradation landforms is much higher when thermo-erosional valleys are included. This was demonstrated for Kurungnakh Island in the central Lena Delta, where only 33.7 % represent flat Yedoma surfaces were found unaffected by thermokarst or thermal erosion (Morgenstern et al., 2011). On the Buor Khaya Peninsula, only 10 % were classified as

undisturbed Yedoma, which implies that 90 % of the site is affected by permafrost degradation (Arcos, 2012).

4.4 Material and methods

Thermo-erosional landforms were manually digitized as line features and subsequently analyzed in a Geographic Information System (GIS) using the software package ArcGIS™ 10.0. The mapping included the whole surficial hydrological discharge system of the study areas, i.e. thermo-erosional gullies and valleys as well as streams and rivers, hypothesizing that all these elements have potentially formed involving thermo-erosional processes.

For the Cape Mamontov Klyk site, data from Grosse et al. (2006) that had been digitized from 1:100,000 topographic map sheets were used and clipped to the Ice Complex extent of Cape Mamontov Klyk, which excludes the hill range in the southwest with outcropping bedrock and rocky slope debris, coastal barrens, and a large sandy floodplain area in the southeast. The mapped features (streams, intermittent streams) were visually compared with panchromatic Landsat-7 ETM+ satellite data (4 August 2000, 15 m spatial resolution) and panchromatic Hexagon data (14 July 1975, 10 m spatial resolution). Because smaller valleys and gullies were not captured in the maps, they were subsequently digitized on the basis of the satellite data. The criterion for the mapping of linear features as thermo-erosional valleys and gullies was their clear incision into the surface with visible slopes. Thermo-erosional features of the Lena Delta site were mapped on the basis of a Landsat-7 ETM+ image mosaic (2000 and 2001, 30 m spatial resolution) (Schneider et al., 2009) and a Hexagon satellite image mosaic (1975, 10 m spatial resolution) (G. Grosse, unpublished data) of the Lena River Delta within the extent of the Lena Delta Ice Complex (Morgenstern et al., 2011). For the Buor Khaya Peninsula, data from Arcos (2012), which had been digitized based on RapidEye satellite data (8 August 2010, 6.5 m spatial resolution) in comparison with 1:100,000 topographic map sheets, were completed for smaller thermo-erosional features using the same RapidEye scene as a mapping basis. The spatial resolution, acquisition date, time of the day, and viewing geometry of the satellite data used (Table 4-1) may have an influence on the identification of thermo-erosional landforms in the images. For Cape Mamontov Klyk and the Lena Delta we therefore used a combination of Hexagon, Landsat, and DEM data that corroborated each other in the degree of detail versus the up-to-date spatial extent of single features that had laterally expanded between 1975 and 2000 by decameters.

Table 4-1. Overview of the satellite data, maps, and DEMs used in this study.

Location	Data type	Year	Equidistance of contour lines / Ground resolution
Cape Mamontov Klyk	Landsat-7 ETM+, pan	2000	15 m
	Hexagon	1975	10 m
	DEM from topographic maps[a]		10 m / 30 m
Lena River Delta	Landsat-7 ETM+ mosaic[b]	2000, 2001	30 m
	Hexagon mosaic[c]	1975	10 m
Parts of Ebe-Basyn and Khardang Islands	DEM from topographic maps[d]		10 m / 30 m
Kurungnakh Island	DEM from topographic maps[e]		10 m / 30 m
Buor Khaya Peninsula	RapidEye[f]	2010	6.5 m
	DEM from topographic maps[c,g]		10 m / 30 m

[a] Grosse et al. (2006)
[b] Schneider et al. (2009)
[c] G. Grosse (unpublished data)
[d] M. Ulrich (unpublished data)
[e] Roessler (2009)
[f] Guenther et al. (2012)
[g] Arcos (2012)

We calculated the drainage density and the valley density as measures of the degree to which the study areas are dissected by streams and valleys, respectively. The drainage density is defined as the total length of streams divided by the area of their drainage basin (Horton, 1932, 1945). On Cape Mamontov Klyk and on the Buor Khaya Pensinsula, some of the streams and valleys and their catchment areas are truncated in the south of the study areas because of the definite study area extent. We still included them in our calculations, because our focus are the characteristics of Ice Complex degradation in the study areas rather than the hydrogeographical characteristics of their whole watersheds. In this study, we therefore calculated the drainage density of each study area as the total length of all streams and rivers divided by the total area. In addition, the valley density was calculated, because large valleys often have well developed floodplains, i.e. broad floors with strongly meandering streams, and a meandering stream has a greater length than its valley. These valley floodplains were delineated as polygon features along the valley floor margins (for Cape Mamontov Klyk we used the data from Grosse et al., 2006) and their center line was digitized to determine the valley length in comparison to the stream length. The valley density was then calculated as the sum of rivers, streams, and intermittent streams outside valley floodplains and the valley floodplain centerlines divided by the total area of the study site.

To illustrate the spatial relation of thermo-erosional landforms to thermokarst lakes and basins, we used GIS datasets from previous studies on Cape Mamontov Klyk (Grosse et al.,

2006) and in the Lena Delta (Morgenstern et al., 2011). On the Buor Khaya Peninsula, only thermokarst lakes could be delineated, because the area has been affected by thermokarst processes to an extent that does not allow for the distinction of individual alas boundaries.

For terrain analyses and deriving valley cross profiles we used Digital Elevation Models (DEM) with a grid cell resolution of 30 m that were derived from the digitized topographic map data. For Cape Mamontov Klyk we used the DEM from Grosse et al. (2006). For the Lena Delta, topographic map sheets at the 1:100,000 scale and derived DEMs were available only for an about 35 by 35 km area in the western delta covering parts of Ebe-Basyn and Khardang Islands (M. Ulrich, unpublished data) and for Kurungnakh Island in the south central delta (Roessler, 2009) (Figure 4-1). Detailed digital terrain analyses in the Lena Delta were therefore confined to these key sites; relief information for the remaining delta areas was retrieved from topographic maps at the scale 1:200,000. For the Buor Khaya Peninsula, the DEM generation was done on a hybrid vector data basis in order to achieve a more up-to-date representation of the alas and thermokarst lake dominated relief. Digitized topographic map contour lines with an equidistance of 10 m, together with mapped streams and standing water bodies that were automatically extracted on the basis of an orthorectified RapidEye image (Günther et al., 2012), served as input data for DEM interpolation. The spatial resolution of the DEMs was too coarse to allow for detailed and statistical analyses of valley cross profiles and further hydrological investigations within the GIS.

Individual thermo-erosional and fluvial landforms were observed during field campaigns to Cape Mamontov Klyk in 2003 (Grosse et al., 2006; Schirrmeister et al., 2004), to the western Lena Delta in 2005 (Schirrmeister et al., 2007; Ulrich et al., 2009), to Kurungnakh Island in 2008 (Morgenstern et al., 2012b; Wagner et al., 2012), and to the Buor Khaya Pensinsula in 2010 (Wetterich et al., 2011).

4.5 Results

The summary characteristics of the three study sites are given in Table 4-2. Cape Mamontov Klyk features the most extensive coverage with valleys and streams (Figure 4-2) and has therefore the highest drainage density (2.0). The values for the Lena Delta and Buor Khaya Peninsula are similar (0.9 and 1.0, respectively). Valley densities are similar or equal to the drainage densities, which implies that largely meandering streams in floodplains only cover a small proportion of the drainage systems of each study area.

Table 4-2. Summary characteristics of the three study sites and their thermo-erosional and thermokarst landforms.

	Cape Mamontov Klyk	Lena Delta	Buor Khaya Peninsula
Study area (km²)	2,109	1,690	2,001
Max. relief height (m asl)	75.5	66	65
Min. relief height (m asl)	0	0	0
Min. distance between highest and lowest relief parts (km)	22	7	7
Total stream length (km)[a]	4,153	1,541	2,047
Drainage density (km/km²)	2.0	0.9	1.0
Valley floodplains (km²)	203.8	8.2	25.6
Maximum floodplain width (km)	4.5	1	1.5
Total length of valley floodplain centerlines (km)	199	25	38
Max. valley depth (m)	35	35	25
Total valley length (km)[b]	3,877	1,541	1,954
Valley density (km/km²)	1.8	0.9	1.0
Alasses (km²)	418.2[d]	337.7[e]	n.d.
Thermokarst lakes (km²)	158.2[d]	88.3[e]	192.9
Thermokarst lakes on Yedoma uplands (km²)	23.0[d]	37.4[e]	n.d.
Total area affected by thermokarst lakes and alasses (km²)[c]	441.2[d]	375.1[e]	n.d.
Thermokarst areal percentage of study site (%)	20.9[d]	22.2[e]	n.d.

[a] Calculated as the sum of all rivers, streams, and intermittent streams.
[b] Calculated as the sum of rivers, streams, and intermittent streams outside valley floodplains and the valley floodplain centerlines.
[c] Calculated as the sum of thermokarst lakes on Yedoma uplands and thermokarst basins.
[d] Data based on Grosse et al. (2006).
[e] Data from Morgenstern et al. (2011).
n.d. – not determined due to lack of data for alas extent.

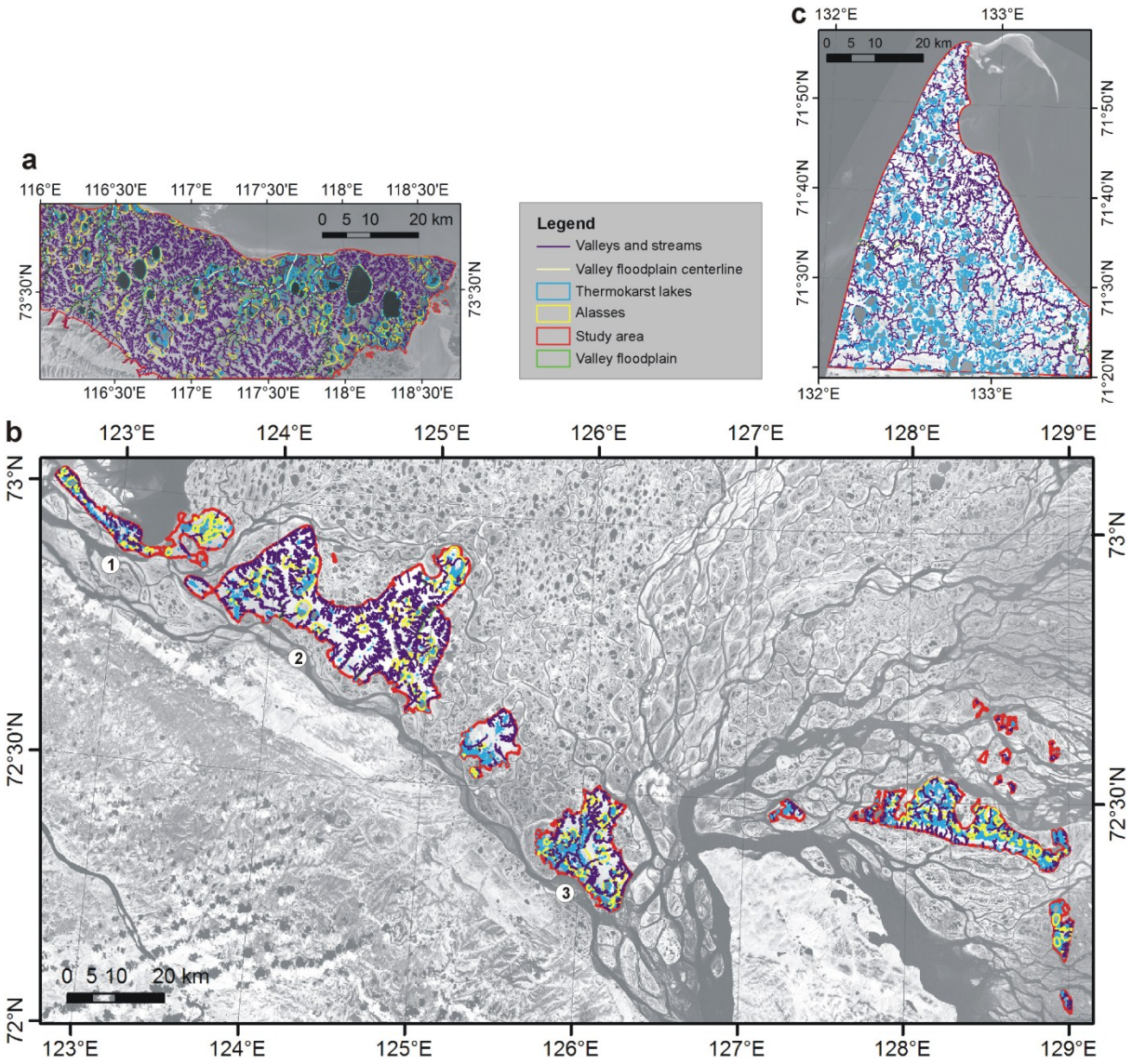

Figure 4-2. Overview of all digitized thermo-erosional and thermokarst landforms in the study areas: **(a)** Cape Mamontov Klyk (panchromatic Landsat-7 ETM+ data), **(b)** Lena River Delta area (Landsat-7 ETM+ mosaic, band 2; GeoCover™ 2000), 1 – Ebe-Basyn Island, 2 – Khardang Island, 3 – Kurungnakh Island, **(c)** Buor Khaya Peninsula (RapidEye data, band 5).

4.5.1 Morphological valley types

Cape Mamontov Klyk is characterized by extensive dendritic valley networks (Figure 4-2a, 4-3a). They start on Yedoma uplands and end at the coast. Some of them cross the whole study area from the Pronchishchev Ridge in the south to the Laptev Sea coast in the north. Smaller networks also start or end in thermokarst lakes and alasses.

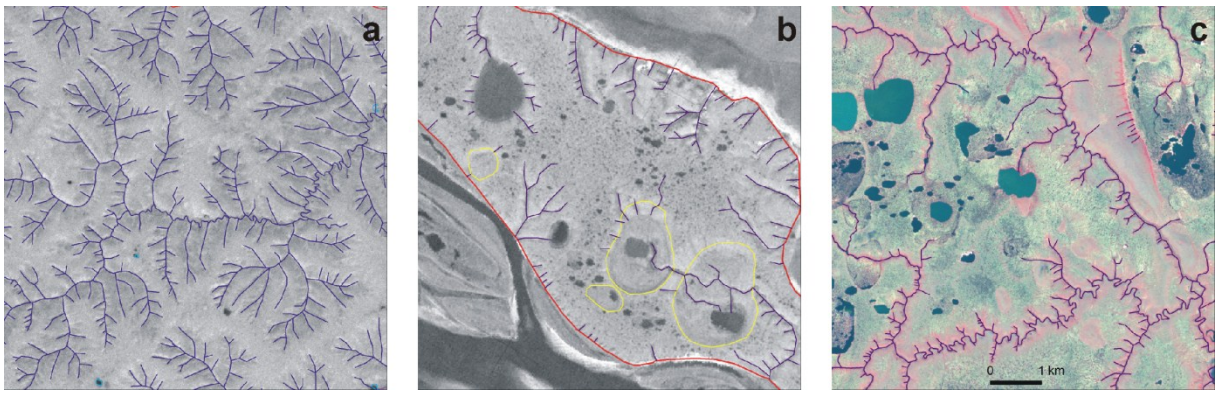

Figure 4-3. Examples of different valley types in the study area: **(a)** extensive dendritic valleys, Cape Mamontov Klyk, **(b)** short parallel valleys along the Ice Complex margin, short radial valleys around thermokarst lakes and on alas slopes, and drainage pathways in alasses, Lena River Delta, **(c)** extensive longitudinal valleys with sharp meanders and short contributing valleys, Buor Khaya Peninsula. Scale bar in (c) applies for all; for color codes see Figure 4-2.

In the Lena River Delta, large dendritic valleys occur only on Khardang Island (Figure 4-2b), which is the largest and highest of the third terrace islands with the greatest distance between the interior and the margins. Most common in the Lena Delta are short thermo-erosional valleys (up to 2 km long, sometimes with short tributary valleys) that are parallel aligned along the margins of the study area, where steep cliffs form an abrupt transition between the Yedoma uplands of the third geomorphological main terrace and the delta channels and floodplains (Figure 4-3b). Longer valleys often interconnect alasses and discharge them into the delta channels. They can be several kilometers long and have several tributary valleys or streams.

All these valley types also occur on the Buor Khaya Pensinsula, but the predominant type here are longitudinal valleys and streams that extend from the interior to the coasts (Figure 4-2c, 4-3c). They do bifurcate, but at distances of several kilometers. In between they feature frequent, very short, parallel side valleys perpendicular to the main valley. They occur on Yedoma uplands as well as in the extensive lower relief areas that resulted from thermokarst subsidence. Sometimes they even start in low areas and then cut through Yedoma remnants that are elevated up to 20 m above these low areas.

In all three study areas, straight, short gullies are often radially located around alasses and thermokarst lakes (Figure 4-3b). They start on the Yedoma uplands, cut into the slopes, and end abruptly at the foot of the alas slope or at the lake level.

4.5.2 Valley profiles

The valley profiles are similar in all three study areas. Short tributary valleys typically have straight longitudinal profiles (Figure 4-3) and V-shaped cross profiles (Figure 4-4d). Higher

order and main valleys mostly follow a winding course from the interior to their mouth on the small scale and meander on the large scale (Figure 4-3a, 4-3c). Narrow valleys with a V- or slightly U-shaped cross profile meander themselves (Figure 4-3a, 4-3c). The meanders bend in sharp angles, obviously following the ice-wedge polygonal network. Broader valleys with a U-shaped cross profile (Figure 4-4e) tend to straighten in their large-scale longitudinal course, but the streams on their floors are meandering with a high frequency.

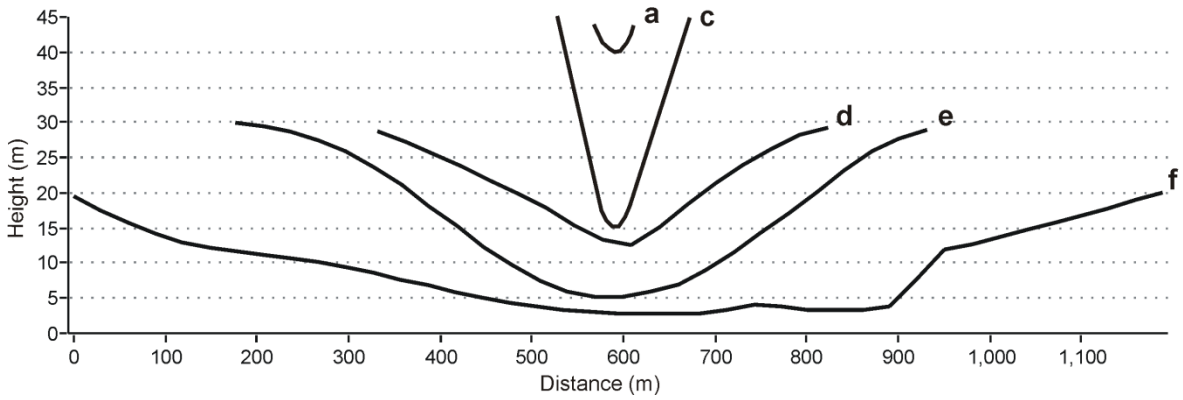

Figure 4-4. Cross profiles of different valley types (letters correspond to the categories in Table 4-3; categories (b) and (g) are not shown because of their shallow depth): **(a)** short, straight gully on alas slope, **(c)** V-shaped ravine, **(d)** V-shaped valley with a straight thalweg of an intermittent stream, **(e)** U-shaped valley with a meandering thalweg of a permanent stream, **(f)** broad valley floodplain with a large meandering river and small oxbow and thermokarst lakes. Profiles (a) and (c) were drawn manually based on field observations, profiles (d)-(e) were derived from the DEM on Mamontov Klyk.

The broad valleys with large floodplains have a flat floor (Figure 4-4f) with a smoothly meandering river and oxbow and small thermokarst lakes. The maximum widths of these valley floodplains are 4.5, 1, and 1.5 km in the Cape Mamontov Klyk, Lena Delta, and Buor Khaya Peninsula study area, respectively. Streams in alasses, and on the Buor Khaya Peninsula also some of the rivers in the large low relief areas, are meandering and only slightly indented into the surface. The maximum valley depth as derived from the DEMs is about 35, 35, and 25 m in the Cape Mamontov Klyk, Lena Delta, and Buor Khaya Peninsula study area, respectively (Table 4-2).

4.5.3 Field observations

During several expeditions to the study region we observed numerous gullies, valleys, and streams (Figure 4-5), which can be assigned to different categories (Table 4-3). Short, straight gullies around thermokarst lakes and alasses cut up to a few meters deep into the slopes of the thermokarst features and mostly follow the same gradient (Table 4-3a, Figure 4-4a). They are densely covered with fresher and higher growing vegetation than the surrounding slope sections. In alasses, small streams often occur as drainage pathways and

connect residual and secondary thermokarst lakes on the alas floor with the hydrological system outside the alasses (Table 4-3b). Deep V-shaped ravines (Table 4-3c, Figure 4-4c) were observed along the cliffs of the third Lena Delta terrace (Figure 4-5f) and along the coasts of the Buor Khaya Peninsula (Figure 4-5g) and Cape Mamontov Klyk. They have a steep to moderate gradient, because they descend from the Yedoma uplands over a distance of only a few tens to hundreds of meters down to almost sea level. Their lower slopes and floors often show a disturbed vegetation cover or are free of vegetation. Some of these ravines have formed due to the drainage of thermokarst lakes. Another type of V-shaped valleys are the small tributary valleys described in section 4.2 (Table 4-3d, Figure 4-4d). They are much wider (up to hundreds of meters) than the V-shaped ravines (up to tens of meters) and therefore have more gentle slopes. U-shaped valleys are widely distributed in the study areas (Table 3e, Figure 4-4e). In many of them the slopes end abruptly at the flat floor, which can be several tens of meters wide (Figure 4-5d). Permanent streams in the lower parts of the Cape Mamontov Klyk and Buor Khaya Peninsula study areas closer to the coast often have broad valleys with distinct floodplains, because they are frequently meandering (Table 4-3f). While their valleys are U-shaped where the meanders are small (Figure 4-5c), they broaden to wide, open floodplains where large streams are meandering in large bends (Figure 4-4f).

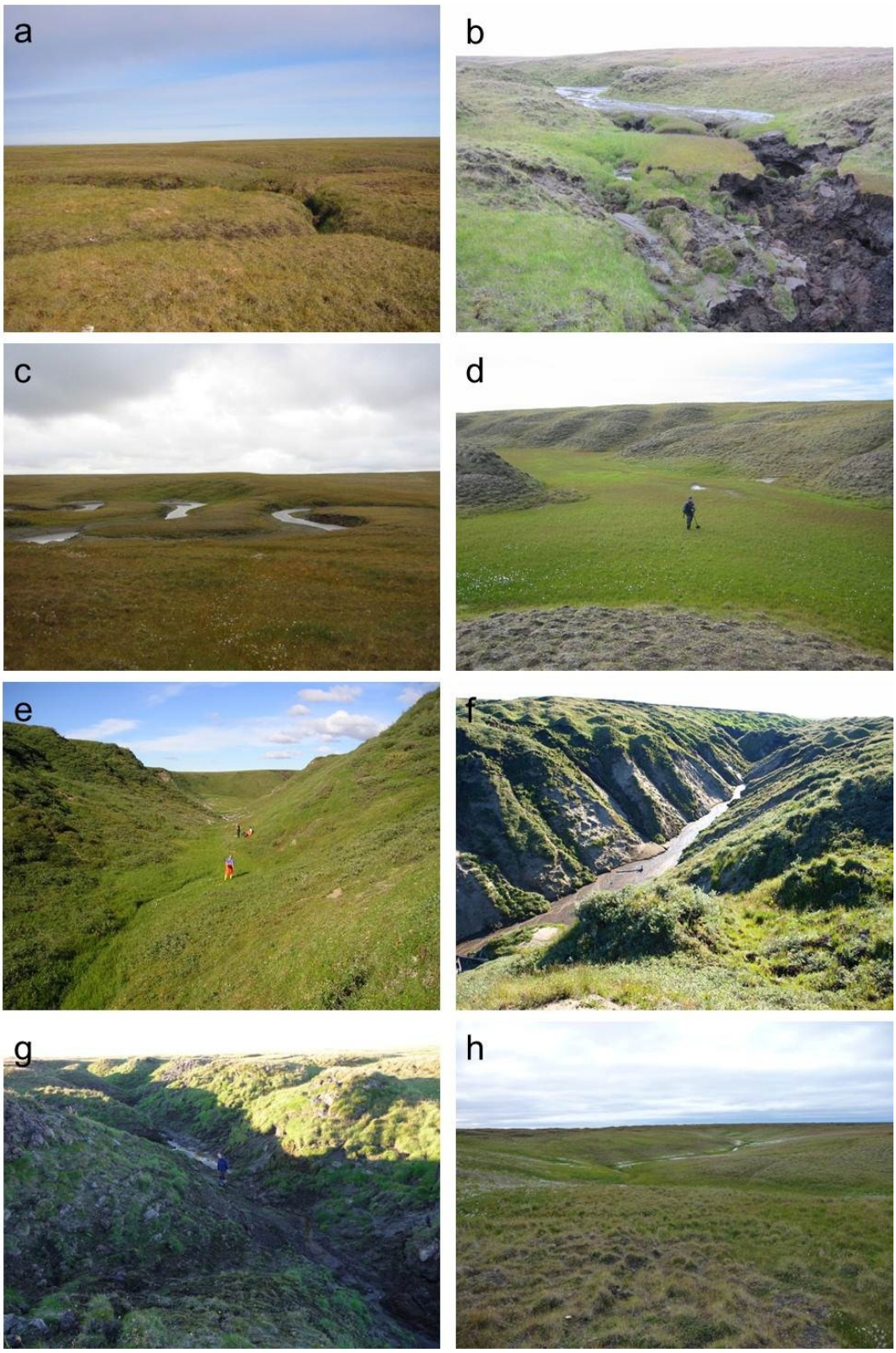

Figure 4-5. Exemplar gullies, valleys, and streams on Cape Mamontov Klyk (a-d), Kurungnakh Island, Lena Delta (e, f), and Buor Khaya Peninsula (g, h). **(a)** Gully initiation due to melting polygonal ice wedges. **(b)** Erosion and disturbed vegetation cover due to strong discharge in an intermittent stream. **(c)** Strongly meandering permanent stream that erodes the ice-rich permafrost along the outer banks. **(d)** U-shaped valley with a broad, flat, densely vegetated floor and little surface water flow.

Continuation of figure caption on next page.

Continuation of figure caption from previous page: **(e)** V-shaped valley on the floor of a large alas. It formed when the primary thermokarst lake was tapped by the neighboring delta channel. The lake drained catastrophically and washed away the unfrozen, predominantly sandy sediments from the lake bottom and underneath into the delta channel, whose water level was several meters below the lake floor. **(f)** Deep, V-shaped valley that retrogressed into the permafrost and drained a small thermokarst lake between 1975 and 2000. Slopes in the lower stratigraphic sand unit are much steeper and less vegetated than in the upper Ice Complex unit, where baydzharakhs are present. See log on valley floor for scale. **(g)** V-shaped valley with small side valleys along polygonal ice wedges and disturbed vegetation cover on the floor and lower parts of the slopes. Position is about 150 m from the coast. **(h)** Smoothly meandering valley with flat slopes.

Table 4-3. Categories of valleys and hydrological features based on field observations in the study region.

Category	Occurrence	Characteristics	Hydrologic regime
a) short, straight gullies	on alas and thermokarst lake slopes	radially arranged around lakes and alasses; V- to U-shaped; steep gradient; up to a few meters deep and wide; dense, fresh vegetation	intermittent streams
b) drainage pathways in alasses	on alas floors	connect residual and secondary thermokarst lakes in partly drained alasses with the stream network outside the alasses; slightly indented into the alas floor; low gradient; up to a few meters wide; dense, fresh vegetation	intermittent and small permanent streams
c) V-shaped ravines	along steep coasts and cliffs; often due to lake drainage	V-shaped; steep to moderate gradient, up to tens of meters deep and wide; vegetation cover on floor and lower slopes often disturbed	intermittent streams
d) V-shaped valleys	in upper parts of the watersheds on Yedoma uplands	mostly tributary valleys; V-shaped; moderate to low gradient, up to tens of meters deep and hundreds of meters wide; intact vegetation cover	Intermittent streams
e) U-shaped valleys	on Yedoma uplands	U-shaped; low gradient, up to tens of meters deep and several to tens of meters wide; flat valley floor with fresh vegetation	intermittent and small permanent streams
f) valleys of permanent streams and rivers	lower parts of long streams close to their mouth	U-shaped; low gradient, up to tens of meters deep and hundreds of meters to kilometers wide; broad floors with distinct floodplains; often bare sediment exposed; oxbow and small thermokarst lakes	permanent, meandering streams
g) water tracks	on gently sloping Yedoma uplands; on large, slightly inclined alas floors	arranged in parallel; low gradient; not or only slightly indented into the surface; dense, fresh vegetation	poorly developed runoff systems

Transitions between these categories down the valleys are common, but not exclusively unidirectional and smooth. In the Cape Mamontov Klyk area we observed, for example, a meandering valley with a U-shaped profile and a small stream in the upper valley section that transformed into a V-shaped ravine with disturbed vegetation at the location of an abrupt drop in elevation (Figure 4-5b).

In addition to these valley landforms analyzed in this study, we have also observed several parallel water tracks on slightly inclined Yedoma uplands and alas floors (Table 4-3g). These water tracks are not included in our analyses, because they are not or only slightly incised into the surface. Similar features have been described for other regions in hill slopes and are sometimes referred to as dells (Mitt, 1959; Katasonova, 1963; McNamara et al., 1999; Grosse et al., 2007).

4.6 Discussion

4.6.1 Valley and stream morphology

The morphometrical characteristics of the mapped features, and partly also the drainage and valley densities, differ greatly between the three study areas. Whereas the drainage density reflects the contemporary extent of active streams, the valley density is a morphometrical indicator integrating valley-forming and valley-filling processes in a study region over large time scales taking into account environmental conditions during the formation and persistence of the valleys (Schmidt, 1984; Tucker et al., 2001).

In ice-rich permafrost lowland regions, stream and valley formation are significantly influenced by the occurrence and abundance of ground ice. Ground ice provides the conditions for thermokarst and thermal erosion, and the ice distribution in the ground can determine the location of stream and valley initiation and its course. Thermal erosion along polygonal ice-wedge systems, for example, results in the formation of zigzag-shaped streams (Czudek and Demek, 1973). Such linear thermal erosion also plays a significant role in the sediment transport down slope, even though it is accomplished by intermittent streams that are only active during the short summers. The large inflow of talus deposits and solifluction material from the slopes leads to a dominance of lateral over downcutting erosion in the formation of river valleys in permafrost regions and to strongly meandering rivers (Yershov, 2004).

In the study region, the development of the modern hydrological system began with the Late Pleistocene-Holocene transition period, when the accumulation of the Ice Complex deposits ceased and the regional climate changed to warmer and wetter conditions, promoting the activation of rivers and widespread permafrost degradation (Grosse et al., 2007;

Schirrmeister et al., 2008, 2011a, 2011c; Kaplina, 2009; Morgenstern et al., 2011). The coastline of the Laptev Sea was located several hundred kilometers further to the north during that time (Bauch et al., 2001), and extensive lowlands with low relief gradients provided favorable conditions for thermokarst. However, thermokarst processes massively occurred only until the mid-Holocene; after that the established thermokarst landscapes experienced minor changes (Romanovskii et al., 2004; Kaplina, 2009; Morgenstern et al., 2012b). The formation of large valley systems presumably started only after higher relief gradients developed in the study region, for example due to the formation of thermokarst lakes and basins and to the transgressing shoreline, which reached its modern position about 5 cal. ka BP (Bauch et al., 2001). As a result, steep bluffs formed on lakes and coasts due to wave and coastal erosion and provided steep relief gradients over shorter distances. At the Cape Mamontov Klyk coast, for example, a steep cliff of up to 30 m height was formed by coastal erosion. In the Lena Delta, the Yedoma surface was cut off from the mountain ranges to the south as well as from the accumulation plains to the north by the large deltaic channels and has been eroded into small disconnected remnants, which are now elevated up to 66 m above deltaic streams and floodplains (Schirrmeister et al., 2002, 2011a). We therefore conclude that the characteristics of the present-day valley networks in the study region basically reflect the climate and relief conditions during the middle and late Holocene period, which is supported by radiocarbon age determinations of valley fillings on Cape Mamontov Klyk that are of late Holocene age (Schirrmeister et al., 2008).

The modern activity of streams is reflected in the drainage density. The high number of intermittent streams contributes substantially to the drainage densities, which would be much lower if only permanent streams were mapped. Because intermittent streams all occupy valleys, and largely meandering rivers and streams only represent a small fraction of all streams mapped, the valley densities do not or only slightly differ from the drainage densities of the study areas.

The high density of valleys in the Cape Mamontov Klyk area (1.8) compared to the other two study areas (0.9 and 1.0 in the Lena Delta and on the Buor Khaya Pensinsula, respectively) indicates that the fluvial and thermal erosion of the Ice Complex deposits was more effective here (Table 4-2). The minimum distances between the highest and lowest point in each study area is longest on Cape Mamontov Klyk (22 km compared to 7 km in the Lena Delta and on the Buor Khaya Pensinsula); it is the largest study area, and represents an integrative and homogenously inclined surface from the mountain ranges to the coast. These characteristics support the accumulation of surface water and concentrated runoff over distances of tens of kilometers. In addition, valley heads and their watersheds are not exclusively situated inside the study area, but start in the Pronchishchev Ridge, which led to

a considerable water supply in addition to precipitation and melt water from thawing Ice Complex deposits within the study area. This effect is still functioning today as evident from the much larger areal extent of valley floodplains with mostly meandering permanent streams and rivers on Cape Mamontov Klyk and from the drainage density being higher than the valley density (Table 4-2).

In the Lena River Delta study area, valleys are predominantly short and rarely form dendritic networks. They are lined up along the steep cliffs of the small islands and cut deep into the Ice Complex and underlying sands along large ice wedge systems perpendicular to the islands' margins. Due to the short distances between the interior of the Yedoma islands and their margins, the valleys follow a high relief gradient, which favors erosion. On the other hand, the watersheds are small and thus the supply of running surface water as eroding agent on the Yedoma uplands is very limited. For the same reason larger streams occur rarely, which is also reflected by the smallest valley floodplain area of all three study areas (8.2 km²) and the smallest maximum floodplain width (1 km) (Table 4-2). Modern changes in the thermo-erosional valleys are stimulated by the activity of the deltaic channels, because the base level of erosion moves inland where the channels erode the islands' margins and retreats where delta floodplains accumulate.

On the Buor Khaya Peninsula, thermokarst processes have degraded the Ice Complex deposits over extensive areas, leaving only a few remnants of undisturbed Yedoma uplands. The surface of the study area is slightly inclined from the center to the coasts; steep gradients are only found around the Yedoma remnants. Therefore, many of the streams do not occupy deep valleys in thick Ice Complex deposits, but have incised up to a few meters deep into the lower, degraded surfaces. Most of them probably do not indicate the location of former valleys that had formed on the Yedoma uplands during the Lateglacial / early Holocene, because they are either drainage channels of thermokarst lakes or have formed on the refrozen surface of extensive and nested alasses as drainage pathways through the low relief areas. In contrast to the Cape Mamontov Klyk area, where additional water supply is derived from the Pronchishchev Ridge, the discharge on the Buor Khaya Peninsula is derived from the local precipitation and melting ground ice only as in the Lena Delta, and the water supply is therefore similarly limited. However, on the Buor Khaya Peninsula longer permanent streams and even rivers as well as larger floodplains exist, which can be explained by the lower overall gradient of this study area compared to the Lena Delta that results from longer distances from the source of the streams and rivers in the interior to the coast.

4.6.2 Valley formation and evolution

Based on our results from field investigations and mapping we propose conceptual models of formation and evolution for the different valley categories in the study areas.

The short, straight gullies in the slopes of thermokarst lakes and alasses (Figure 4-3b, Table 4-3a) form due to concentrated surface runoff from the Yedoma uplands into the lakes and alasses. Sediments are transported down slope and can form small alluvial fans on alas floors (Morgenstern et al., 2012b). In the negative relief features on the slopes, snow preferentially accumulates and promotes further erosion, because it insulates the permafrost from cold temperatures during winter and supplies more water during snowmelt in spring. Such feedback from nivation is also highly relevant for all other valley types described in this study.

The drainage pathways in alasses (Figure 4-3b, Table 4-3b) as well as a large percentage of the streams on the degraded surface of the Buor Khaya Peninsula (Figure 4-3c) are either primary pathways created during the drainage of primary thermokarst lakes or secondary pathways that formed after permafrost aggradation on the alas floor. Figure 4-5e shows a very large and deep example for the first drainage pathway type. It has formed by eroding the unfrozen sediments up to 10 m deep from the lake floor during catastrophic drainage of the large primary lake. The second type often forms along Holocene polygonal ice-wedge networks on alas floors when surplus water from precipitation and snowmelt collects in polygon troughs and discharges to lower relief parts and into larger drainage streams and valleys. The polygon troughs widen, and in cases where small ponds form at polygon junctions, beaded drainage occurs (Morgenstern et al., 2012b). Larger streams further erode the alas floor so that they are not confined to the polygonal pattern anymore, but evolve similar to the other permanent streams in the study areas as described below.

V-shaped ravines along steep Yedoma cliffs (Figure 4-3b, Table 4-3c) mostly result from retrogressive, headward erosion. They initiate at small incisions in cliff edges and reinforce due to accumulating snow and water until they stabilize when equilibrium is reached between erosion and sedimentation. The retrogressive erosion can occur along ice wedges or independently from them and develop at rates of up to several tens of meters per year (Czudek and Demek, 1973). When such ravines encounter a thermokarst lake and drain it catastrophically, they can significantly deepen and widen by thermal erosion during a short amount of time (Figure 4-5f). After stabilization they become completely vegetated.

The V-shaped valleys (Table 4-3d), U-shaped valleys (Table 4-3e), and valleys of permanent streams (Table 4-3f) are usually part of extensive valley networks and evolve

interdependently. Their development on the slightly inclined surface of the Yedoma uplands starts from shallow bands of concentrated, but intermittent surface runoff like water tracks or dells (Table 4-3g). Due to active layer deepening and sediment outwash, which can be significant even with the vegetation cover staying intact, the bands deepen and create V-shaped valleys with long, slightly inclined slopes (Figure 4-4d). In areas with higher relief gradients valley initiation can also occur by gullying along polygonal ice-wedge systems. Due to the confluence of several valleys more water accumulates downstream, so that further valley development is characterized by an intensification of the erosion laterally as well as into depth, but nivation and solifluction may even play a more significant role in the lateral erosion and widening of the valleys. As a result, the valley shapes transform from V to U. Finally, when large, permanent streams become meandering rivers broad flood plains develop. In the case of abrupt relief changes, for example at the junctions of streams or valleys of different orders, valley cross profiles can change from one type to another. Figure 4-5b shows such an example, where a steep V-shaped ravine is retrograding into a small and shallow U-shaped valley.

4.7 Conclusion

The existing valley and stream networks in the study areas reflect the late Holocene development of the regional hydrological system. It was initiated in the extensive lowland landscapes after a more pronounced relief formed due to the eroding effects of the transgressed Laptev Sea, delta channels, and thermokarst subsidence. The morphology and spatial distribution of the valley systems vary greatly between the study areas and depend basically on the:

- relief gradient,
- size of the catchments,
- previous degradation of the initial Ice Complex surface by thermokarst.

In the Cape Mamontov Klyk area, extensive dendritic valley networks have formed on a broad Ice Complex plain between the Pronchishchev mountain range and the Laptev Sea. Large catchments and a water surplus from the mountain range led to the formation of large permanent rivers and streams. On the small Ice Complex remnants of the Lena River Delta, predominantly short, but deep valleys have incised into the steep cliffs, and larger networks occur only on the largest island Khardang. Streams and valleys on the Buor Khaya Peninsula mainly evolved on low surfaces that had been degraded by extensive thermokarst. Valleys therefore have a more longitudinal character with short tributaries.

The formation processes in all three study areas were strongly influenced by thermal erosion of the ice-rich, fine-grained permafrost deposits, on the original Ice Complex surface as well as in the polygonal tundra of degraded surfaces. The abundance of valleys and streams shows that thermal erosion, besides thermokarst, played a key role in the degradation of the ice-rich permafrost of the study areas in the past. Most of the valleys that developed during the late Holocene have stabilized, but thermal erosion continues to be active today. Under a continued arctic warming with increasing permafrost temperatures, active layer depths, and changing precipitation patterns, thermal erosion might substantially contribute to further degradation of ice-rich permafrost landscapes, but further investigations are needed to shed light on the interplay between degrading and stabilizing factors in this system.

Acknowledgements

We thank R. Spröte for digitizing the Lena Delta main valleys, M. Ulrich for digitizing portions of the topographic maps of the Lena Delta and constructing the DEMs, and A. Sandakov for digitizing the main valleys of the Buor Khaya Peninsula. We greatly appreciate the efforts of all German and Russian colleagues in organizing and supporting the expeditions to the study areas. RapidEye imagery was kindly provided by DLR through the RapidEye Science Archive (RESA). A. Morgenstern was supported by the German National Academic Foundation and the Christiane Nüsslein-Volhard-Foundation. G. Grosse was supported by NASA grant NNX08AJ37G.

5 Synthesis

This thesis aimed at deriving new insights on the degradation of Siberian ice-rich permafrost by thermokarst and thermal erosion. The detailed analysis of currently existing degradational landforms in three lowland sites adjacent to the Laptev Sea underlain by Ice Complex deposits leads to a better understanding of the impact that thermokarst and thermal erosion have had on these sensitive landscapes since the beginning of their activation. Based on the results, conclusions on the potential of future permafrost degradation by thermokarst and thermal erosion can be drawn.

In the frame of this thesis, detailed analyses of thermokarst have concentrated on the third Lena Delta terrace. Thermal erosion was studied in three areas underlain by Ice Complex deposits, Cape Mamontov Klyk, the third Lena Delta terrace, and the Buor Khaya Peninsula (Figure 1-4). This synthesis extends the results of the individual manuscripts (Chapters 2, 3, 4) by including additional thermokarst data for the Cape Mamontov Klyk and Buor Khaya Peninsula areas from previous studies to provide a comprehensive discussion of permafrost degradation by thermokarst and thermal erosion for all three study areas. Sections 5.1 to 5.5 directly address the thesis' objectives stated in Section 1.2, and Section 5.6 points out directions for future research on the degradation of ice-rich permafrost.

5.1 Quantification of thermokarst and thermal erosion

All three study areas are widely affected by thermokarst and thermal erosion. GIS calculations of all thermokarst lakes and thermokarst basins (alasses) mapped within the Ice Complex extent of the Lena Delta show that 22.2 % are covered by thermokarst (Chapter 2). Data from Grosse et al. (2006) reveal a similar thermokarst areal percentage of 20.9 % for the Cape Mamontov Klyk area (Table 4-2). On the Buor Khaya Peninsula area, thermokarst lakes cover 9.6 % (Arcos, 2012), and the visual interpretation of the satellite data points to an areal percentage of alasses that by far exceeds that of the Cape Mamontov Klyk and Lena Delta areas. While thermokarst lake area percentages and their changes over several years or decades have been calculated on the basis of remote sensing analyses for various regions throughout the Arctic (Côté and Burn, 2002; Payette et al., 2004; Smith et al., 2005; Riordan et al., 2006; Labrecque et al., 2009; Kravtsova and Tarasenko, 2011), only few studies also provide data on drained thermokarst basin areas (Frohn et al., 2005; Hinkel et al., 2003) (Chapter 2), in particular for Yedoma regions. On the Bykovsky Peninsula, which is located at the Eastern Laptev Sea coast between the Lena Delta and the Buor Khaya Peninsula, 53 % of its Ice Complex area is affected by thermokarst (Grosse et al., 2005), and in the Siberian

Kolyma lowland, which is also situated within the area of Ice Complex distribution (Figure 1-2), thermokarst lakes and alasses cover between <25 to >75 % of the study sites (Kaplina et al., 1986).

The coverage of Yedoma regions with thermo-erosional landforms and their characteristics had not been investigated over large areas so far as to the author's knowledge. In the study region, the abundance of thermo-erosional landforms has been measured by the valley density, which was calculated for each of the three study areas as the total valley length divided by the total area. The valley densities amount to 1.8 in the Cape Mamontov Klyk area, 0.9 in the Lena Delta area, and 1.0 in the Buor Khaya Peninsula area (Table 4-2).

An assessment of the Ice Complex area that has been degraded by thermokarst and thermal erosion is possible with a combination of methods including DEM analyses that also account for the slope areas of thermo-erosional valleys and around thermokarst lakes, which are not captured by the linear valley digitization and the automatic water body extraction, respectively. On Kurungnakh Island in the Lena River Delta, the area of flat undisturbed Yedoma uplands outside existing thermokarst features was calculated based on a DEM and was found to be 33.7 % (Chapter 2). This means that 66.3 % of the Kurungnakh Island area has been affected by thermokarst and thermal erosion. Based on a multispectral classification of Landsat-7 ETM+ data including DEM derived relief characteristics, Grosse et al. (2006) found that 78 % of the Cape Mamontov Klyk area is affected by thermokarst, thermal erosion, and related slope processes. However, their study area extent also comprises coastal barrens and a large sandy floodplain area with numerous thermokarst lakes in the southwest that were excluded from the calculations within Chapter 4 of this thesis. The areal percentages for the thesis' study area extent therefore might slightly deviate from the one given by Grosse et al. (2006). For the Buor Khaya Peninsula area, a similar approach, which combined a multispectral classification of RapidEye data with DEM derived relief characteristics, revealed a degradation of 90 % (Arcos, 2012).

5.2 Characteristics of degradational landforms in different settings

The previous paragraph showed great differences in the overall areal percentage of degradational landforms between the study areas, but also the morphometric characteristics and spatial distribution of thermokarst and thermo-erosional landforms vary considerably. On Cape Mamontov Klyk, degradational landforms are deeply incised into the Yedoma surface, and thermo-erosional valleys dominate the relief, even though very large thermokarst lakes and alasses also occur (Figure 4-2). On the Buor Khaya Peninsula, only a few Yedoma remnants are elevated over large areas of flat surfaces that resulted from

extensive degradation by thermokarst. In the Lena Delta, the situation on Khardang Island (western delta, for location see Figure 2-4) resembles that in the Cape Mamontov Klyk area, while the characteristics of Sobo Island (eastern delta, for location see Figure 2-4) are similar to the Buor Khaya Peninsula (Figure 4-2).

These differences in the surface characteristics and coverage with degradational landforms resulted from different relief situations. Higher relief gradients are present in the western part of the study region due to the widespread presence of elevated Yedoma uplands, while lower gradients are found in the low-lying plains of the eastern part. This marked difference between the western and eastern region possibly also reflects neotectonic activity. The study region is seismotectonically very active, because it is located at the zone of intense deformation between the North American and Eurasian plates, which transforms from extension in the Laptev Sea to transpression further south (Grigoriev et al., 1996; Grachev et al., 2003; Fujita et al., 2009) (Figure 5-1). Modern seismicity records show particularly high concentrations of epicenters of earthquakes with magnitudes of up to 5 along the Olenyokskaya and Bykovsky channels bordering the Lena Delta to the south. In the Lena Delta, a dichotomy between uplift in the western and subsidence in the eastern part has been inferred from stratigraphical investigations (Grigoriev, 1993; Schwamborn et al., 2002). Tectonic movements of significant amplitudes (30 m and more) are reported for the Holocene (Galabala, 1987). Khardang Island, which is the largest island of the third Lena Delta terrace, has an elevated central part in the east originating from block uplift (Grigoriev, 1993). Other islands of the third terrace also indicate neotectonic movements since at least the late Pleistocene because of their different land surface inclinations. For the original late-Pleistocene accumulation plain a consistent inclination from the mountain ranges to the sea would be assumed, i.e. from SSW (high) to NNE (low). The erosional remnants of this accumulation plain, which today form the third Lena Delta terrace, should in general show the same inclination. However, the generalized surface of the Yedoma upland of Kurungnakh Island is inclined from SE to NW and the surface of Dzhangylakh Island (west of Kurungnakh Island, Figure 2-4) from NNE to SSW. Khardang Island shows an even more complex situation with its central block uplift in the eastern part and an inclination from N to S in the western part of the island. The Buor Khaya Pensinsula is situated in an area of subsidence, the Omoloi Graben, and therefore provides conditions similar to the eastern subsiding Lena Delta sector, whereas the Cape Mamontov Klyk area is situated in the Lena-Taimyr Uplift and is comparable to the third terrace islands in the western Lena Delta section (Drachev et al., 1998) (Figure 5-1).

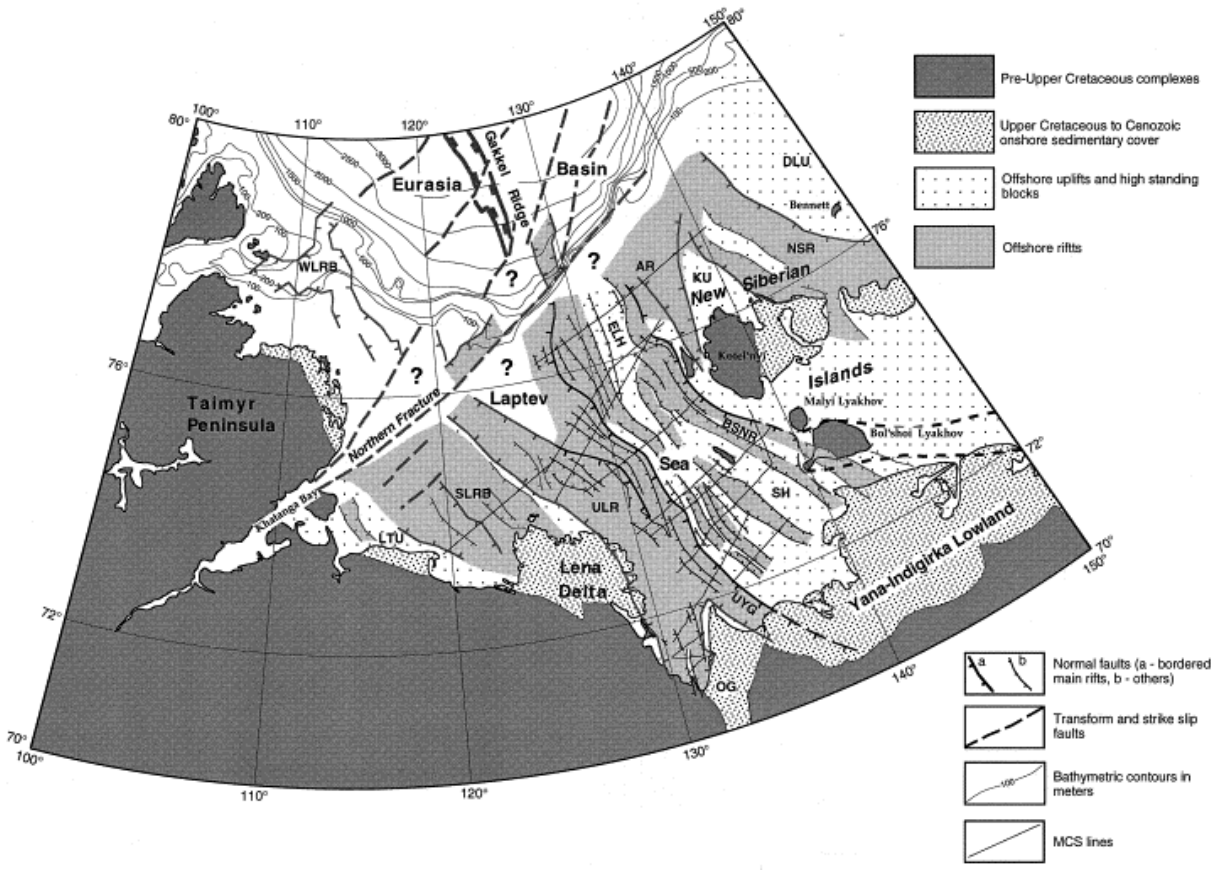

Figure 5-1. Tectonic context of the study region (map from Drachev et al., 1998). WLRB - West Laptev Rift Basin, LTU - Lena–Taimyr Uplift, SLRB - South Laptev Rift Basin, ULR - Ust' Lena Rift, UYG - Ust' Yana Graben, OG - Omoloi Graben, ELH - East Laptev Horst, AR - Anisin Rift, BSNR - Bel'kov-Svyatoi Nos Rift, SH - Stolbovoi Horst, KU - Kotel'nyi Uplift, NSR - New Siberian Rift, DLU - De Long Uplift. The grey-coloured faults are mainly delineated by the gravity data.

In regions of tectonic uplift, permafrost degradation creates distinct landforms that are deeply incised into the ice-rich deposits, and thermal erosion prevails thermokarst, whereas the surface in lowered regions degrades almost completely and predominantly by thermokarst (Kaplina et al., 1986; Kaplina, 2009). The characteristics of the degradational landforms and the present-day relief confirm an uplift situation in the western part of the study region (including Kurungnakh Island) and a subsidence situation in the eastern part (east of Kurungnakh Island). The alas on Kurungnakh Island, which has been investigated in high detail in Chapter 3, represents a typical example of thermokarst in regions of tectonical uplift, because of its distinct outline, great depth, and connection to a deep thermo-erosional valley that led to the drainage of the primary thermokarst lake and limitation of subsequent thermokarst activity.

The present-day cryolithology of the study areas is also a result of the described relief situations. The massive thermokarst development in the lowered regions led to the thawing

and compaction of the Ice Complex deposits over extensive areas, which consequently resulted in an overall lower ice volume. Even though aggrading Holocene permafrost on these degraded surfaces can also be ice-rich, the large ice volume of the late Pleistocene deposits as well as their initial surface level is not reached. In the uplifted areas, thermal erosion has been the dominating type of permafrost degradation over thermokarst. In the valleys, the Ice Complex has been thawed and much of the sediments eroded, and in alasses, the Ice Complex deposits have been transformed similar to that in the lowered regions. Undegraded Yedoma uplands remained in some areas that still feature the original late Pleistocene deposits with high ice contents.

The altered cryolithological conditions in degraded parts of the landscapes significantly influence the morphometric characteristics of subsequently evolving degradational landforms (Table 5-1). Newly developing thermokarst and thermo-erosional processes are generally restricted in depth because of the lower total ice volume (Chapters 2, 3, 4). Maximum measured depths of lakes in alasses were about 4 m, while alasses themselves are up to 35 m deep (Chapter 2). Similarly, thermo-erosional valleys in degraded areas are up to about 10 m deep, while those that have incised into Yedoma surfaces reach maximum depths of 35 m (Chapter 4). Thermokarst lakes that form on Yedoma uplands usually have smooth, circular outlines, because their lateral expansion proceeds evenly in all directions (Table 2-5). In contrast, the formation of lakes on degraded surfaces takes place in a setting that has been affected by an interplay of different, partly concurrent processes like previous lake expansion and stepwise drainage, permafrost aggradation and polygonal ice-wedge growth, and the formation of drainage channels and pingos (Chapter 3). This leads to a higher micro- and meso-relief differentiation and differences in ground ice distribution, resulting in more irregular outlines of subsequently evolving lakes. Thermo-erosional valleys that form on Yedoma uplands mostly follow a steeper relief gradient and develop dendritic networks, whereas streams that drain flat degraded surfaces follow a more longitudinal course over small relief gradients (Chapter 4).

Table 5-1. Comparison between degradational landforms that have formed on undisturbed Yedoma uplands and those that have formed on previously degraded surfaces.

	Yedoma uplands		Degraded surfaces	
	Thermokarst	Thermal erosion	Thermokarst	Thermal erosion
Max. depth (m)	35	35	4	10
Morphometry	smooth, circular outlines	dendritic networks	irregular outlines	longitudinal valleys

5.3 Types and developmental stages of degradational landforms

Thermokarst and thermo-erosional landforms have been categorized into different morphometric types and developmental stages. Thermokarst lakes on Yedoma uplands that completely fill their basins represent the first stage of thermokarst development in the ice-rich permafrost of the study region (Chapters 2, 3). After drainage of the primary lake, residual lakes can remain in the newly formed alas and continue to erode previously unaffected Ice Complex deposits by lateral expansion into the initial alas slopes (Chapter 3). On the exposed alas floor, permafrost starts to aggrade, providing the conditions for secondary thermokarst lake formation. The formation and subsequent partial or complete drainage of secondary thermokarst lakes can occur several times in the same area, but is rather limited in regions of tectonic uplift compared to regions of subsidence. In uplifted regions, primary thermokarst lakes form deep, distinct alasses. After their first drainage they are usually well connected to the hydrological network that follows a high relief gradient. Further water supply will therefore rather lead to the drainage of the secondary thermokarst lakes than to their continuing lateral expansion. As has been summarized in Section 5.2, substantial further subsidence of secondary thermokarst lakes in deep alasses will not occur because ground ice contents of underlying deposits are mostly not sufficient to sustain deep thermokarst development due to previous talik formation underneath the primary thermokarst lake. In regions of tectonic subsidence, however, several generations of thermokarst landforms are superimposed on each other. The original late Pleistocene Yedoma surface has been degraded over extensive areas, creating broad lowlands with low relief gradients that provide only poor drainage conditions, hence promoting the repeated ponding of water and formation of larger, but shallow secondary thermokarst lakes.

Morphological types of large thermo-erosional valley systems, dendritic networks and longitudinal valleys, have already been discussed in the context of the different relief and cryolithological settings which they predominantly form in (Chapter 5.2). Furthermore, a categorization can be established for individual thermo-erosional landforms or sections of the valley systems (Table 4-3). Some of these categories, for example V-shaped valleys, U-shaped valleys, and valleys of permanent rivers and streams, represent different evolutionary stages that often succeed one another in the longitudinal profile of a longer valley or valley system. The degree to which they develop depends mainly on the size of the catchment and the respective relief gradient. Only in large catchments, which accumulate considerable amounts of surface water to large meandering permanent streams and rivers, broad valleys and valley floodplains are able to form (Chapter 4).

Most of the thermo-erosional valleys in the study region can be considered primary thermo-erosional landforms, no matter whether they have formed on Yedoma uplands (like V-shaped ravines and valleys) or on surfaces that had previously been degraded by thermokarst (like drainage pathways in alasses). However, thermal erosion that reactivates on previously stabilized thermo-erosional valley floors can create secondary thermo-erosional landforms. The secondary features can belong to a different morphometric category than the primary landforms which they form in, for example a V-shaped ravine can form on the floor of a U-shaped valley.

The different types discussed in this chapter are the result of the different character of geomorphological processes that can occur simultaneously within the study region in dependence on relief and cryolithological conditions, but under the same climatic conditions. The study region has experienced climatic variations that affected the evolution of the degradational landforms. The onset of massive and widespread degradation of the ice-rich permafrost in the region at the transition from late Pleistocene to Holocene was triggered by a significant change to warmer and moister climate conditions (Chapter 2, 3). The dominating form of degradation in all three study areas during that time was thermokarst. After the Holocene thermal maximum, which was the period between 10,000 and ca. 8,500-8,200 a BP (Kuzmina and Sher, 2006), thermokarst activity in the region decreased. The reconstruction of the evolution of an individual alas on Kurungnakh Island revealed that the thermokarst lakes in the alas expanded during two phases of high water availability between 5 and 3 ka BP that were attributed to regional variations in the precipitation regime (Chapter 3). Such regional climatic changes most likely influenced the overall thermokarst development in the study areas. The wetter phases probably also enhanced thermo-erosional processes that had been activated since the mid to late Holocene due to the formation of higher relief gradients.

5.4 Interaction between thermokarst and thermal erosion

The previous chapters indicate that thermokarst and thermal erosion are interrelated. Thermokarst, among other processes such as the transgression of the sea or the fluvial and deltaic erosion of the Lena Delta Ice Complex, created relief differences that initiated thermal erosion. Retrogressive thermo-erosional valleys can drain thermokarst lakes on Yedoma uplands by tapping, thereby regulating and limiting the active development of thermokarst (Chapter 2, 3). The drainage event itself is an interaction between the thermokarst lake and the thermo-erosional valley. This has been described for the drainage of the studied alas in Chapter 3 and is further illustrated by Figure 5-2, which shows a small

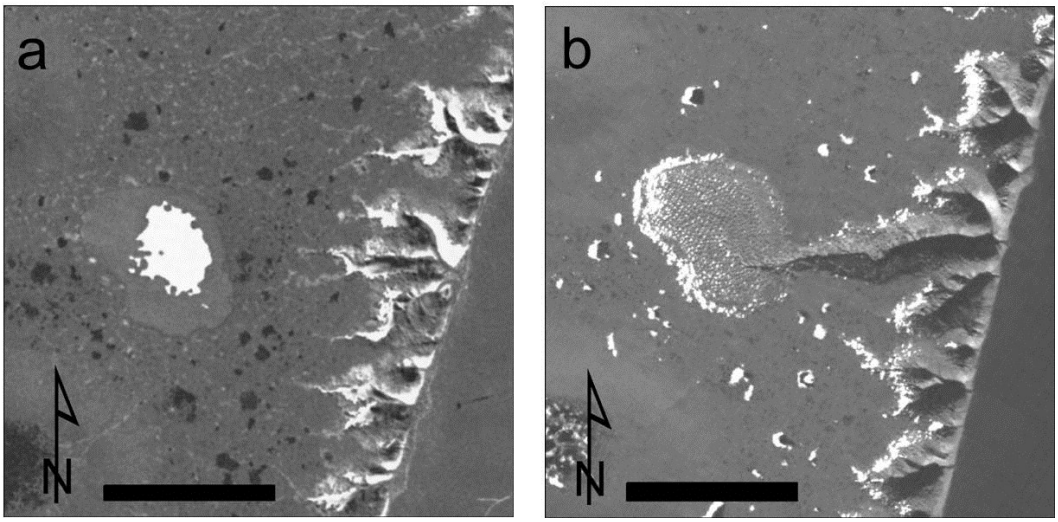

Figure 5-2. Thermokarst and short thermo-erosional landforms on Kurungnakh Island, Lena Delta, **(a)** before (Corona, 22 June 1964) and **(b)** after lake drainage (ALOS PRISM, 21 September 2006). Scale bars are 500 m, white patches on lake ice and in upper valley sections in (a) and at the margins of drained basin and small ponds in (b) indicates snow.

thermokarst lake on Yedoma uplands and a short thermo-erosional valley before and after a drainage event. The draining thermo-erosional valley is one of several short V-shaped ravines that have incised into the about 50 m high eastern bluff of Kurungnakh Island, Lena Delta. Figure 5-2a shows that the valley bifurcates at a distance of about 300 m from the island's margin, presumably along polygonal ice wedge systems. The thermokarst lake completely fills its basin, no slopes are visible around its margin. A small light-colored band between the southeastern shoreline of the lake and the southern valley branch in Figure 5-2a indicates the location of overflow during times of high water availability related to a slight micro-topographic depression along polygonal troughs on the Yedoma surface (Simova, 1964). It can be assumed that during a summer with high precipitation warm water discharged from the lake via this outflow band and into the southern valley branch. It thermally eroded the ice-wedge ice, thereby eventually lowering the drainage sill of the lake and establishing a direct connection between the lake and the southern branch of the thermo-erosional valley, which triggered lake drainage. Similar processes involving channel headward erosion, lake bank overflow, and lake drainage have been reported for other regions such as the Mackenzie region (Marsh and Neumann, 2001) or the Seward Peninsula (Jones et al., 2011). The warm water of the draining lake further eroded the Yedoma surface and the lake drained rapidly. The result of this self-reinforcing process is shown in Figure 5-2b; the lake has drained completely and a new, deep valley section has formed between the lake basin and the previous head of the southern valley branch. The exact date of the drainage event is unknown, but occurred about 20 ± 5 years after the acquisition of the satellite image in Figure 5-2a as inferred from the comparison of further satellite imagery

(Ulrich et al., 2009). The valley therefore might have retrogressed further into the direction of the lake before the drainage event, thereby reducing the drainage barrier, but the drainage process and the rapid deepening of the valley floor by thermal erosion still would have proceeded similar to the description presented here.

5.5 Future development of thermokarst and thermal erosion

The results of this thesis consistently emphasize the necessity of understanding the previous degradation history of ice-rich permafrost landscapes and its conditions before scenarios about the future development of permafrost degradation by thermokarst and thermal erosion and implications for its impacts can be inferred. It is particularly important to include both major types of permafrost degradation, thermokarst and thermal erosion, and their interplay in the investigation of particular landscapes. For example, calculations of Yedoma areas that are available for future permafrost degradation by thermokarst and the extrapolation of associated potential carbon release will yield significantly lower values for areas of tectonic uplift if thermo-erosional landforms are included compared to calculations that are based on thermokarst landforms only.

In the study region, less than one third of the area represents original Yedoma surfaces unaffected by thermokarst and thermal erosion (Section 5.2). The future development of thermokarst lakes on Yedoma uplands is restricted due to the increasing proximity of existing degradational landforms and other topographic lows that will lead to lake drainage (Chapter 2). Even if the regional climate continued to change to warmer and moister conditions, thermokarst processes on Yedoma uplands will not lead to such a widespread formation of large thermokarst lakes as during the early Holocene. The degradation of the remaining Ice Complex deposits will continue, but lateral erosion by thermo-erosional landforms and by the expansion of lakes in alasses might have a more important effect than thermokarst subsidence. This has important implications for the mobilization of the fossil organic carbon that had been stored in the frozen deposits for several thousands of years (Tarnocai et al., 2009). While carbon from thawing organic matter underneath thermokarst lakes becomes available for local biogeochemical processes and can be released to the atmosphere as greenhouse gases, it will be at least partly transported to the fluvial system by thermal erosion (Grosse et al., 2011).

Thermokarst and thermo-erosional processes evolving or reactivating on surfaces that had previously been affected by thermokarst activity were shown to have a smaller impact on the alteration of ice-rich permafrost landscapes than those occurring on undisturbed Yedoma uplands (Chapters 1, 2, 3). They are restricted to the Ice Complex deposits that had

already experienced thaw, compaction, and old carbon mobilization, and to Holocene deposits that have formed after the drainage of the primary thermokarst lake.

5.6 Outlook

The study region can be regarded a key region for the investigation of permafrost degradation, because it features sensitive ice-rich deposits in different relief settings and stages of degradation. The implications derived from this thesis can be transferred to other regions with similar characteristics. The Siberian Yedoma extent has been estimated to cover an area of about 10^6 km² (Zimov et al., 2006a), and similar ice-rich deposits have also been described for North American regions (Kanevskiy et al., 2011; Schirrmeister et al., 2013) (Figure 1-2). However, despite the fact that permafrost degradation and thermokarst have been studied for decades, many of the complex interactions between process factors and landscape components remain to be investigated (Jorgenson et al., 2010; Grosse et al., 2011) and are still not included or adequately represented in climate models (Jorgenson et al., 2010; Burke et al., 2012). This applies in particular to thermal erosion, which is a largely understudied phenomenon. In Alaska, integrated investigations are underway to quantify landscape and biogeochemical changes related to thermo-erosional processes in permafrost hillslopes (Bowden et al., 2012). In Siberian ice-rich permafrost regions, however, systematic studies of thermo-erosional processes and landforms over large areas have been lacking. The investigations on the spatial characteristics of thermo-erosional landforms in different relief and cryolithological settings based on remote sensing and geoinformation techniques that were presented in Chapter 4 should therefore be extended in the future in order to assess the impact of thermal erosion on the degradation of Siberian ice-rich permafrost and to relate it to ongoing changes of the water and carbon cycle in the Arctic. In particular, future studies should:

- extend the investigations of this thesis to other study areas,
- quantify thermo-erosional landform changes over the past 60 years by means of multitemporal remote sensing,
- investigate the interactions of thermal erosion, not only with thermokarst, but also hydrological landscape conditions, vegetation, snow cover, etc.,
- conduct water sampling as baseline for nutrient and sediment load,
- deduce more detailed scenarios for the potential evolution of thermo-erosional landforms and related permafrost landscape components under a warming climate,
- evaluate subsequent impacts on the arctic water and carbon cycle.

Ideally, such studies would combine remote sensing and geoinformation methods with detailed field investigations of exemplar sites in different environments. Furthermore, the acquisition of higher resolution remote sensing imagery (e.g. IKONOS, Geoeye) and DEMs (e.g. TanDEM-X) would allow for more precise areal quantifications and detailed hydrological analyses.

References

ACIA, 2004. Impacts of a warming Arctic – Arctic Climate Impact Assessment, Cambridge, Cambridge University Press, 146.

AMAP, 2011. Snow, water, ice and permafrost in the Arctic (SWIPA). Oslo: Arctic Monitoring and Assessment Programme (AMAP).

Andreev, A., Tarasov, P., Schwamborn, G., Ilyashuk, B., Ilyashuk, E., Bobrov, A., Klimanov, V., Rachold, V., Hubberten, H.-W., 2004. Holocene paleoenvironmental records from Nikolay Lake, Lena River Delta, Arctic Russia. Palaeogeography, Palaeoclimatology, Palaeoecology 209, 197-217, doi:10.1016/j.palaeo.2004.02.010.

Anisimov, O. A., Reneva, S. A., 2006. Permafrost and changing climate: The Russian perspective. Ambio 35, 169-175.

Anisimova, N. P., 1961. Geothermal investigations in taliks underneath several water bodies and streams in central Yakutia. Permafrost and accompanying phenomena on the territory of the Yakutian ASSR, USSR Academy of Sciences, Moscow, 89-95. (in Russian)

Arcos, D. R., 2012. Classification of periglacial landforms based on high resolution multispectral remote sensing data. A contribution to the landscape description of the north Siberian Buor Khaya Pensinsula. Unpublished diploma thesis, University of Potsdam, 71 p. (in German)

Bauch, H. A., Mueller-Lupp, T., Taldenkova, E., Spielhagen, R. F., Kassens, H., Grootes, P. M., Thiede, J., Heinemeier, J., Petryashov, V. V., 2001. Chronology of the Holocene transgression at the North Siberian margin, Global and Planetary Change 31, 125–139.

Billings, W.D., Peterson, K.M., 1980. Vegetational change and ice-wedge polygons through the thaw-lake cycle in arctic Alaska. Arctic and Alpine Research 12 (4), 413-432.

Boike, J., Abramova, K., Bolshiyanov, D., Grigoriev, M., Herzschuh, U., Kattner, G., Knoblauch, C., Kutzbach, L., Mollenhauer, G., Schneider, W. (Eds.), 2009. Russian-German Cooperation SYSTEM LAPTEV SEA: The Expedition Lena 2009. Reports on Polar and Marine Research 600, Alfred Wegener Institute for Polar and Marine Research, Bremerhaven.

Bosikov, N. P., 1991. Evolution of Central Yakutian alasses, Permafrost Institute Yakutsk, Siberian Branch, USSR Academy of Sciences, Yakutsk, 128 p. (in Russian)

Bowden, W. B., Gooseff, M. N., Balser, A., Green, A., Peterson, B. J., Bradford, J., 2008. Sediment and nutrient delivery from thermokarst features in the foothills of the North Slope, Alaska: Potential impacts on headwater stream ecosystems. Journal of Geophysical Research 113, G02026, doi:10.1029/2007JG000470.

Bowden, W. B., Larouche, J. R., Pearce, A. R., Crosby, B. T., Krieger, K., Flinn, M. B., Kampman, J., Gooseff, M. N., Godsey, S. E., Jones, J. B., Abbott, B. W., Jorgenson, M. T., Kling, G. W., Mack, M., Schuur, E. A. G., Baron, A. F., Rastetter, E. B., 2012. An integrated assessment of the influences of upland thermal-erosional features on landscape structure and function in the foothills of the Brooks Range, Alaska. In: Hinkel, K. M. (Ed.), Tenth International Conference on Permafrost, Vol. 1: International Contributions, The Northern Publisher, Salekhard, Russia, 61-66.

Boytsov, M. N., 1965. Morphological evolution of thaw lake basins. Anthropogenic period in the Arctic and Subarctic, 143, edited by NEDRA, Research Institute Geology of the Arctic, Moscow, Russia, 327–340. (in Russian)

Burke, E. J., Hartley, I. P., Jones, C. D., 2012. Uncertainties in the global temperature change caused by carbon release from permafrost thawing. The Cryosphere Discussions 6, 1367-1404, doi:10.5194/tcd-6-1367-2012.

Carson, C. E., Hussey, K. M., 1962. The oriented lakes of Arctic Alaska. Journal of Geology 70, 417-439.

CAVM Team, 2003. Circumpolar Arctic Vegetation Map (1:7,500,000 scale). Conservation of Arctic Flora and Fauna (CAFF) Map No. 1., U.S. Fish and Wildlife Service, Anchorage, Alaska.

Chapin, F., Sturm, M., Serreze, M., McFadden, J., Key, J. R., Lloyd, A. H., McGuire, A. D., Rupp, T. S., Lynch, A. H., Schimel, J. P., Beringer, J., Chapman, W. L., Epstein, H. E., Euskirchen, E. S., Hinzman, L. D., Jia, G., Ping, C.-L., Tape, K. D., Thompson, C. D. C., Walker, D. A., Welker, J. M., 2005. Role of land-surface changes in Arctic summer warming. Science 310, 657-660, doi:10.1126/science.1117368.

Costard, F., Dupeyrat, L., Gautier, E., Carey-Gailhardis, E., 2003. Fluvial thermal erosion investigations along a rapidly eroding river bank: application to the Lena River (central Siberia). Earth Surface Processes and Landforms 28 (12), 1349-1359.

Côté, M. M., Burn, C. R, 2002. The oriented lakes of Tuktoyaktuk Peninsula, western arctic coast, Canada: A GIS-based analysis. Permafrost and Periglacial Processes 13, 61–70, doi: 10.1002/ppp.407.

Czudek, T. , Demek, J., 1970. Thermokarst in Siberia and its influence on the development of lowland relief. Quaternary Research 1 103–120.

Czudek, T., Demek, J., 1973. Die Reliefentwicklung während der Dauerfrostboden-degradation (The relief development during the degradation of permafrost). Rozpravy Československé Akademie věd, Řada matematických a přírodních věd 83 (2), Academie nakladatelství Československé Akademie věd, Praha, 68 p. (in German)

Downing, J. A., Prairie, Y. T., Cole, J. J., Duarte, C. M., Tranvik, L. J., Striegl, R. G., McDowell, W. H., Kortelainen, P., Caraco, N. F., Melack, J. M., Middelburg, J. J., 2006. The global abundance and size distribution of lakes, ponds, and impoundments. Limnology and Oceanography 51, 2388–2397.

Drachev, S. S., Savostin, L. A., Groshev, V. G., Bruni, I. E., 1998. Structure and geology of the continental shelf of the Laptev Sea, Eastern Russian Arctic. Tectonophysics 298, 357-393.

Dupeyrat, L., Costard, F., Randriamazaoro, R., Gailhardis, E., Gautier, E., Fedorov, A., 2011. Effects of ice content on the thermal erosion of permafrost: implications for coastal and fluvial erosion. Permafrost and Periglacial Processes 22 (2), 179-187, doi: 10.1002/ppp.722.

Faegri, K., Iversen, J., 1989. Textbook of Pollen Analysis. John Wiley & Sons, New York.

Fortier, D., Allard, M., Shur, Y., 2007. Observation of rapid drainage system development by thermal erosion of ice wedges on Bylot Island, Canadian Arctic Archipelago. Permafrost and Periglacial Processes 18 (3), 229-243, doi: 10.1002/ppp.595.

Franke, D., Hinz, K., Block, M., Drachev, S. S., Neben, S., Kos'ko, M. K., Reichert, C., Roeser, H. A., 2000. Tectonics of the Laptev Sea region in Northeastern Siberia. Polarforschung 68, 51-58.

French, H. M., 2007. The periglacial environment. Third Edition, John Wiley & Sons, Chichester.

Frohn, R. C., Hinkel, K. M., Eisner, W. R., 2005. Satellite remote sensing classification of thaw lakes and drained thaw lake basins on the North Slope of Alaska. Remote Sensing of Environment 97, 116-126, doi: 10.1016/j.rse.2005.04.022.

Fujita, K., Koz'min, B. M., Mackey, K. G., Riegel, S. A., McLean, M. S., and Imaev, V. S., 2009. Seismotectonics of the Chersky Seismic Belt, eastern Sakha Republic (Yakutia) and Magadan District, Russia, Stephan Mueller Special Publication Series 4, 117-145, doi:10.5194/smsps-4-117-2009.

Galabala, R. O., 1987. New data on the composition of the Lena Delta. Quaternary of Northeast Asia, Academy of Sciences of the USSR, Magadan, Russia, 152-172.

Gavrilov, A. V., Romanovskii, N. N., Romanovsky, V. E. Hubberten, H. W., Tumskoy, V. E., 2003. Reconstruction of ice complex remnants on the eastern Siberian arctic shelf. Permafrost and Periglacial Processes 14 (2), 187-198.

Godin, E., Fortier, D., 2012. Fine-scale spatio-temporal monitoring of multiple thermo-erosion gully development on Bylot Island, Eastern Canadian Archipelago. In: Hinkel, K. M. (Ed.), Tenth International Conference on Permafrost, Vol. 1: International Contributions, The Northern Publisher, Salekhard, Russia, 125-130.

Goslar, T., Czernik, J., Goslar, E., 2004. Low-energy 14C AMS in Poznań Radiocarbon Laboratory, Poland. Nuclear Instruments and Methods in Physics Research Section B: Beam Interactions with Materials and Atoms 223–224 (0), 5-11, doi:10.1016/j.nimb.2004.04.005.

Grachev, A. F., 2003. The Arctic rift system and the boundary between the Eurasian and North American lithospheric plates: New insight to plate tectonic theory. Russian Journal of Earth Sciences 5 (5), 307-345.

Grigoriev, M. N., 1993. Cryomorphogenesis of the Lena River mouth area, Siberian Branch, USSR Academy of Sciences, Yakutsk, 176 p. (in Russian).

Grigoriev, M. N., Imaev, V. S., Imaeva, L. P., Kozmin, B. M., Kunitskiy, V. V., Lationov, A. G., Mikulenko, K. I., Skryabin, R. M., Timirshin, K. V., 1996. Geology, Seismicity and Cryogenic Processes in the Arctic Areas of Western Yakutia. Yakut Scientific Centre SB RAS, Yakutsk, 84 p. (in Russian)

Grimm, E.C., 1987. CONISS: A FORTRAN 77 program for stratigraphically constrained cluster analysis by the methods of incremental sum of squares. Computers and Geoscience 13, 13-35.

Grimm, E.C., 1991. TILIA and TILIAGRAPH Software. Springfield, Illinois.

Grosse, G., Schirrmeister, L., Kunitsky, V. V., Hubberten, H.-W., 2005. The use of CORONA images in remote sensing of periglacial geomorphology: An illustration from the NE Siberian coast. Permafrost and Periglacial Processes 16, 163–172, doi: a 10.1002/ppp.509.

Grosse, G., Schirrmeister, L., Malthus, T. J., 2006. Application of Landsat-7 satellite data and a DEM for the quantification of thermokarst-affected terrain types in the periglacial Lena-Anabar coastal lowland. Polar Research 25, 51-67.

Grosse, G., Schirrmeister, L., Siegert, C., Kunitsky, V. V., Slagoda, E. A., Andreev, A. A., Dereviagyn, A. Y., 2007. Geological and geomorphological evolution of a sedimentary periglacial landscape in Northeast Siberia during the Late Quaternary. Geomorphology 86, 25–51, doi:10.1016/j.geomorph.2006.08.005.

Grosse, G., Romanovsky, V., Walter, K., Morgenstern, A., Lantuit, H., Zimov, S., 2008. Distribution of thermokarst lakes and ponds at three Yedoma sites in Siberia. Proceedings of the 9th International Conference on Permafrost, Fairbanks, Alaska, 29 June - 3 July 2008, Kane, D. L. and Hinkel, K. M. (Eds.), Institute of Northern Engineering, University of Alaska Fairbanks, 551-556.

Grosse, G., Harden, J., Turetsky, M., McGuire, A. D., Camill, P., Tarnocai, C., Frolking, S., Schuur, E. A. G., Jorgenson, T., Marchenko, S., Romanovsky. V., Wickland, K. P., French, N., Waldrop, M., Bourgeau-Chavez, L., Striegl, R. G., 2011. Vulnerability of high latitude soil carbon in North America to disturbance. Journal of Geophysical Research 116, G00K06, doi:10.1029/2010JG001507.

Grosse, G., Jones, B., Arp, C., 2012. Thermokarst lakes, drainage, and drained basins. In: Shroder, J. (Editor in Chief), Giardino, R., Harbor, J. (Eds.), Treatise on Geomorphology, Academic Press, San Diego, CA, vol. 8 (in press).

Günther, F., 2009. Investigation of thermokarst evolution in the southern Lena Delta using multitemporal remote sensing and field data, unpublished diploma thesis, Technical University of Dresden, Dresden, Germany, 96 pp. (in German)

Günther, F., Ulrich, M., Morgenstern, A., Schirrmeister, L., 2010. Planimetric and volumetric thermokarst change detection on ice rich permafrost, using remote sensing and field data. Third European Conference on Permafrost: Thermal state of frozen ground in a changing climate during the IPY, Svalbard, Norway.

Günther, F., Overduin, P.P., Sandakov, A.V., Grosse, G., Grigoriev, M.N., 2012. Thermo-erosion along the Yedoma coast of the Buor Khaya Peninsula, Laptev Sea, East Siberia. In: Hinkel, K. M. (Ed.), Tenth International Conference on Permafrost, Vol. 1: International Contributions, The Northern Publisher, Salekhard, Russia, 137-142.

Hinkel, K. M., Eisner, W. R., Bockheim, J. G., Nelson, F. E., Peterson, K. M., Dai, X. Y., 2003. Spatial extent, age, and carbon stocks in drained thaw lake basins on the Barrow Peninsula, Alaska. Arctic, Antarctic and Alpine Research 35, 291-300.

Hinkel, K. M., Frohn, R. C., Nelson, F. E., Eisner, W. R., Beck, R. A., 2005. Morphometric and spatial analysis of thaw lakes and drained thaw lake basins in the western Arctic Coastal Plain, Alaska. Permafrost and Periglacial Processes 16, 327–341, doi: 10.1002/ppp.532.

Hopkins, D.M., 1949. Thaw lakes and thaw sinks in the Imuruk lake area, Seward Peninsula, Alaska. Journal of Geology 57 (2), 119-131.

Horton, R. E., 1932. Drainage basin characteristics. American Geophysical Union, Transactions 13, 348-352.

Horton, R. E., 1945. Erosional development of streams and their drainge basins; Hydrophysical approach to quantitative morphology. Bulletin of the Geological Society of America 56, 275-370.

Hubberten, H. W., Andreev, A., Astakhov, V. I., Demidov, I., Dowdeswell, J. A., Henriksen, M., Hjort, C., Houmark-Nielsen, M., Jakobsson, M., Kuzmina, S., Larsen, E., Lunkka, J. P., Lysa, A., Mangerud, J., Moller, P., Saarnisto, M., Schirrmeister, L., Sher, A. V., Siegert, C., Siegert, M. J., Svendsen, J. I., 2004. The periglacial climate and environment in northern Eurasia during the Last Glaciation. Quaternary Science Reviews 23, 1333–1357.

Jeffries, M.O., Morris, K., Liston, G.E., 1996. A method to determine lake depth and water availability on the North Slope of Alaska with spaceborne imaging radar and numerical ice growth modeling. Arctic 49 (4), 367-374.

Jones, B. M., Grosse, G., Arp, C. D., Jones, M. C., Walter Anthony, K. M., Romanovsky, V. E., 2011. Modern thermokarst lake dynamics in the continuous permafrost zone, northern Seward Peninsula, Alaska. Journal of Geophysical Research 116, G00M03, doi:10.1029/2011JG001666.

Jorgenson, M. T., Shur, Y. L., Pullman, E.R., 2006. Abrupt increase in permafrost degradation in Arctic Alaska. Geophysical Research Letters 33, L02503. doi:10.1029/2005GL024960.

Jorgenson, M. T., Shur, Y., 2007. Evolution of lakes and basins in northern Alaska and discussion of the thaw lake cycle. Journal of Geophysical Research 112, F02S17. doi:10.1029/2006JF000531.

Jorgenson, M. T., Romanovsky, V., Harden, J., Shur, Y., O'Donnell, J., Schuur, E. A. G., Kanevskiy, M., Marchenko, S., 2010. Resilience and vulnerability of permafrost to climate change. Canadian Journal of Forest Research 40 (7), 1219–1236, doi:10.1139/X10-060.

Kanevskiy, M., Shur, Y., Fortier, D., Jorgenson, M. T., Stephani, E., 2011. Cryostratigraphy of late Pleistocene syngenetic permafrost (yedoma) in northern Alaska, Itkillik River exposure. Quaternary Research 75, 584-596, doi: 10.1016/j.yqres.2010.12.003.

Kaplina, T. N., 2009. Alas complex of Northern Yakutia, Kriosfera Zemli (Earth Cryosphere) 13, 3-17. (in Russian)

Kaplina, T. N., Lozhkin, A. V., 1979. Age of alas deposits of the Yakutian coastal plain, Geologiya (Geology), 2, USSR Academy of Sciences, 69-76. (in Russian)

Kaplina, T. N., Kostalyndina, N. K., Leibman, M. O., 1986. Relief analysis of the Kolyma lowlands for cryolithological mapping. Formation of frozen ground and prognosis of cryogenic processes, Nauka, Moscow, 51-60. (in Russian)

Karlsson, J., Christensen, T. R., Crill, P., Förster, J., Hammarlund, D., Jackowicz-Korczynski, M., Kokfelt, U., Roehm, C., Rosén, P., 2010. Quantifying the relative importance of lake emissions in the carbon budget of a subarctic catchment. Journal of Geophysical Research 115, G03006, doi: 10.1029/2010JG001305.

Katasonova, E. G., 1963. The role of thermokarst in the development of dells. In: Katasonov, E.M. (Ed.), Conditions and special features of the formation of frozen horizons in Siberia and in Far-East, Publishing House AN SSSR, Moscow, pp. 91–100. (in Russian)

Katasonov, E. M., 1960. On the deposits of the thermokarst lakes "alasses" in the Yana maritime lowlands, Geologiya i Geofisika (Geology and Geophysics), 2, Siberian Branch, USSR Academy of Sciences, 103-112. (in Russian)

Khvorostyanov, D. V., Ciais, P., Krinner, G., Zimov, S. A., 2008. Vulnerability of east Siberia's frozen carbon stores to future warming. Geophysical Research Letters 35, L10703, doi: 10.1029/2008GL033639.

Kienast, F., Wetterich, S., Kuzmina, S., Schirrmeister, L., Andreev, A. A., Tarasov, P., Nazarova, L., Kossler, A., Frolova, L., Kunitsky, V. V., 2011. Paleontological records indicate the occurrence of open woodlands in a dry inland climate at the present-day Arctic coast in western Beringia during the last interglacial. Quaternary Science Reviews 30, 2134-2159. doi:10.1016/j.quascirev.2010.11.024.

Kravtsova, V. I., Bystrova, A. G., 2009. Changes in thermokarst lake sizes in different regions of Russia for the last 30 years. Kriosfera Zemli (Earth Cryosphere) 13, 16-26. (in Russian)

Kravtsova, V. I., Tarasenko, T. V., 2011. The dynamics of thermokarst lakes under climate changes since 1950, Central Yakutia. Kriosphera Zemli (Earth Cryosphere) 15 (3), 31-42. (in Russian)

Kuzmina, S., Sher, A., 2006. Some features of the Holocene insect faunas of northeastern Siberia. Quaternary Science Reviews 25 (15–16), 1790-1820.

Kuznetsova, T. P., 1961. Oriented lakes of the Yano-Indigirka coastal lowland. In: Questions on the Geography of Yakutia, USSR Academy of Sciences, Yakutsk, 68-70. (in Russian)

Labrecque, S., Lacelle, D., Duguay, C. R., Lauriol, B., Hawkings, J., 2009. Contemporary (1951-2001) evolution of lakes in the Old Crow Basin, Northern Yukon, Canada: Remote sensing, numerical modeling, and stable isotope analysis. Arctic 62 (2), 225-238.

Ling, F., Zhang, T., 2004. Modeling study of talik freeze-up and permafrost response under drained thaw lakes on the Alaskan Arctic Coastal Plain. Journal of Geophysical Research 109, D01111, doi:10.1029/2003JD003886.

Marsh, P., Neumann, N. N., 2001. Processes controlling the rapid drainage of two ice-rich permafrost-dammed lakes in NW Canada. Hydrological Processes 15 (18), 3433-3446, doi: 10.1002/hyp.1035.

McNamara, J. P., Kane, D. L., Hinzman, L. D., 1999. An analysis of an arctic channel network using a digital elevation model. Geomorphology 29, 339-353.

Medeanic S., 2006. Freshwater algal palynomorph records from Holocene deposits in the coastal plain of Rio Grande do Sul, Brazil. Review of Palaeobotany and Palynology 141, 83–101.

Meyers, P.A., 1994. Preservation of elemental and isotopic source identification of sedimentary organic matter. Chemical Geology 114, 289-302.

Mitt, K. L., 1959. K voprosu o prirode delley Daaldynskovo rayona (On the question of the nature of dells in the Daaldynskiy region). Voprosy Geografii 46, 28-34. (in Russian)

Morgenstern, A., Grosse, G., Schirrmeister, L., 2008a. Genetic, morphological, and statistical characterization of lakes in the permafrost-dominated Lena Delta, in: Proceedings of the 9th International Conference on Permafrost, Fairbanks, Alaska, 29 June - 3 July 2008, Kane, D. L. and Hinkel, K. M. (Eds.), Institute of Northern Engineering, University of Alaska Fairbanks, 1239-1244.

Morgenstern, A., Ulrich, M., Guenther, F., Roessler, S., Lantuit, H., 2008b. Combining ALOS data and field investigations for the reconstruction of thermokarst evolution in the North Siberian Lena Delta, in: Proceedings of the Second ALOS PI 2008 Symposium (CD-ROM), ESA SP-664, ESA Communication Production Office, ESA, Noordwijk, Netherlands, http://hdl.handle.net/10013/epic.31924.

Morgenstern, A., Grosse, G., Günther, F., Fedorova, I., Schirrmeister, L., 2011. Spatial analyses of thermokarst lakes and basins in Yedoma landscapes of the Lena Delta. The Cryosphere 5, 849-867, doi:10.5194/tc-5-849-2011.

Morgenstern, A., Grosse, G., Arcos, D. R., Günther, F., Overduin, P. P., Schirrmeister, L., 2012a. The role of thermal erosion in the degradation of Siberian ice-rich permafrost. In preparation for Journal of Geophysical Research – Earth Surface.

Morgenstern, A., Ulrich, M., Günther, F., Roessler, S., Fedorova, I. V., Rudaya, N. A., Wetterich, S., Boike, J., Schirrmeister, L., 2012b. Evolution of thermokarst in East-Siberian ice-rich permafrost: A case study. Geomorphology, under review.

Muster, S., Langer, M., Heim, B., Westermann, S., Boike, J., 2012. Subpixel heterogeneity of ice-wedge polygonal tundra: a multi-scale analysis of land cover and evapotranspiration in the Lena River Delta, Siberia. Tellus B 64, 17301, doi:10.3402/tellusb.v64i0.17301.

Osterkamp, T. E., Viereck, L., Shur, Y., Jorgenson, M. T., Racine, C., Doyle, A., Boone, R. D., 2000. Observations of thermokarst and its impact on boreal forests in Alaska, U.S.A. Arctic, Antarctic and Alpine Research 32, 303-315.

Osterkamp, T. E., Jorgenson, M. T., Schuur, E. A. G., Shur, Y. L., Kanevskiy, M. Z., Vogel, J. G., Tumskoy, V. E., 2009. Physical and ecological changes associated with warming permafrost and thermokarst in Interior Alaska. Permafrost and Periglacial Processes 20, 235–256, doi: 10.1002/ppp.656.

Pavlova, E. Yu., Dorozhkina, M., 2000. Geomorphological studies in the western and central sectors of the Lena Delta. In: Rachold, V. (Ed.) Expeditions in Siberia in 1999, Reports on Polar Research 354, Alfred Wegener Institute for Polar and Marine Research, Bremerhaven.

Payette, S., Delwaide, A., Caccianiga, M., Beauchemin M., 2004. Accelerated thawing of subarctic peatland permafrost over the last 50 years. Geophysical Research Letters 31, L18208, doi:10.1029/2004GL020358.

Pfeiffer, E.-M., Janssen, H., 1994. Characterization of organic carbon, using the δ^{13}C-value of a permafrost site in the Kolyma-Indigirka-Lowland, northeast Siberia. In: Kimble, J. M., Ahrens, R. J. Proceedings of the Meeting on the Classification, Correlation, and Management of Permafrost-Affected Soils. July, 1994. USDA, Soil Conservation Service, National Soil Survey Center, Lincoln, NE. pp. 90-98. Publ. Co., Houston, Texas, 323 pp.

Reimer, P. J., Baillie, M. G. L., Bard, E., Bayliss, A., Beck, J. W., Blackwell, P. G., Bronk Ramsey, C., Buck, C. E., Burr, G. S., Edwards, R. L., Friedrich, M., Grootes, P. M., Guilderson, T. P., Hajdas, I., Heaton, T. J., Hogg, A. G., Hughen, K. A., Kaiser, K. F., Kromer, B., McCormac, F. G., Manning, S. W., Reimer, R. W., Richards, D. A., Southon, J. R., Talamo, S., Turney, C. S. M, van der Plicht, J., Weyhenmeyer, C. E., 2009. IntCal09 and Marine09 Radiocarbon Age Calibration Curves, 0-50,000 Years cal BP. Radiocarbon 51 (4), 1111-1150.

Riordan, B., Verbyla, D., McGuire, A. D., 2006. Shrinking ponds in subarctic Alaska based on 1950–2002 remotely sensed images. Journal of Geophysical Research 111, G04002, doi:10.1029/2005JG000150.

Roessler, S., 2009. Charakterisierung von Oberflächen- und Thermokarstformen auf eisreichen Permafrostablagerungen im Lena-Delta (Russland) (Characterization of surface and thermokarst features in ice-rich permafrost deposits in the Lena Delta (Russia)). Diploma Thesis, University of Augsburg, Augsburg, Germany. (in German)

Romanovskii, N. N., 1961. Erosion-thermokarst basins in the northern coastal lowlands of Yakutia and the New Siberian Islands, in: Permafrost Investigations, l, Moscow State University, Moscow, 124-14. (in Russian)

Romanovskii, N. N., Hubberten, H.-W., Gavrilov, A. V., Tumskoy, V. E., Tipenko, G. S., Grigoriev, M. N., Siegert, C., 2000. Thermokarst and land-ocean interactions, Laptev Sea Region, Russia. Permafrost and Periglacial Processes 11, 137-152.

Romanovskii, N. N., Hubberten, H. W., Gavrilov, A. V., Tumskoy, V. E., Kholodov, A. L., 2004. Permafrost of the east Siberian Arctic shelf and coastal lowlands. Quaternary Science Reviews 23 (11-13), 1359-1369. doi:10.1016/j.quascirev.2003.12.014.

Romanovsky, V. E., Smith, S. L., Christiansen, H. H., 2010. Permafrost thermal state in the polar Northern Hemisphere during the International Polar Year 2007–2009: A synthesis. Permafrost and Periglacial Processes 21, 106–116, doi: 10.1002/ppp.689.

Rowland, J. C., Jones, C. E., Altmann, G., Bryan, R., Crosby, B. T., Geernaert, G. L., Hinzman, L. D., Kane, D. L., Lawrence, D. M., Mancino, A., Marsh, P., McNamara, J. P., Romanovsky, V. E., Toniolo, H., Travis, B. J., Trochim, E., Wilson, C. J., 2010. Arctic landscapes in transition: responses to thawing permafrost. Eos Transactions AGU 91 (26), 229-230.

Schirrmeister, L., Kunitsky, V. V., Grosse, G., Schwamborn, G., Andreev, A. A., Meyer, H., Kuznetsova, T., Bobrov, A., Oezen, D., 2003. Late Quaternary history of the accumulation plain north of the Chekanovsky Ridge (Lena Delta, Russia) - a multidisciplinary approach. Polar Geography 27, 277-319.

Schirrmeister, L., Grigoriev, M. N., Kutzbach, L., Wagner, D., Bolshiyanov, D. (Eds.), 2004. Russian-German Cooperation SYSTEM LAPTEV SEA: The Expedition Lena-Anabar 2003. Reports on Polar and Marine Research 489, Alfred Wegener Institute for Polar and Marine Research, Bremerhaven.

Schirrmeister, L., Wagner, D., Grigoriev, M. N., Bolshiyanov, D. Yu. (Eds.), 2007. Russian-German Cooperation SYSTEM LAPTEV SEA: The Expedition Lena 2005. Reports on Polar and Marine Research 550, Alfred Wegener Institute for Polar and Marine Research, Bremerhaven.

Schirrmeister, L., Grosse, G., Kunitsky, V., Magens, D., Meyer, H., Dereviagin, A., Kuznetsova, T., Andreev, A., Babiy, O., Kienast, F., Grigoriev, M., Overduin, P.P., Preusser, F., 2008. Periglacial landscape evolution and environmental changes of Arctic lowland areas for the last 60,000 years (Western Laptev Sea coast, Cape Mamontov Klyk). Polar Research 27 (2), 249-272. doi:10.1111/j.1751-8369.2008.00067.x.

Schirrmeister, L., Grosse, G., Schnelle, M., Fuchs, M., Krbetschek, M., Ulrich, M., Kunitsky, V., Grigoriev, M., Andreev, A., Kienast, F., Meyer, H., Babiy, O., Klimova, I., Bobrov, A., Wetterich, S., Schwamborn, G., 2011a. Late Quaternary paleoenvironmental records from the western Lena Delta, Arctic Siberia. Palaeogeography, Palaeoclimatology, Palaeoecology 299 (1-2), 175–196, doi:10.1016/j.palaeo.2010.10.045.

Schirrmeister, L., Grosse, G., Wetterich, S., Overduin, P. P., Strauss, J., Schuur, E. A. G., Hubberten, H.-W., 2011b. Fossil organic matter characteristics in permafrost deposits of the northeast Siberian Arctic. Journal of Geophysical Research 116, G00M02, doi:10.1029/2011JG001647.

Schirrmeister, L., Kunitsky, V., Grosse, G., Wetterich, S., Meyer, H., Schwamborn, G., Babiy, O., Derevyagin, A., Siegert, C., 2011c. Sedimentary characteristics and origin of the Late

Pleistocene Ice Complex on north-east Siberian Arctic coastal lowlands and islands – A review. Quaternary International 241, 3–25, doi:10.1016/j.quaint.2010.04.004.

Schirrmeister, L., Froese, D., Tumskoy, V., Grosse, G., Wetterich, S., 2013. Yedoma: Late Pleistocene ice-rich syngenetic permafrost of Beringia. Encyclopedia of Quaternary Science, 2nd edition, Elsevier, in press.

Schmidt, K.-H., 1984. Der Fluss und sein Einzugsgebiet (The river and his watershed). Franz Steiner Verlag, Wiesbaden. (in German)

Schneider, J., Grosse, G., Wagner, D., 2009. Land cover classification of tundra environments in the Arctic Lena Delta based on Landsat 7 ETM+ data and its application for upscaling of methane emissions. Remote Sensing of Environment 113, 380-391, doi:10.1016/j.rse.2008.10.013.

Schuur, E. A. G., Bockheim, J., Canadell, J. G., Euskirchen, E., Field, C. B., Goryachkin, S. V., Hagemann, S., Kuhry, P., Lafleur, P. M., Lee, H., Mazhitova, G., Nelson, F. E., Rinke, A., Romanovsky, V. E., Shiklomanov, N., Tarnocai, C., Venevsky, S., Vogel, J. G., Zimov, S. A., 2008. Vulnerability of permafrost carbon to climate change: Implications for the global carbon cycle. Bioscience 58, 701-714, doi:10.1641/B580807.

Schuur, E., Vogel, J., Crummer, K., Lee, H., Sickman, J., and Osterkamp, T., 2009. The effect of permafrost thaw on old carbon release and net carbon exchange from tundra. Nature 459, 556-559, doi:10.1038/nature08031.

Schwamborn, G., Andreev, A. A., Rachold, V., Hubberten, H. W., Grigoriev, M. N., Tumskoy, V., Pavlova, E. Y., Dorozhkina, M. V., 2002a. Evolution of Lake Nikolay, Arga Island, Western Lena River delta, during Late Pleistocene and Holocene time. Polarforschung 70, 69-82.

Schwamborn, G., Rachold, V., Grigoriev, M. N., 2002b.Late Quaternary sedimentation history of the Lena Delta. Quaternary International 89, 119–134.

Sher, A. V., Kaplina, T. N., Ovander, M. G., 1987. Unified regional stratigraphic chart for the Quaternary deposits in the Yana-Kolyma Lowland and its mountainous surroundings: Explanatory note in: Decisions of the Interdepartmental Stratigraphic Conference on the Quaternary of the Eastern USSR, Magadan, 1982, USSR Academy of Sciences, Far-Eastern Branch, North-Eastern Complex Research Institute, Magadan, 29-69. (in Russian)

Simova, L.E., 1964. Origin, development, and degradation of thermokarstic lakes in Anadyr tundra. In: Proceedings of the northeast complex scientific research institute 10, Vechnaya merzlota Chukotki, USSR Academy of Sciences, Siberian Branch, Magadan, 130-137. (in Russian)

Smith, L. C., Sheng, Y., MacDonald, G. M., Hinzman, L. D., 2005. Disappearing Arctic lakes. Science 308, 1429.

Soloviev, P. A., 1962. Alas relief of Central Yakutia and its formation. In: Permafrost and accompanying phenomena on the territory of the Yakutian ASSR, USSR Academy of Sciences, Moscow, 38-53. (in Russian)

Soloviev, P. A., 1959. Cryolithozone of the northern part of the Lena and Amga interfluve, USSR Academy of Sciences, Moscow. (in Russian)

Star, J., Estes, J., 1990. Geographic Information Systems – an introduction, Prentice-Hall, Englewood Cliffs, New Jersey, 303 pp.

Strauss, J., Schirrmeister, L., Wetterich, S., Borchers, A., Davydov, S. P., 2012. Grain-size properties and organic-carbon stock of Yedoma Ice Complex permafrost from the Kolyma lowland, northeastern Siberia. Global Biogeochemical Cycles, doi:10.1029/2011GB004104, in press.

Svendsen, J. I., Alexanderson, H., Astakhov, V. I., Demidov, I., Dowdeswell, J. A., Funder, S., Gataullin, V., Henriksen, M., Hjort, C., Houmark-Nielsen, M., Hubberten, H.-W., Ingolfsson, O., Jakobsson, M., Kjaer, K. H., Larsen, E., Lokrantz, H., Lunkka, J. P., Lysa, A., Mangerud, J., Matiouchkov, A., Murray, A., Moller, P., Niessen, F., Nikolskaya, O., Polyak, L., Saarnisto, M., Siegert, C., Siegert, M. J., Spielhagen, R. F., Stein, R., 2004. Late quaternary ice sheet history of northern Eurasia. Quaternary Science Reviews 23, 1229–1271.

Tarnocai, C., Canadell, J. G., Schuur, E. A. G., Kuhry, P., Mazhitova, G., Zimov, S. A., 2009. Soil organic carbon pools in the northern circumpolar permafrost region. Global Biogeochemical Cycles 23, GB2023, doi:10.1029/2008GB003327.

Tomirdiaro, S.V., 1965. The physics of lake thermokarst in the arctic lowlands and Antarctica and the cryogenic reworking of soils. Kolyma 7, 30-34, Kolyma 8, 36-41. (in Russian)

Toniolo, H., Kodial, P., Hinzman, L. D., Yoshikawa, K., 2009. Spatio-temporal evolution of a thermokarst in Interior Alaska. Cold Regions Science and Technology 56 (1), 39-49, doi: 10.1016/j.coldregions.2008.09.007.

Trask, P. D., 1932. Origin and environment of source sediments of petroleum. Gulf Publ. Co., Houston, Texas, 323 pp.

Treshnikov, A. F., 1985. Atlas Arktiki (Atlas of the Arctic). National Commission of Hydro-Meteorology and Environmental Protection, Major Department of Geodesy and Cartography, USSR, Moscow, 204 pp. (in Russian)

Tucker, G. E., Catani, F., Rinaldo, A., Bras, R. L., 2001. Statistical analysis of drainage density from digital terrain data. Geomorphology 36, 187-202.

Tumskoy, V. E., 2002. Thermokarst and its role in the development of the Laptev sea region in the late Pleistocene and Holocene. Authors' abstract of the Candidate Sci. (Geol.) Dissertation, Moscow State University, Moscow. (in Russian).

Ulrich, M., Grosse, G., Chabrillat, S., Schirrmeister, L., 2009. Spectral characterization of periglacial surfaces and geomorphological units in the Arctic Lena Delta using field spectrometry and remote sensing. Remote Sensing of Environment 113, 1220-1235, doi:10.1016/j.rse.2009.02.009.

Ulrich, M., Morgenstern, A., Günther, F., Reiss, D., Bauch, K. E., Hauber, E., Rössler, S., Schirrmeister, L., 2010. Thermokarst in Siberian ice-rich permafrost: Comparison to asymmetric scalloped depressions on Mars. Journal of Geophysical Research 115, E10009, doi: 10.1029/2010JE003640.

Ulrich, M., Günther, F., Morgenstern, A., Schirrmeister, L., 2011. High-resolution digital elevation model (DEM) of a thermokarst depression in Siberian ice-rich permafrost deposits. doi:10.1594/PANGAEA.759573.

van Everdingen, R. O. (Ed.), 2005. Multi-language glossary of permafrost and related ground-ice terms, National Snow and Ice Data Center/World Data Center for Glaciology, Boulder, available at: http://nsidc.org/fgdc/glossary.

van Geel, B., van der Hammen, T., 1978. Zygnemataceae in Quaternary Colombian sediments. Review of Paleobotany and Palynology 25, 377-392.

Veremeeva, A., Gubin, S., 2009. Modern tundra landscapes of the Kolyma Lowland and their evolution in the Holocene. Permafrost and Periglacial Processes 20, 399-406, doi: 10.1002/ppp.674.

Wagner, D., Overduin, P., Grigoriev, M., Knoblauch, C., Bolshiyanov, D. (Eds.), 2012. Russian-German Cooperation SYSTEM LAPTEV SEA: The Expedition LENA 2008. Reports on Polar and Marine Research 642, Alfred Wegener Institute for Polar and Marine Research, Bremerhaven.

Walter, K. M., Zimov, S., Chanton, J. P., Verbyla, D., Chapin III, F. S., 2006. Methane bubbling from Siberian thaw lakes as a positive feedback to climate warming. Nature 443, 71-75, doi:10.1038/nature05040.

Walter, K. M., Edwards, M. E., Grosse, G., Zimov, S., Chapin III, F. S., 2007. Thermokarst lakes as a source of atmospheric CH4 during the last deglaciation. Science 318, 633-636, doi: 10.1126/science.1142924.

West, J. J., Plug, L. J., 2008. Time-dependent morphology of thaw lakes and taliks in deep and shallow ground ice. Journal of Geophysical Research 113, F01009, doi: 10.1029/2006JF000696.

Wetterich, S., Kuzmina, S., Andreev, A. A., Kienast, F., Meyer, H., Schirrmeister, L., Kuznetsova, T., Sierralta, M., 2008. Palaeoenvironmental dynamics inferred from late Quaternary permafrost deposits on Kurungnakh Island, Lena Delta, Northeast Siberia, Russia. Quaternary Science Review 27, 1523-1540, doi:10.1016/j.quascirev.2008.04.007.

Wetterich S., Schirrmeister, L., Andreev, A. A., Pudenz, M., Plessen, B., Meyer, H., Kunitsky, V. V., 2009. Eemian and Late Glacial/Holocene palaeoenvironmental records from permafrost sequences at the Dmitry Laptev Strait (NE Siberia, Russia). Palaeogeography, Palaeoclimatology, Palaeoecology 279, 73-95, doi: 10.1016/ j.palaeo.2009.05.002.

Wetterich, S., Overduin, P. P., Grigoriev, M. (Eds.), 2011. Russian-German Cooperation SYSTEM LAPTEV SEA: The expedition Eastern Laptev Sea – Buor Khaya Peninsula 2010. Reports on Polar and Marine Research 629, Alfred Wegener Institute for Polar and Marine Research, Bremerhaven.

Yershov, E. D., 2004. General geocryology. Studies in polar research. Cambridge: Cambridge University Press.

Zimov, S. A., Voropaev, Y. V., Semiletov, I. P., Davidov, S. P., Prosiannikov, S. F., Chapin III, F. S., Chapin, M. C., Trumbore, S., Tyler, S., 1997. North Siberian lakes: A methane source fueled by Pleistocene carbon. Science 277, 800-802, doi:10.1126/science.277.5327.800.

Zimov, S. A., Davydov, S. P., Zimova, G. M., Davydova, A. I., Schuur, E. A. G., Dutta, K., Chapin III, F. S., 2006a. Permafrost carbon: Stock and decomposability of a globally significant carbon pool. Geophysical Research Letters 33, L20502, doi:10.1029/2006GL027484.

Zimov, S. A., Schuur, E. A. G., Chapin III, F. S., 2006b. Permafrost and the global carbon budget. Science 312, 1612–1613, doi:10.1126/science.1128908.

Zona, D., Oechel, W. C., Kochendorfer, J., Paw U, K. T., Salyuk, A. N., Olivas, P. C., Oberbauer, S. F., Lipson, D. A., 2009. Methane fluxes during the initiation of a large-scale water table manipulation experiment in the Alaskan Arctic tundra. Global Biogeochemical Cycles 23, GB2013, doi:10.1029/2009GB003487.

Note: The reference list has been updated and arranged according to the structure of the thesis. Therefore, slight differences to citations in the original papers may occur.

Acknowledgements

I would like to express my gratitude to my supervisor Prof. Hans-Wolfgang Hubberten for his continuous support of my scientific career and for providing me with working conditions that allowed both flexibility and continuity throughout my PhD time.

I am very grateful to Dr. Lutz Schirrmeister for accompanying my work with ongoing enthusiasm, exceptional support, and experienced guidance since the beginning of my time at the AWI in Potsdam, which he was even ready to provide from remote Siberian field camps. I would like to thank Dr. Guido Grosse for inviting me to study the fascinating field of permafrost degradation almost ten years ago and for sustaining our cooperation ever since. I very much benefited from both of their vast permafrost-related knowledge and field experience, which they were always willing to share.

I am thankful to Dr. Christine Siegert, Dr. Mikhail Grigoriev, Dr. Tatjana Kaplina, and Dr. Vladimir Tumskoy for giving me many opportunities to gain deeper insights into the Russian perspective on permafrost and periglacial research, not only by extensive discussions, but also by providing me with numerous books and articles from the vast pool of the Russian scientific literature.

I thank all colleagues that have supported me and my work at the AWI and were always available for critical discussions and introductions into their field of expertise, in particular Dr. Julia Boike, Prof. Ulrike Herzschuh, Dr. Georg Schwamborn, Dr. Birgit Heim, Dr. Hugues Lantuit, Dr. Paul Overduin, Dr. Sebastian Wetterich, Prof. Bernhard Diekmann, and Dr. Hanno Meyer. I enjoyed being part of the virtual working group “REmote Sensing of POlar Non-glaciated and Sensitive Environments” (RESPONSE) and thank all members for sharing the efforts in remote sensing and GIS data acquisition and archiving and for exchanging methodological expertise. I thank Ute Bastian, Cindy Springer, Lutz Schönicke, Janina Stapel, Christin Orfert, Martin Lamottke (all AWI), and Dr. Birgit Plessen (GFZ) for their support with lab analyses, and Roland Spröte for his digitizing efforts. Tobias Schmidt and Heiko Gericke are thanked for assuring smooth IT working conditions and quick problem solving. Many thanks go to Dr. Inga May and Dr. Thomas Opel for their quick help and proof-reading during the last days. I want to thank Dr. Mathias Ulrich, Frank Günther, and Sebastian Rößler for their “Kurungnakh cooperation”. I also thank all other fellow PhD students and senior colleagues for the enjoyable working atmosphere at the AWI.

I greatly acknowledge the engagement and support of all members of the Lena 2008 expedition team, particularly the valuable help of Dr. Irina Fedorova and Dr. Dmitry

Bolshiyanov. I would also like to thank my other co-authors of the presented research papers for their contributions and discussions, and Dr. Natalya Rudaya for conducting the pollen analyses and according interpretation so quickly but carefully.

I highly appreciate the financial support of my PhD work by the German National Academic Foundation (Studienstiftung des deutschen Volkes), the Christiane Nüsslein-Volhard-Foundation, the Faculty of Mathematics and Natural Science of the University of Potsdam, and the AWI directorate. I also thank the DAAD and several other funding organizations for supporting my participation in various scientific conferences.

Finally, I wish to thank my family and friends for their support, interest, and confidence during the past years. I want to express a very special thank you to Gesine Frenzel for her exceptional efforts and loving care for the girls, which enormously helped to keep the balance in their lives during rough times.

With all my heart I thank you, Tom, for sharing this life with me and for your great support in so many ways and you, Lilia and Maja, for reminding me every day what life really is about and, above all, for being the most wonderful daughters in the world.